



# DISSERTATION

Titel der Dissertation

„Chip Electrophoresis of Human Rhinovirus and  
Receptor Decorated Liposomes as Model Membranes  
for the Analysis of Key Steps in the Viral Infection  
Pathway“

Band 1 von 1 Bänden

Verfasser

Mag. rer. nat. Victor U. Weiss

angestrebter akademischer Grad

Doktor der Naturwissenschaften (Dr. rer. nat.)

Wien, Oktober 2009

Studienkennzahl lt. Studienblatt: A 091 419

Dissertationsgebiet lt. Studienblatt: Dr.-Studium der Naturwissenschaften Chemie UniStG

Betreuerin / Betreuer: Prof. Dr. Ernst Kenndler

# Acknowledgements

Prof. Dr. Ernst Kenndler and Prof. Dr. Dieter Blaas as group leaders

Klaus Witt and Agilent Technologies (Waldbronn, Germany) for support in material and technical matters

Gerhard Bilek, Leopold Kremser, Angela Pickl-Herk, Irene Goesler, Abdul Ghafoor, Christoph Weber, Katharina Huszar, Xavier Subirats, Viliam Kolivoška, Nena Matscheko, Adolfo Téllez, Matthias Rizzi, my colleagues



Verena, Sophie, Waltraud, Werner and Rainer, my family

# Contents

	Page
Acknowledgements	2
Contents	3
Abbreviations	4
1 Abstract	5
2 Introduction	6
2.1 Biological Background	6
2.1.1 Human Rhinoviruses	6
2.1.2 From Plasma Membranes to Liposomes	10
2.2 Technical Background	13
2.2.1 Capillary Electrophoresis	13
2.2.1.1 Migration of Analytes	13
2.2.1.2 Peak Dispersion	17
2.2.2 Chip Electrophoresis on the Agilent 2100 Bioanalyzer System	21
2.3 Analytical Background	25
2.3.1 Capillary Electrophoresis of HRVs	25
2.3.2 Electrophoresis of HRV2 on the Agilent 2100 Bioanalyzer System	30
2.3.3 Capillary Electrophoresis of Liposomes	34
3 Results and Discussion	35
3.1 Capillary Electrophoresis of Subviral 135S Particles	37
3.2 Receptor Mediated Attachment of Virions to Liposomes	53
3.3 Determination of Leakage from Lipid Vesicles via Electrophoresis	84
3.4 Investigation of Membrane Disrupting Abilities of HRV2	88
3.5 RNA Transfer of HRV2 through Membranes	99
4 Method Development on the Agilent 2100 Bioanalyzer System	114
4.1 Application of a Fluorescent EOF Marker	114
4.1.1 Calcein	114

4.1.2 Atto 495	118
4.2 Determination of Stable Electrophoresis Conditions for Chip Analysis	123
4.3 Fluorescence Labeling of HRV2	126
6 Conclusion	130
Literature	131
Curriculum Vitae	138
Zusammenfassung der Dissertation (dt.)	141
Lebenslauf (dt.)	142

## **Abbreviations**

CMC ... critical micellar concentration

EOF ... electroosmotic flow

FITC ... fluorescein isothiocyanate

FL ... fluorescence

HRV2 ... human rhinovirus serotype 2

LDL ... low density lipoprotein

SDS ... sodium dodecyl sulphate

TEM ... transmission electron microscopy

# 1 Abstract

Human Rhinoviruses (HRVs) constitute the most frequent causative agents of common cold infections. Roughly 100 serotypes are differentiated, which are divided into two classes according to receptor specificity upon cell infection. Major group viruses bind to intercellular adhesion molecule 1 (ICAM-1), minor group viruses to members of the low-density-lipoprotein receptor (LDLR) family. We demonstrated previously that chip electrophoresis allows for analysis of fluorescence labeled virus and its bioaffinity reactions, for instance binding of minor group HRV2 to receptor fragments derived from the Very-Low-Density-Lipoprotein Receptor (VLDLR) [Weiss *et al.* (2007): Virus analysis by electrophoresis on a microfluidic chip, *J. Chromatogr. B* 860, 173 – 179 and Kolivoška *et al.* (2007): Electrophoresis on a microfluidic chip for analysis of fluorescence-labeled human rhinovirus, *Electrophoresis* 28, 4734 – 4740].

In continuation of our previous work this thesis will be dedicated to the specific, receptor mediated attachment of HRV2 to cells via chip electrophoresis. However, instead of working with living cells, receptor decorated unilamellar vesicles (liposomes) were employed. Such, binding experiments between model membranes and virions could be carried out under well defined conditions.

In addition to binding experiments of HRV2 to liposomes, the transfer of the HRV2 genome into the aqueous lumen of model vesicles was investigated. *In vivo*, HRVs are internalized into cells via receptor mediated endocytosis. Endosomes undergo acidification which induces conformational changes in encapsulated HRVs. Through these changes virions are able to transfer their RNA genome through the plasma membrane into the cytosol of the infected cell. Therefore, I took interest in membrane disrupting abilities of viral proteins as well as of complete virions. Furthermore, experiments were carried out setting the stage for monitoring of the RNA transfer itself via so-called molecular beacons, fluorescence labeled oligonucleotide probes that bind specifically to corresponding nucleotide sequences. Binding to target sequences renders beacons fluorescent, which can be followed by chip electrophoresis.

# 2 Introduction

## 2.1 Biological Background

### 2.1.1 Human Rhinoviruses [3]

Human Rhinoviruses (HRVs) from the picornavirus family are non-enveloped, acid labile viruses of icosahedral symmetry with about 30 nm diameter. 60 copies each of the four viral proteins VP1 - VP4 form the viral capsid and encapsulate a single stranded, positive sense RNA of about 7100 nucleotides (figure 1). VP4 lies on the inner side of the virus capsid and is externalized upon virus conversion during the infection process together with the N-terminus of VP1. Other areas of VP1 together with VP2 and VP3 form the outer virus surface. According to their receptor specificity the roughly 100 different HRV serotypes are classified into a major and a minor group [4, 5]. Major group HRVs bind ICAM-1 for cell entry, whereas the minor group binds members of the LDL receptor family – LDL receptor (LDLR), very-LDL receptor (VLDLR) and LDLR related protein (LRP) [6]. This thesis concentrates on HRV2, the best studied minor group HRV member. Recombinant soluble receptor fragments derived from VLDLR were shown to bind in a circular way around the fivefold axis on the HRV2 capsid surface. According to the number of available binding modules per receptor fragment even multi-module binding was experienced [7 – 11]. Another classification of the several HRV serotypes is based on their sensitivity against a number of antiviral drugs, termed WIN compounds after the synthesizing company [12].

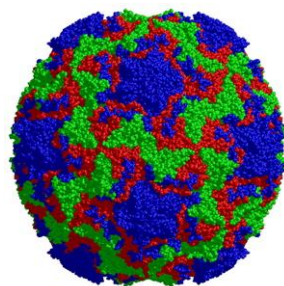


Fig. 1: Human Rhinoviruses are particles of icosahedral symmetry formed of four viral proteins: VP1 – blue , VP2 – green, VP3 – red, VP4 lies at the inside of the capsid and is not visible. Image taken from [http://www.mediresource.com/CPNews/images/x021226A\\_2009.jpg](http://www.mediresource.com/CPNews/images/x021226A_2009.jpg)

Binding of virions to plasma membrane receptors is defined as the first step in the HRV infection cycle. Following steps include (figure 2):

- (i) Endocytosis of receptor bound virions to early endosomes [13]
- (ii) Dissociation of the virus / receptor complex as well as changes in the virus conformation (uncoating) upon further transport along the endosomal route
- (iii) Release of the viral RNA from the inside of the capsid through the encapsulating membrane into the cytosol of the infected cell
- (iv) Synthesis of new infectious viral particles from internalized RNA

HRV2 enters target cells mainly via clathrin dependent pathways. Internalized virions cumulate in early endosomes (within 5 min), membrane enclosed organelles of a mildly acidic pH value (pH 6.0 to 6.5). Under these conditions bound virus particles dissociate from respective plasma membrane receptors. Virions are then transported via endosomal carrier vesicles (ECV) to late endosomes (within 15 min). Both cell compartments exhibit pH values below 5.6, the pH threshold for HRV2 uncoating. In the course of virus uncoating the structure of the virus capsid is altered – VP4 is expelled from the virion and the N-termini of VP1, which lay previously at the inner side of the virus shell, are externalized. In a second step the viral RNA is expelled from the inside of the virus capsid. Viral and subviral particles can be differentiated via their sedimentation upon centrifugation. Native virions sediment at 150S, whereas viral particles still including the RNA but already without VP4 sediment at 135S. Subviral particles, that have expelled the RNA as well, sediment at 80S. Conversely to major group HRVs, uncoating of HRV2 *in vivo* is solely pH dependant, whereas *in vitro* HRV conversion can also be induced via heating to temperatures of 56°C or more. pH triggered RNA release could be visualized via dynamic force microscopy [14].

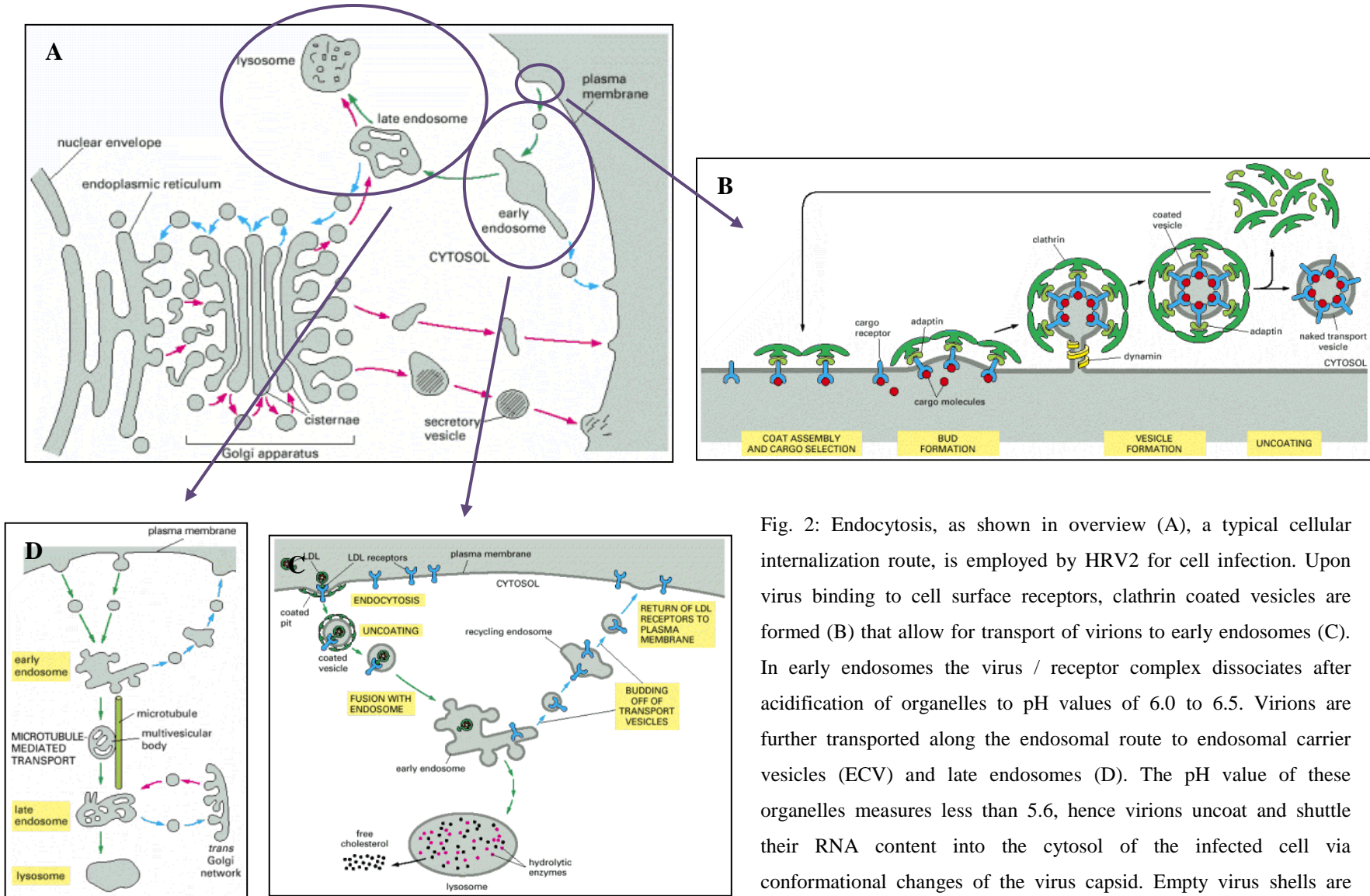


Fig. 2: Endocytosis, as shown in overview (A), a typical cellular internalization route, is employed by HRV2 for cell infection. Upon virus binding to cell surface receptors, clathrin coated vesicles are formed (B) that allow for transport of virions to early endosomes (C). In early endosomes the virus / receptor complex dissociates after acidification of organelles to pH values of 6.0 to 6.5. Virions are further transported along the endosomal route to endosomal carrier vesicles (ECV) and late endosomes (D). The pH value of these organelles measures less than 5.6, hence virions uncoat and shuttle their RNA content into the cytosol of the infected cell via conformational changes of the virus capsid. Empty virus shells are degraded in lysosomes. Images taken from [15].



*De novo* virus synthesis takes place after viral RNA has reached the cytosol of an infected cell. Therefore, HRVs have to shuttle their RNA through the endosomal plasma membrane. In principal two mechanisms are possible – (i) rupture of the endosomal membrane or (ii) formation of pores in the membrane that allow for passing of the virus RNA over the lipid barrier. For HRV2 co-uptake of fluid phase markers has demonstrated the latter case. Only fluorescence labeled dextrans of small size were found to enter the cytosol of infected cells, whereas larger molecules were retained in late endosomes. Moreover the acidic pH of ECVs and late endosomes was maintained during HRV infection which also argues against endosomal rupture. Such, formation of a roughly 10Å wide pore via the N-terminus of VP1 as well as via VP4 was suggested [16, 17]. Externalized N-termini of VP1 are thought to insert into the endosomal lipid bilayer during HRV2 uncoating to arrange the direction of RNA expulsion. After release of the viral genome to the cytoplasm, subviral 80S particles are degraded in lysosomes at pH values of 4.0 to 4.5.

Ribosomal translation of the viral RNA is error prone, thus accounting for the large number of different HRV serotypes [18]. Small changes in the amino acid sequence lead to serological completely different rhinoviruses. For the pharmaceutical industry this variety of serotypes hinders the development of vaccines and antiviral drugs against HRVs. Therefore, rhinoviruses present the most frequent causative agents of common cold infections, reaching from annoying but else harmless mild infections of the upper respiratory tract to more serious lower respiratory tract infections like pneumonia and exacerbations of other diseases like bronchial asthma. HRVs are typically transmitted via self-infection (contact of hands contaminated with virus containing secretions with eyes or the nasal mucosa) or via aerosols. After initial contact, virions are transported to target cells in the posterior nasal areas, where binding to respective receptors occurs [19 – 22].

## 2.1.2 From Plasma Membranes to Liposomes [23]

Cells are confined from their extracellular environment via plasma membranes. Also in the cytosol of a respective cell, are membranes needed for the confinement of different intracellular compartments to maintain specific organelle characteristics, for instance pH values. Plasma membranes are bilayers formed from phospholipids (figure 3).

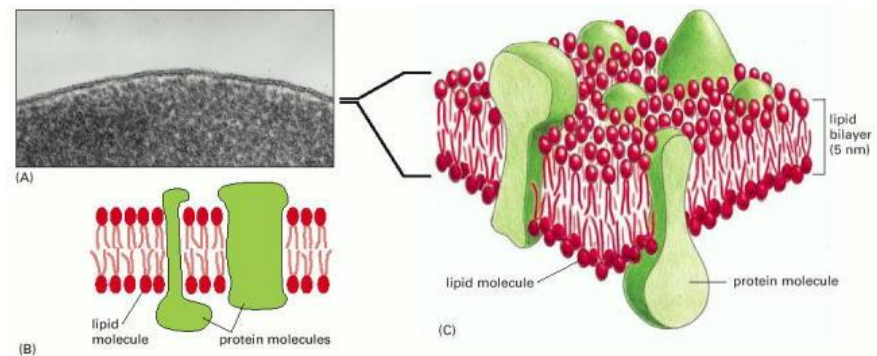


Fig. 3: Electron microscope image of a plasma membrane cross section (A), a two dimensional plasma membrane view (B) and a three dimensional model (C). Phospholipids are depicted in red, membrane proteins in green. Image taken from [23].

Phospholipids are amphipathic molecules – they consist of a polar headgroup and two hydrophobic fatty acid chains. When introduced to aqueous solutions, amphipathic molecules spontaneously form aggregates to minimize their impact on the three dimensional structure of the aqueous medium (figure 4), thus minimizing the resulting increase in free energy (*similia similibus solvuntur*).

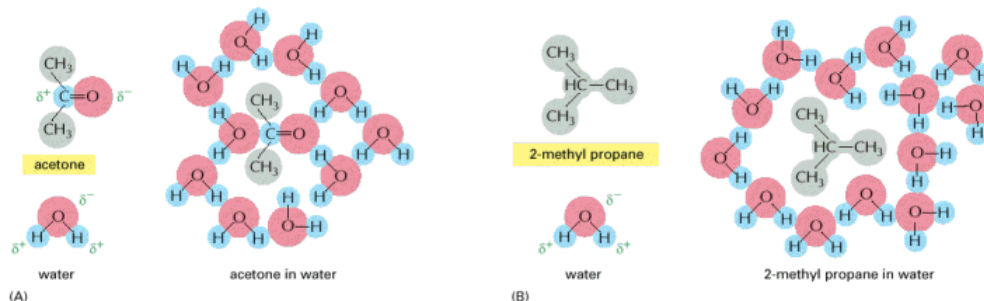


Fig. 4: Impact of hydrophilic and hydrophobic molecules on the three dimensional structure of an aqueous solution. Polar molecules, for instance acetone (A), form electrostatic interactions with water and are therefore incorporated in the three dimensional structure of the solution. Isobutane (B) on the other hand is not able to form electrostatic interactions with water molecules thus

forcing the aqueous solution to reorganize into ice like cages. This entropy reduction leads to an increase of the free energy of the solution. In order to keep this increase as small as possible hydrophobic molecules form clusters, e.g. oil droplets in water. Image taken from [23].

Clustering of phospholipids in aqueous media leads to energetically favorable spherical structures formed of lipid bilayers. Lipid bilayers are in fact fluids themselves, where individual phospholipids are able to diffuse laterally, to flex or to rotate. Crossovers of phospholipids from one leaflet of the bilayer to the other only seldom occur. Proteins are inserted into the bilayer either via hydrophobic anchors or transmembrane domains. Together with heterogeneity in membrane composition, attached proteins yield cellular lipid bilayers their biological functionality. For membrane research experiments living cells are often replaced by liposomes, i.e. artificial, spherical lipid bilayers that encapsulate an aqueous core. Such liposomes offer the possibility to concentrate on basic traits related to the plasma membrane itself.

Liposomes are distinguished according to their size and lamellarity (figure 5 A and [24, 25]).

- (i) MLVs – multilamellar vesicles of 0.15 - 1  $\mu\text{m}$  diameter
- (ii) SUVs – small unilamellar vesicles of 25 - 50 nm diameter
- (iii) LUVs – large unilamellar vesicles of 100 nm - 1  $\mu\text{m}$  diameter
- (iv) GUVs – giant unilamellar vesicles of 1 - 200  $\mu\text{m}$  diameter
- (v) MVVs – multivesicular vesicles of 1.6 - 10.5  $\mu\text{m}$  diameter

Liposomes are thermodynamical stable structures, formed spontaneously upon hydration of a lipid film. Modification of liposome size and lamellarity can be achieved upon processing of the initially formed material via e.g. sonication or extrusion through filters of a well defined pore size [24, 25]. Functionalization of liposomes can be achieved through several means (figure 5B and [24, 25]).

- (i) Encapsulation of water soluble molecules

- (ii) Entrapment of hydrophobic molecules in the lipid bilayer
- (iii) Interaction of the lipid bilayer with amphipathic molecules
- (iv) Anchoring molecules on the liposome surface (*NB*, we opted in previous work (refer to 2.3.3) for this approach to decorate liposomes with recombinant receptor fragments: a  $\text{Ni}^{2+}$  chelating lipid, DOGS-NTA – 1,2-dioleoyl-*sn*-glycero-3-[*N*-(5-amino-1-carboxypentyl)iminodiacetic acid)succinyl] (nickel salt) – was incorporated into the liposomal bilayer. Free coordinative sites on  $\text{Ni}^{2+}$  could be targeted by recombinant receptor fragments expressing a His6-tag – six histidines in tandem – at their C-terminus.)

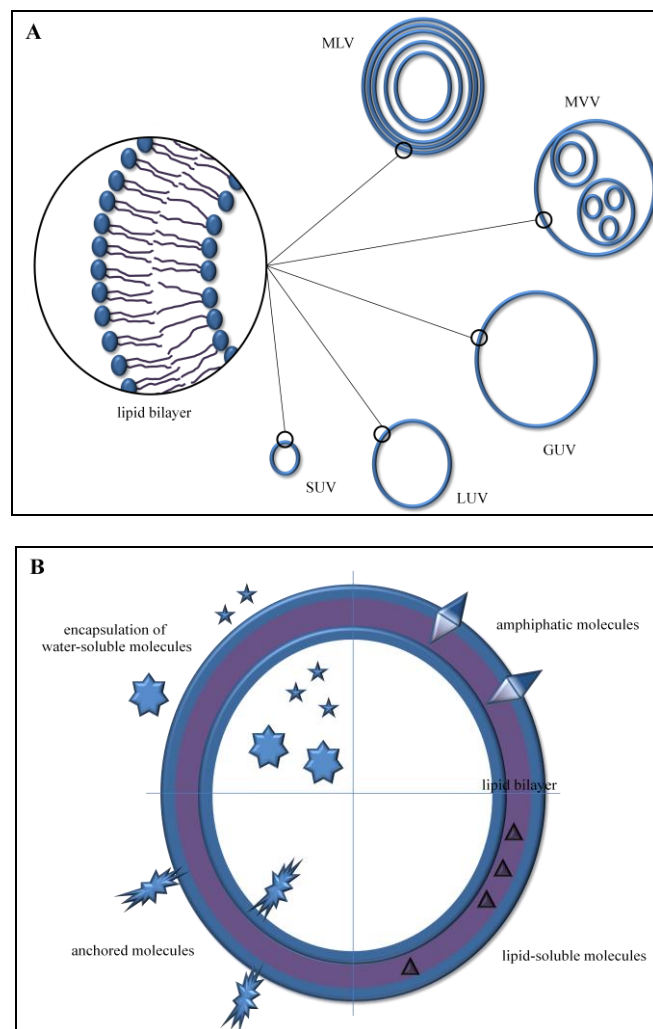


Fig. 5: Difference in liposome size and lamellarity (A) MLV: multilamellar vesicles, SUV: small unilamellar vesicles, LUV: large unilamellar vesicles, GUV: giant unilamellar vesicles, MVV: multivesicular vesicles. Liposomes can be functionalized via various methods (B) – e.g. encapsulation of hydrophilic molecules into their aqueous core or interaction of hydrophobic or amphipathic molecules with the lipid bilayer.

## 2.2 Technical Background

### 2.2.1 Capillary Electrophoresis [26 – 30]

#### 2.2.1.1 Migration of Analytes

Capillary electrophoresis (CE) allows for separation of analytes in open tubes, i.e. capillaries, filled with a background electrolyte (BGE) upon application of an electric field. Figure 6A shows a schematic drawing of a typical CE setup: A capillary is placed between two buffer reservoirs that are additionally connected via electrodes and a high voltage power supply. Sample injection is carried out on one end, analyte zones are detected at the opposite end of the capillary after analyte separation in an electric field. Figure 6B demonstrates a typical CE instrument as found in our laboratory.

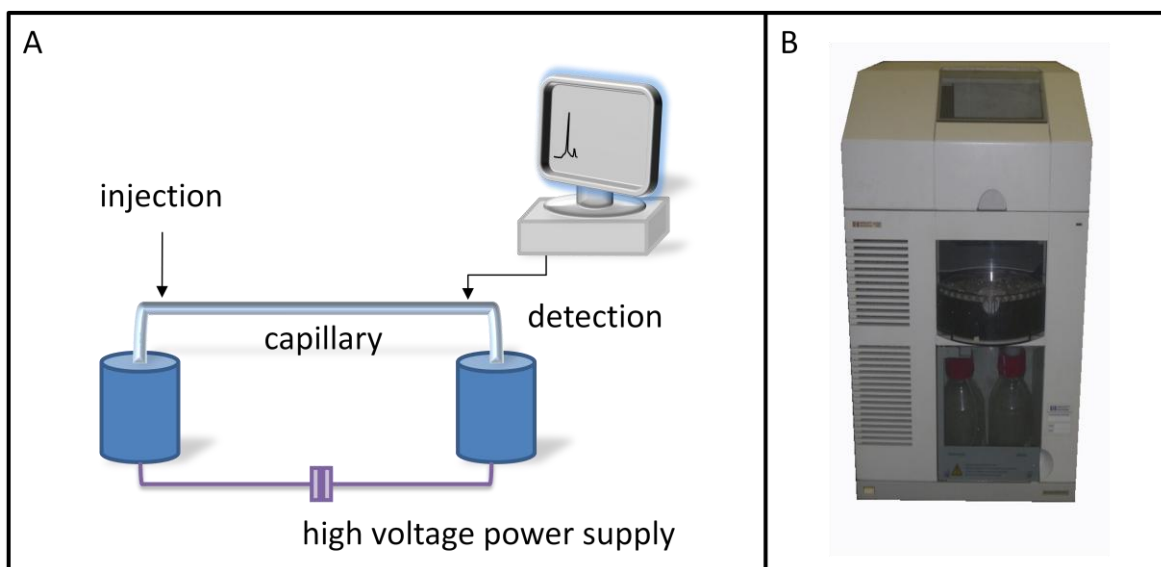


Fig. 6: Schematic drawing of a capillary electrophoresis setup (A). Image of a commercially available Agilent CE instrument (B). Image 6B was taken from <http://www.spectralabsci.com/images/HP-3D-CE-G1600AX.jpg>

Analytes subjected to CE are separated according to their migration velocity in the applied electric field.

$$v_i = E \cdot \frac{z \cdot e}{\xi}$$

The velocity of migration  $v_i$  is directly proportional the applied field  $E$  times an analyte specific factor. This factor can be expressed as  $\frac{v_i}{E} = \frac{z \cdot e}{\xi}$  and is termed  $\mu_i^0$ , or absolute mobility of a substance. It is a result of two counterdirected forces working in steady state on a particle during electrophoresis: (i) an accelerating term  $z \cdot e$  reflecting the electric force being proportional to the charge of the respective analyte and (ii) a retarding term  $\xi$  considering hydrodynamic friction according to Stokes law (described by the frictional coefficient). The frictional coefficient itself is defined as  $\xi = 6 \cdot \pi \cdot a_i \cdot \eta$  reflecting the particle geometry as well as the dynamic viscosity  $\eta$  of the BGE. Via the viscosity dependence temperature as well as solvent effects are taken into account. The absolute mobility can therefore be described as:

$$\mu_i^0 = \frac{z \cdot e}{6 \cdot \pi \cdot a_i \cdot \eta}$$

However, the term  $6 \cdot \pi \cdot a_i$  defines an idealized, rigid and non changing sphere. Furthermore, the absolute mobility describes the electrophoretic behaviour of an analyte in the absence of any ions, i.e. a BGE diluted to an infinitely low concentration. Both these facts illustrate that the concept of an absolute electrophoretic mobility can only be understood as a first approximation in describing the migrational behaviour of an analyte in CE.

According to the Debye-Hückel-Onsager theory the absolute mobility is modified through solvent dependant parameters to consider the finite ionic strength of the BGE.  $\mu_i^0$  is corrected for the relaxation (A) and the electrophoretic (B) effect as well as for the ionic strength (I) of the employed solvent, thus yielding the concept of an actual mobility  $\mu_i^{act}$ .

$$\mu_i^{act} = \mu_i^0 - A\sqrt{I}\mu_i^0 - B\sqrt{I}$$

$$I = \frac{1}{2} \sum c_i z_i^2$$

Both, relaxation (A) and electrophoretic effect (B) decelerate analytes in CE. The relaxation effect describes the retardation of molecules by displacement of charged particles out of the centre of a sphere of counter ions and the time needed thereafter for formation of such a sphere anew. The electrophoretic effect on the other hand describes the

retardation due to solvent molecules transported by counter-moving counter-charged ions. Both effects are shown schematically in figure 7.

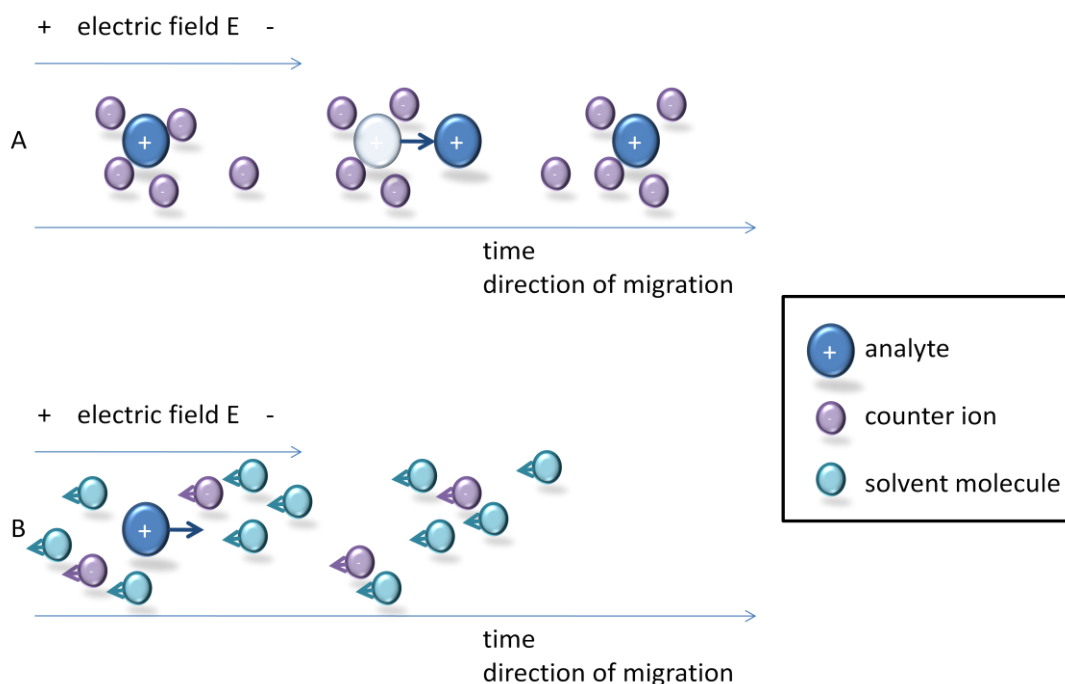


Fig. 7: Retarding effects in CE: relaxation effect (A) and electrophoretic effect (B)

Furthermore all kinds of equilibria, such as ion pair formation, conjugation or complex formation have to be considered upon description of the migrational behaviour of analytes in CE. For weak acids or bases the effective mobility  $\mu_i^{eff}$  accounts for the pH value of the BGE, since proteolysis of analytes is of course affected by the pH. For a monovalent acid thus the following expression is obtained:

$$\mu_i^{eff} = \frac{\mu_i^{act}}{1 + 10^{pKa-pH}}$$

For fused silica capillaries also the electroosmotic flow (EOF) has to be considered in dependence of the pH value of the BGE. Silanol groups ( $pK_a = 4-6$ ) are ionized upon application of BGEs with intermediate or high pH, thus attracting cationic species from the buffer to the capillary surface. Hence an electric bilayer is formed from deprotonized silanol groups and cationic species from the solution. Upon application of an electric field the cationic species of the electric bilayer migrate in the direction of the cathode inducing movement of the whole electrolyte bulk inside the capillary in the same direction. This effect is termed EOF and induces an additional electroosmotic mobility  $\mu^{EOF}$ . Effective

and EOF mobility are combined to form the apparent mobility  $\mu_i^{app}$  of an analyte in CE. The apparent mobility can be visualized as vectorial sum of its two constituents (figure 8).

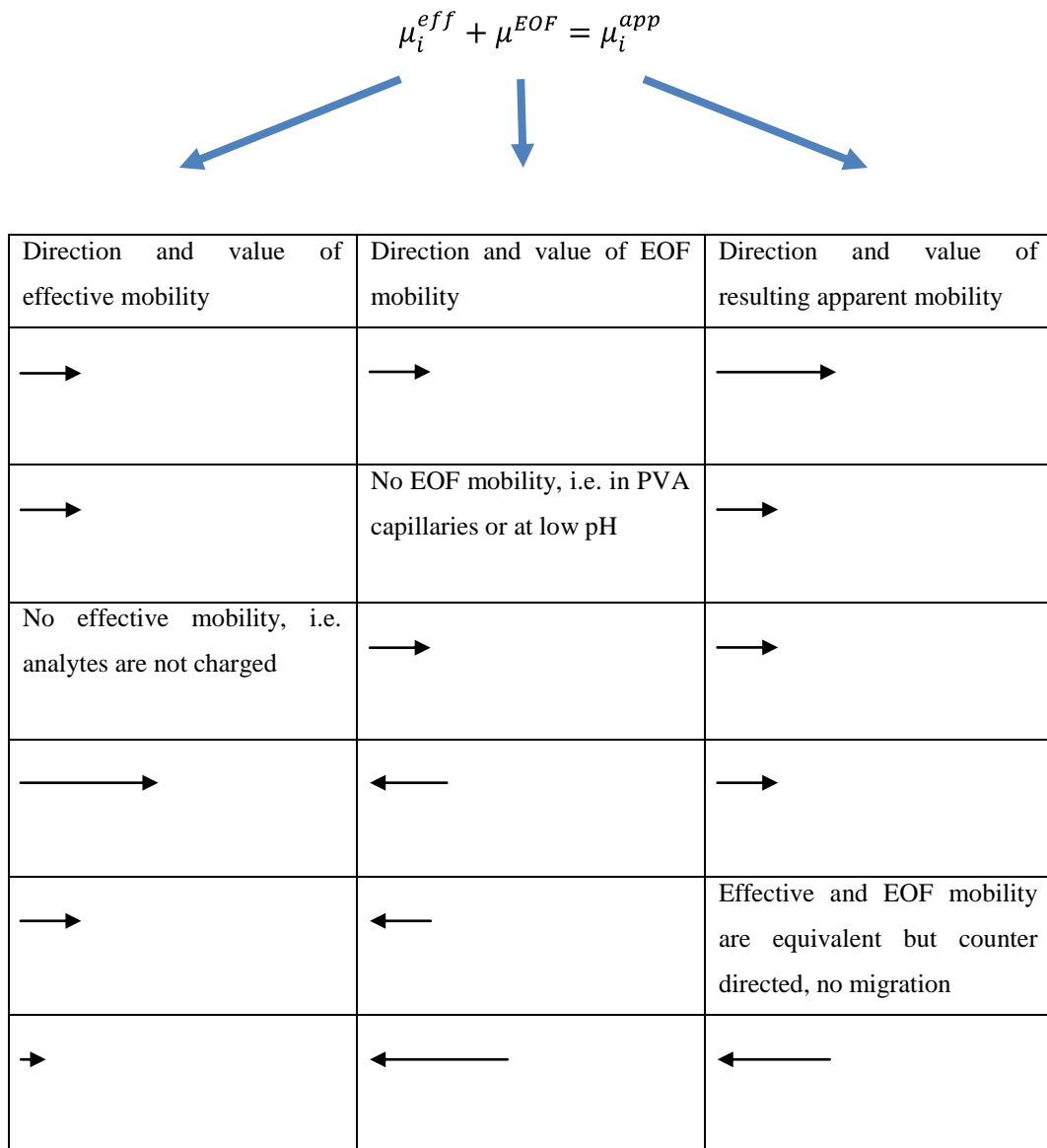


Fig. 8: Effective and EOF mobility are visualized as vectors for calculation of the apparent mobility of an analyte.

The electroosmotic mobility  $\mu^{EOF}$  is dependent on the zeta-potential  $\zeta$  of the BGE as well as on its viscosity  $\eta$ ;  $\epsilon_r$  describes the relative permittivity and  $\epsilon_0$  the permittivity of vacuum.

$$\mu^{EOF} = -\frac{\epsilon_r \cdot \epsilon_0 \cdot \zeta \cdot E}{\eta}$$



### 2.2.1.2 Peak Dispersion [31 – 33]

Even if the analyte zone forms a Dirac function upon injection to the capillary, at analyte detection the peak shape resembles a Gauss function. The width of this function can be expressed via the peak variance  $\sigma_z^2$  after analyte migration for a distance  $z$ .  $\sigma_z$ , the standard deviation of the Gaussian distribution expressed in the space domain, is half of the distance between the inflection points of the curve (at approximately 0.6 of the peak height). The peak variance  $\sigma_z^2$  and the migrational distance  $z$  can be related via a proportional factor  $H$ , which is according to Martin and Synge termed plate height and which indicates peak broadening after migration for the distance  $z$ .

$$\sigma_z^2 = H \cdot z$$
$$H = \frac{\sigma_z^2}{z}$$

In CE the position of the detector is normally fixed, which implies that not the peak variance in dependence on the migrational distance of the analyte peak from the point of injection is of importance but the time needed for the analyte zone to pass the detection window. Nevertheless the plate model of Martin and Synge can also be employed for CE since  $\sigma_z^2$  and  $\sigma_t^2$ , the peak variances in the space and time domain, respectively, can be related via the analyte velocity  $v_i$ .

$$\sigma_{t,i}^2 = \frac{\sigma_{z,i}^2}{v_i^2}$$

A number of individual effects contribute to the total peak broadening in CE. The resulting total peak variance as well as the total plate height can be understood as sum of those individual effects.

$$\sigma_{tot}^2 = \sum \sigma_{ind}^2$$
$$H_{tot} = \sum H_{ind}$$

Effects influencing the total plate height in CE include:

- (i) Extracolumn effects – Sample injection as well as detection influence the peak variance due to finite zone width independent of the migrational process itself.

- (ii) Longitudinal diffusion – Longitudinal diffusion results from a respective concentration gradient across the zonal boundary. It depends on the diffusional coefficient of the analyte  $D_i$  in a direct proportional and from the velocity of the analyte  $\mu_i^{app} \cdot E$  in an indirect proportional way.
- (iii) Radial temperature gradient – Joule heat is generated by the passing of an electric current through the capillary. High capillary surface-to-volume ratios (narrow capillaries) allow for efficient heat dissipation. Narrow capillary diameters on the other hand increase the current density inside the capillary. Therefore, to reduce the amount of generated Joule heat, the current itself has to be reduced, either by application of lower field strengths or by reduction of the ionic strength of the BGE.
- (iv) Wall adsorption – Wall adsorption especially in conjunction with slow kinetics of analyte sorption from the capillary wall contributes to peak broadening in CE as well. Irreversible adsorption to the capillary wall can even lead to loss of the analyte peak. On the other hand, however, adsorption of molecules to the capillary wall can be employed for coating procedures.
- (v) Electromigration dispersion – In capillary zone electrophoresis the same current is applied across the capillary. However, the presence of analyte ions in the sample zone influences the conductivity in that particular capillary volume. Thus, the field strength in the sample zone is lower (for zones of higher conductivity) than in adjacent capillary sections. Analyte ions therefore exhibit different migration velocities according to their relative position in the capillary. Analytes after the terminating front of the sample zone exhibit higher velocities (because of higher field strength) in the direction of overall migration than analytes in the sample zone itself. As soon as the analyte reaches the sample zone again it is confronted with its lower field strength and is slowed down. This effect results in peak sharpening at the terminating front of the sample zone. However, the same effect at the leading front of the sample zone leads to peak broadening since the direction of longitudinal diffusion and analyte acceleration due to a higher field strength point at the same direction.

- (vi) Minor effects – Capillary bending results in different path lengths for analyte ions passing the capillary and thus as well to peak broadening. Also the presence of EOF causes peak broadening as do laminar flows inside the capillary or even the cut of the capillary. In overall, for short capillaries and even more so on electrophoretic microchips, peak broadening effects resulting from channel geometry as well as from extracolumn effects gain more influence on the total peak variance than for longer separation distances.

The plate number  $N$  relates the effective length of the capillary to the plate height  $H$ .

$$N = \frac{L}{H}$$

The plate number  $N$  in CE is analyte specific and is accessible from the resulting peak variance after analyte migration. For  $\sigma_{tot}^2 = H \cdot L$  it can be further reasoned:

$$N = \frac{L}{H} = \frac{L^2}{\sigma^2}$$

$$N = \frac{(\mu_{avg} \cdot E \cdot t)^2}{\sigma^2}$$

$$\sqrt{N} = \frac{\mu_{avg} \cdot E \cdot t}{\sigma}$$

$\mu_{avg}$  corresponds to the average mobility of two solutes. Likewise the separation of two analytes is described via the resolution  $R$  as ratio between the difference in peak migration distance  $\Delta x_i$  and peak width. For Gauss peaks baseline separation is obtained at  $4\sigma$  which leads to:

$$R = \frac{\Delta x_i}{4\sigma} = \frac{\Delta\mu_i^{app} \cdot E \cdot t}{4\sigma}$$

Comparison of equations for  $N$  and  $R$  finally relates the resolution between two peaks to a selectivity (comparison of mobilities) and an efficiency term (related to peak dispersion via the square root of the plate number  $N$ ). Therefore baseline separation between two peaks in CE depends on both factors, migration and dispersion. However, since the plate number is

considered only as square root, the resolution between two analytes is more easily adjusted via the selectivity term.

$$\sigma = \frac{\mu_{avg} \cdot E \cdot t}{\sqrt{N}}$$
$$\sigma = \frac{1}{4} \frac{\Delta\mu_i^{app} \cdot E \cdot t}{R}$$

$$\frac{\mu_{avg} \cdot E \cdot t}{\sqrt{N}} = \frac{1}{4} \frac{\Delta\mu_i^{app} \cdot E \cdot t}{R}$$
$$\frac{\mu_{avg}}{\sqrt{N}} = \frac{1}{4} \frac{\Delta\mu_i^{app}}{R}$$

$$R = \frac{1}{4} \sqrt{N} \frac{\Delta\mu_i^{app}}{\mu_{avg}}$$

## 2.2.2 Chip Electrophoresis on the Agilent 2100 Bioanalyzer System

The Agilent 2100 Bioanalyzer system (figure 9) was developed for chip electrophoretic separation of proteins, DNA and RNA as well as for cell flow-cytometry. Protein separation is described in literature in detail [34 – 36]; other applications work similarly.

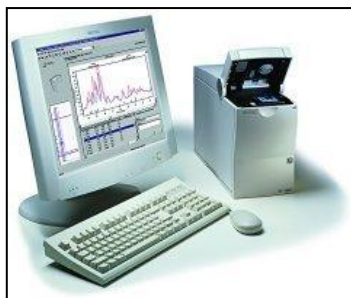


Fig. 9: Agilent 2100 Bioanalyzer workstation; image taken from <http://www.chem.agilent.com/>

Agilent 2100 Bioanalyzer chips (figure 10) are single-use products manufactured from Caliper Technologies Corp. (Mountain View, CA) and fabricated from soda lime glass. Channels are etched photolithographically to 13  $\mu\text{m}$  depth and 36  $\mu\text{m}$  width on square chips of 17.5 mm edge length. In the case of the protein application up to 10 samples can be analyzed per chip, DNA and RNA chips even allow analysis of up to 12 samples. Upon purchase, chips are supplied with background electrolyte, dye and standard solutions to allow for quick lab-on-a-chip sample analysis.



Fig. 10: Chips for Agilent 2100 Bioanalyzer – blue for DNA, green for RNA and violet for protein analysis. Yellow chips are employed for cell flow-cytometry. Image taken from [http://www.bcm.edu/cms\\_web/110/biolabchips.jpg](http://www.bcm.edu/cms_web/110/biolabchips.jpg)

Channels of protein chips are filled on the supplied chip priming station via pressurization (12.0  $\mu\text{L}$  for 60 sec from well A4) with a polymer containing BGE as sieving matrix

(120 mM Tricine, 42 mM Tris, pH 7.6, 8.7 mM SDS, 3.25 % polydimethylacrylamide, 4  $\mu$ M FL dye with  $\lambda_{\text{ex}} / \lambda_{\text{em}} = 650 / 680\text{nm}$ ). Remaining BGE is removed from well A4 before 12.0  $\mu$ L of BGE are pipetted to wells A4, B4, C4 and D3, respectively. Well D4 is filled with 12.0  $\mu$ L BGE not including SDS or dye, hence termed destaining solution. Well D2 is used for application of a protein size standard solution. All other wells are filled with 6.0  $\mu$ L of denatured protein samples. Notation of wells as described above is according to literature [34] and shown below (figure 11).

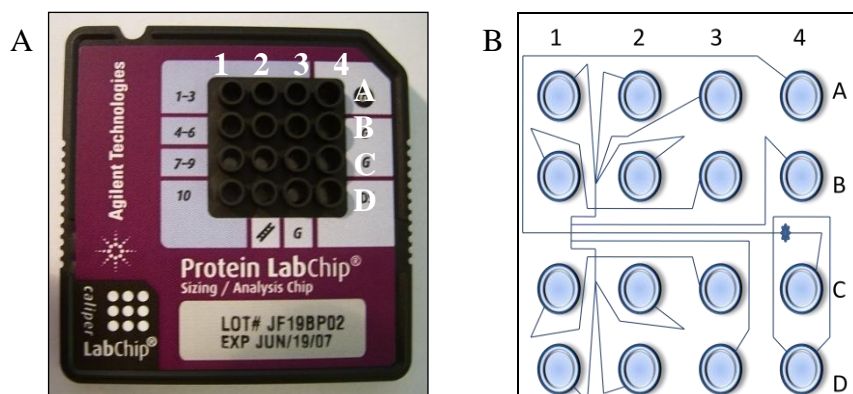


Fig. 11: Protein chip for Agilent 2100 Bioanalyzer (A); the scheme (B) reflects the chip geometry.

All processes during analysis of samples on Agilent 2100 Bioanalyzer chips are controlled via a computer script, which is embedded in the assay surface of the instrument and hence usually not accessible to the user. The script allows individual targeting of 16 high voltage power supplies. Thus, samples are injected electrophoretically to the separation channel on the chip via a two step process as shown in figure 12. This two step process allows for injection of a sharp sample zone into the separation channel; the volume of the respective sample plug was calculated to 25 pL [34].

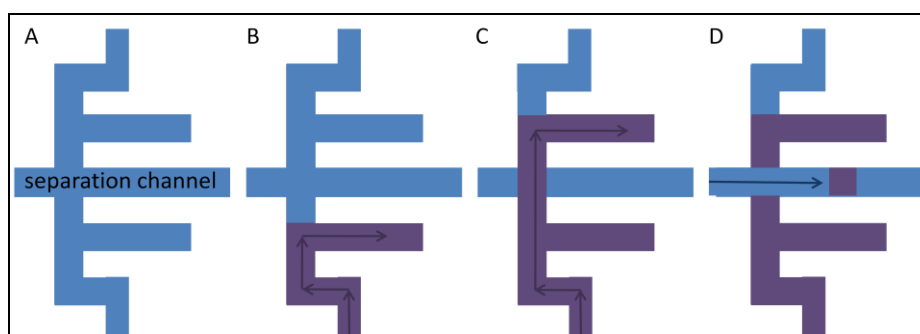


Fig. 12: Electrophoretic sample injection to the chip separation channel (A). An example for sample injection from a well of the lower chip part is detailed. In a first step, molecules are

electrophoresed to well D3 (B), in a second step across the separation channel to well B4 (C). A short sample plug of approximately 25 pL is then analyzed in the separation channel (D). Samples from the upper chip part are injected upon electrophoresis to according wells.

The instrument is equipped for FL detection at two wavelengths; a red laser allows for detection at a maximum  $\lambda_{\text{ex}} = 630 \text{ nm}$ , a blue LED for detection at a maximum  $\lambda_{\text{ex}} = 470 \text{ nm}$ . Upon migration in the separation channel proteins are separated in the polymer sieving matrix according to their respective size. Furthermore, proteins are FL labeled via a dye included in the BGE to allow for detection with the red laser of the instrument. Dye molecules interact with SDS/protein complexes and SDS micelles likewise, rendering both fluorescent. However, interaction of the FL dye with detergent micelles greatly diminishes the sensitivity of the analytical system. Therefore, Agilent developed a so called virtual destain (figure 13), that dilutes the SDS concentration in the BGE after analyte separation below the detergent CMC value with destaining solution (BGE not including dye or SDS). Dye molecules are reported not to interact with SDS monomers but attach to the proteinaceous analytes instead, rendering them even more fluorescent and thus increasing the sensitivity of protein detection.

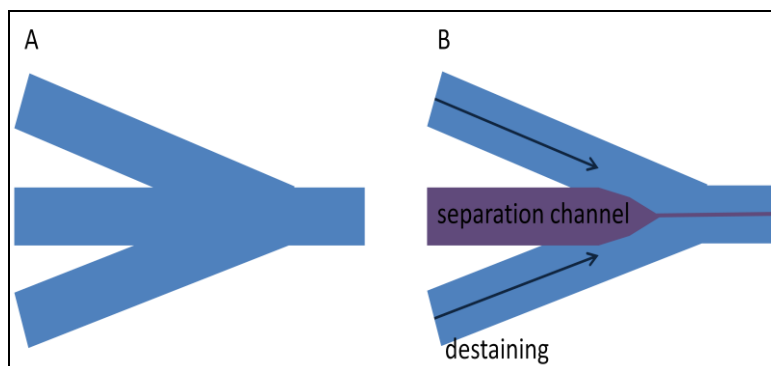


Fig. 13: Online virtual destain in the course of protein analysis on Agilent 2100 Bioanalyzer chips: Chip geometry (A) and direction of flows (B). The SDS concentration of the BGE is diluted below the CMC of the detergent after separation of analytes via a destaining solution, thus greatly improving the sensitivity of the instrument for FL labeled protein detection.

Results of protein analysis can either be read out in the form of electropherograms or can be converted to simulate SDS-PAGE gels. An electropherogram obtained after analysis of a protein ladder size standard can be found in figure 14. Peaks for 7 marker proteins and for the dye as lower marker (sizing from 4.5 - 240 kDa) are baseline separated. The second peak of the electropherogram is described as system peak [37].

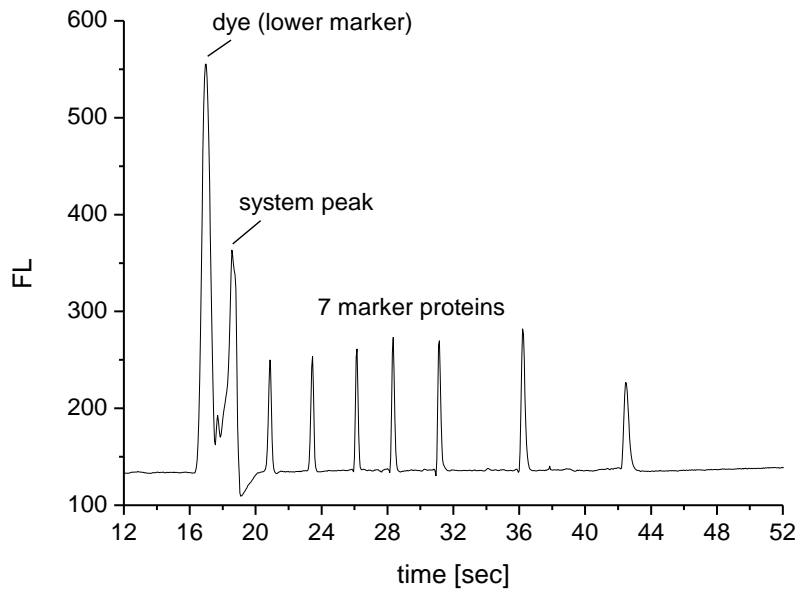


Fig. 14: Electropherogram of a ladder sample analyzed on a protein chip of Agilent 2100 Bioanalyzer. Peaks correspond to seven marker proteins, a peak for the FL dye as lower marker and a system peak (second peak).

DNA analysis is carried out presumably in a likewise fashion although the exact composition of the BGE has not been published so far. The most striking difference between protein and DNA chips is the chip geometry itself. Whereas protein chips include a destaining cycle, this cycle is omitted with DNA chips. Thus up to twelve DNA samples can be analyzed per chip (figure 15 and [38]).

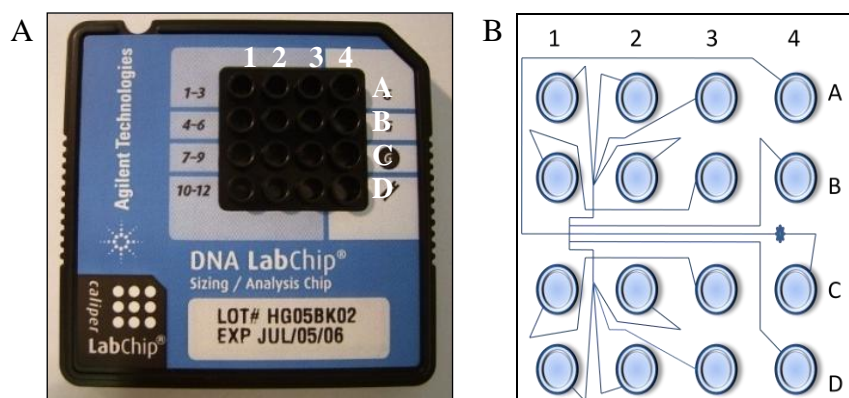


Fig. 15: DNA chip for Agilent 2100 Bioanalyzer (A); the scheme on the right side demonstrates the chip geometry (B).



## 2.3 Analytical Background

### 2.3.1 Capillary Electrophoresis of HRVs

After initial capillary electrophoresis experiments with tobacco mosaic virus by Hjertén et al. [39] during the late 1980s, CE has more and more evolved as a powerful tool for the analysis of viruses. Electrophoresis in the capillary format offers the great advantage over other analysis methods that virions can be followed in free solution, therefore allowing for tracking of virions in the fluid phase. In such a way, for instance binding of virus particles to receptor molecules or antibodies can be monitored. CE has thus been successfully employed for the study of several virus families, like togaviridae [40] comoviridae [41], adenoviridae [42] and picornaviridae [43 – 45].

Human rhinoviruses, belonging to the latter virus family, have been extensively characterized via CE in a series of papers [46, 47] (for reviews refer to [43, 44, 48, 49]). As has been stated (refer to 2.1.1) HRVs consist of a proteinaceous capsid of 60 copies each of the four viral proteins VP1 - 4 encapsulating a viral RNA genome. The pI of such a protein capsid assembly – that of HRV serotype 2 – was found to be 6.8 via capillary isoelectric focussing (CIEF, [50]). Therefore, HRV2 particles are negatively charged at pH 8.3, the pH of the BGE normally employed for rhinovirus analysis in CE. The basic pH value of the BGE was chosen to allow for electrophoresis with reasonable virus mobility – the BGE pH should value at least  $\pm 1$  pH units of the analyte pI. However, virus uncoating at acidic pH values anticipates application of BGEs with pH values lower than 5.8. Thus sodium borate at pH 8.3 was introduced as BGE for CE of HRVs.

Furthermore, it was found that virions tend to yield aggregates upon subjection to CE in plain sodium borate. Therefore, to reduce virus aggregation and to suppress spike formation, detergents like sodium dodecyl sulphate (SDS), sodium deoxycholate, Triton X-100R or dodecylpolyethyleneglycol ether (Thesit) were introduced to the BGE. Surfactants had to be applied above their respective critical micellar concentration (CMC) to show the desired effect on virus electrophoresis [51]. Depending on the choice of the detergent applied to the BGE, native virions as well as subviral 80S particles or even viral proteins and the virus RNA genome were accessible for CE. Figure 16, A displays an

electropherogram of native 150S viral particles in CE obtained after application of 10 mM SDS to the BGE. DMSO was included in samples as EOF marker. The peak obtained for native 150S particles shows an UV absorption maximum at 260 nm because of encapsulated RNA within the virion (figure 16, B). Under such BGE conditions (100 mM boric acid, adjusted to pH 8.3 including 10 mM SDS) determination of concentration and purity of virus preparations via comparison to a standard electropherogram is possible and carried out routinely in our laboratory.

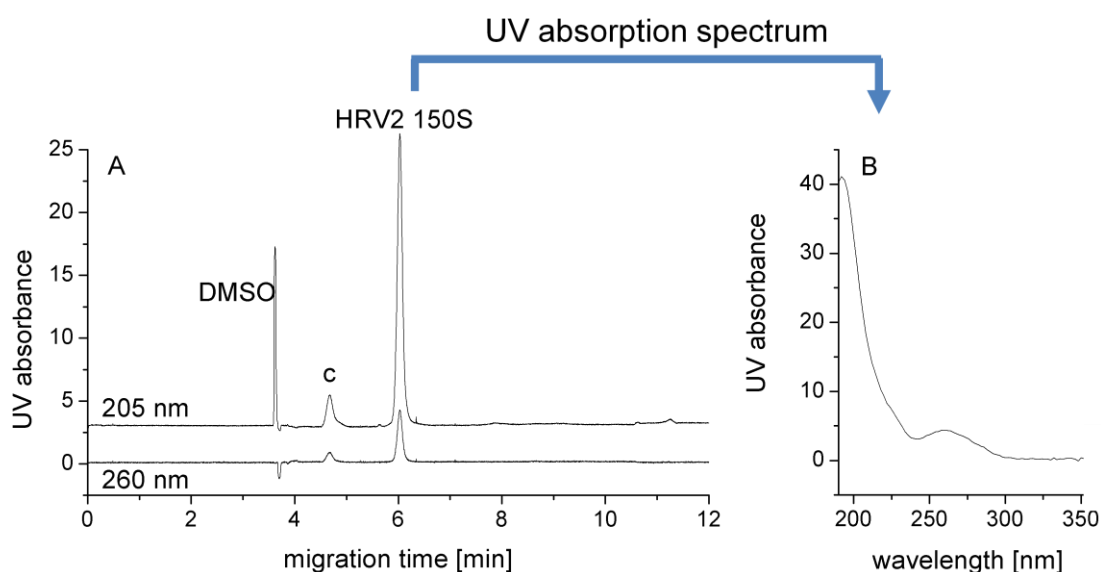


Fig. 16: Virus analysis on an Agilent 3D CE (A). The HRV2 stock solution valued 4.7 mg/mL; Sample preparation: 1:20 dilution of virus and  $1:4 \times 10^3$  dilution of DMSO in BGE; BGE: 100 mM sodium borate, pH 8.3, 10 mM SDS; CE at + 25 kV, 20°C, injection at 50 mbar x 9 sec, detection at 200/205/260 nm, BW 10 nm; Capillary: fused silica, 50  $\mu$ m inner diameter, 375  $\mu$ m outer diameter,  $L_{tot} / L_{eff} = 60.0 / 51.5$  cm. Native 150S particles exhibit an UV absorption maximum at 260 nm (B)

Heat denaturation of such virus samples (10 min heating to 56°C in SDS containing BGE) leads to disintegration of viral capsids. Instead of one peak for 150S particles four peaks corresponding to viral proteins and one peak corresponding to the viral RNA (again UV absorption maximum at 260 nm) are obtained. Figure 17 displays a respective electropherogram.

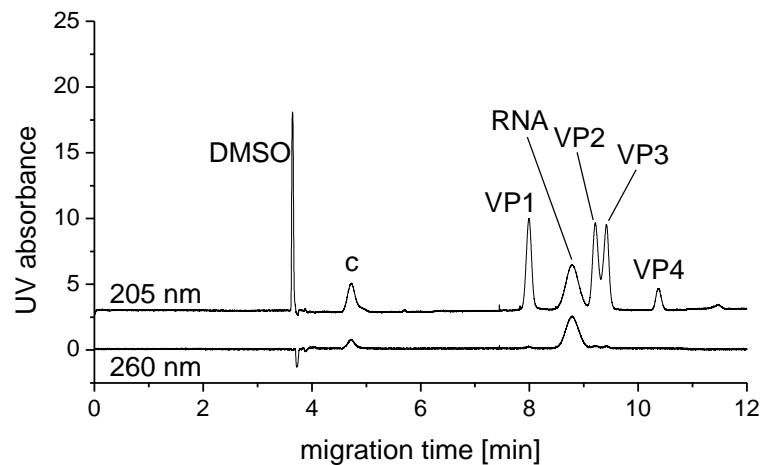


Fig. 17: CE as with figure 16; Sample was heated for 10 min to 56°C prior to analysis.

Substitution of SDS with Thesit no longer permits electrophoretic separation of native virions and a contaminant of the virus preparation (figure 18). However, heat denaturation and CE of corresponding virus samples now allow for analysis of subviral B particles sedimenting at 80S instead of VPs (figure 19). Therefore, the choice of detergents and sample pre-treatment allows for specific targeting of several species of the virus uncoating process. Subviral A particles sedimenting at 135S were only reported once in CE so far [52] and could until now not be reproducibly targeted.

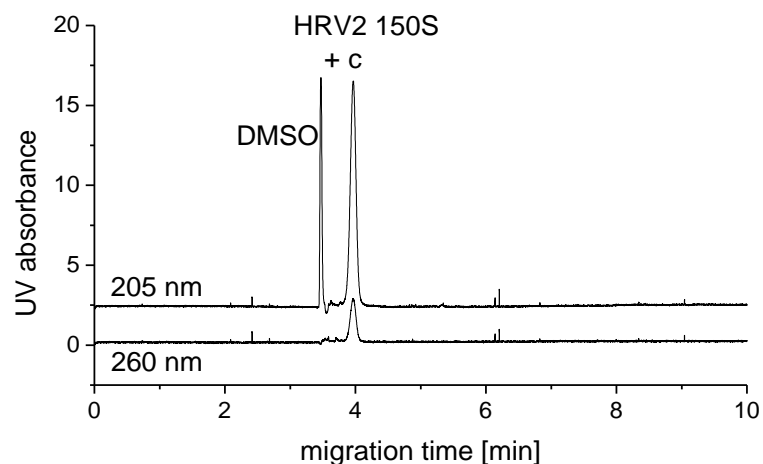


Fig. 18: Virus analysis on an Agilent 3D CE. HRV2 stock solution as with figure 16; Sample preparation: 1:20 dilution of virus and  $1:4 \times 10^3$  dilution of DMSO in BGE not including any detergents; BGE: 100 mM sodium borate, pH 8.3, 10 mM Thesit; CE as with figure 16; Capillary: fused silica, 50  $\mu$ m inner diameter, 375  $\mu$ m outer diameter,  $L_{tot} / L_{eff} = 60.2 / 51.8$  cm

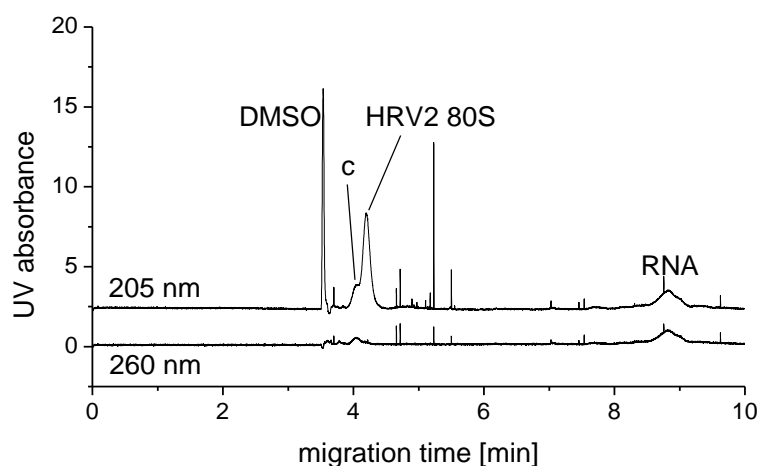


Fig. 19: CE as with figure 18; Sample was heated for 10 min to 56°C prior to analysis.

Upon application of the described CE conditions reaction of viral as well as subviral particles to recombinant soluble receptors, antibodies and antibody fragments was reported [53 – 58]. Also the kinetics of thermal denaturation in the presence or absence of antiviral compounds (WIN) was accessible for analysis [52]. Postcolumn infectivity assays enabled the differentiation of HRV serotypes [59]. To allow for more sensitive virus detection, also FL labeling was introduced. In principle two possible approaches of FL labeling of virions exist: (i) FL modification of the proteinaceous capsid or (ii) labeling of the encapsulated viral RNA genome [60 – 62]. Although labeling of the encapsulated genome promised to offer the great advantage of unmodified capsids yet still FL viral particles and thus to allow for sterical unhindered reactions of virions with receptor molecules upon cell infection experiments, only few dye molecules could be attached to the RNA. Therefore, only low FL signals were obtained. Furthermore, dye molecules did not covalently attach to the RNA but probably intercalated to double stranded regions of the virus genome. Upon RNA release and unfolding, FL dye molecules therefore detached from their target, no longer allowing for FL tracking of the viral genome. Thus, for most experiments FL modification of the viral capsid was chosen instead to enhance virus detectability in CE. A corresponding electropherogram for FITC ( $\lambda_{\text{ex}} / \lambda_{\text{em}}$  at 488 / 518 nm) modified HRV2 is presented in figure 20. A contaminant of the virus preparation was as well heavily labeled with the amine reactive dye, yielding a FL peak even larger than that of the labeled virus particle. Also, unreacted dye molecules could not be completely removed from samples by application of column size exclusion chromatography (SEC) as demonstrated below. Furthermore, SEC led to quite high sample dilution. Finally, covalent modification of

primary amines of the proteinaceous virus capsid (mainly of VP1) limited the ability of modified virions for receptor attachment (modified amines of VP1 lay most probably at the starshaped dome of the capsid where receptor binding takes place). Nevertheless, some of the virus receptor binding properties were maintained. Therefore, virions still exhibited infectivity albeit at much lower levels than unmodified viruses. Despite all these drawbacks, FL modification of HRV capsids is widely employed for improvement of virus detectability in CE.

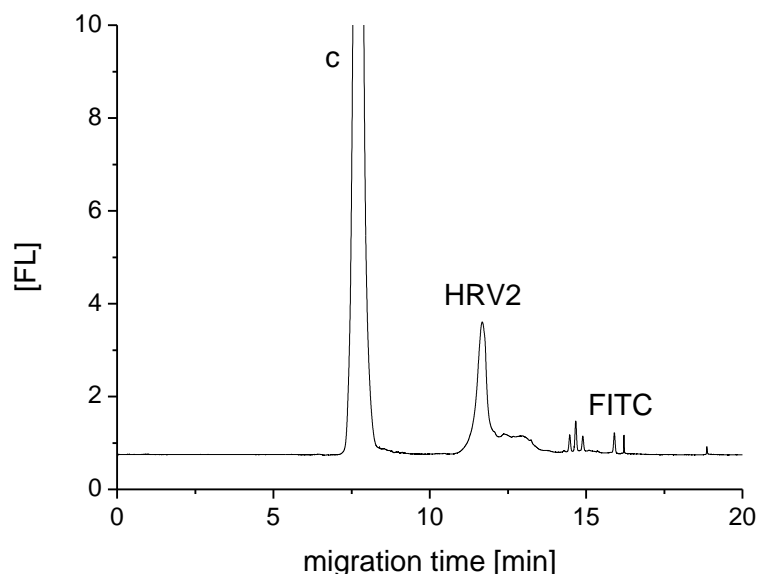


Fig. 20: CE of FITC labeled HRV2 after SEC. Sample was applied undiluted after SEC with 50 mM sodium borate, pH 8.3 as elution buffer; BGE: 100 mM sodium borate, pH 8.3, 10 mM SDS; Capillary: fused silica, 75  $\mu\text{m}$  inner diameter,  $L_{\text{tot}} = 73.0$  cm,  $L_{\text{UV}} = 23.5$  cm,  $L_{\text{FL}} = 58.0$  cm; CE at 20°C, + 20 kV ( $\sim 27$  kV/m), 200/260 nm UV detection, FL detection with external FL detector from Picometrics (Ramonville, France) equipped with a red argon laser ( $\lambda_{\text{ex}} = 488$  nm) from Spectra-Physics (Mountain View, USA), 25 mbar x 10 sec injection

Lately, FL modification of the viral capsid via the amine reactive probe Cy5 ( $\lambda_{\text{ex}} / \lambda_{\text{em}}$  at 649 / 670 nm) was reported [1, 2] to allow for chip electrophoresis of virus samples employing the commercially available Agilent Bioanalyzer system.

## 2.3.2 Electrophoresis of HRV2 on the Agilent 2100 Bioanalyzer System

In the course of our previous research we extended the applicability of Agilent 2100 Bioanalyzer to another type of analytes – viruses and subviral particles [1, 2]. In order to do so, the script of the instrument, originally intended for DNA analysis, was adapted to our needs. The following changes were implemented:

- (i) **Change in polarity:** According to CE data (refer to 2.3.1), we decided to opt for 100 mM boric acid adjusted to pH 8.3 via sodium hydroxide and including the detergent SDS as BGE. Under these conditions, we experienced EOF values comparable to CE. However, since chip DNA analysis was developed with a polymer containing sieving matrix with highly reduced EOF we had to change the polarity of all electrophoretic steps on the chip, i.e. sample injection to the separation channel and electrophoretic sample analysis. In the end, we opted for 1300 V potential for sample injection and 800 V (approx. 19 kV/m) potential for electrophoretic sample analysis, both applied in positive polarity, i.e. lower potentials were set for the respective outlet than for the respective inlet wells.
  
- (ii) **Setup of the instrument optics:** Changing the BGE to sodium borate, pH 8.3, including SDS as surfactant had also a significant impact on the optical adjustment of the instrument. Normal polymer containing BGE for DNA analysis includes a FL dye as well, in order to stain DNA in the course of electrophoresis on the chip. Under these conditions adjustment of the instrument optics to the detection window of the separation channel filled with a FL BGE is possible. Omitting the FL dye in the BGE causes severe problems in the system setup process. Therefore, we included some modifications in our script allowing for flushing of the separation channel with Cy5 containing BGE prior to setup of the instrument optics. After setup of the optics was complete, we again removed the dye electrophoretically from the separation channel. With this setup we could sustain the high detection sensitivity upon chip electrophoresis and could greatly improve the baseline stability during analyses.

- (iii) Further changes affected chip handling and sample preparation: DNA chips were filled with 12.0  $\mu\text{L}$  BGE on the Priming Station (20 s, upper syringe clip position, position C of the base plate) from the BGE outlet well. Twelve  $\mu\text{L}$  of Cy5 containing sample buffer (62.5 nM dye concentration) were applied to the ladder well for adjustment of the instrument optics and 12.0  $\mu\text{L}$  BGE to the remaining two wells marked 'G'. Six  $\mu\text{L}$  of the samples were applied to the remaining wells. After the run, electrodes were cleaned with the Electrode Cleaning Chip (filled with 380  $\mu\text{L}$  doubly distilled water). Samples consisted of prestained FL analytes. Cy5 ( $\lambda_{\text{ex}} / \lambda_{\text{em}}$  at 649 / 670 nm) was employed for analyte modifications.

After implementation of our modifications we were able to run Cy5-labeled virus samples on DNA chips. Modification of the SDS content of the BGE allowed for separation of all sample constituents: labeled HRV2, free dye molecules, which had not been completely removed from samples via SEC and a contaminant of the virus preparation which was as well heavily modified by the amine reactive probe Cy5. Resulting electropherograms taken from [2] are depicted in figure 21.

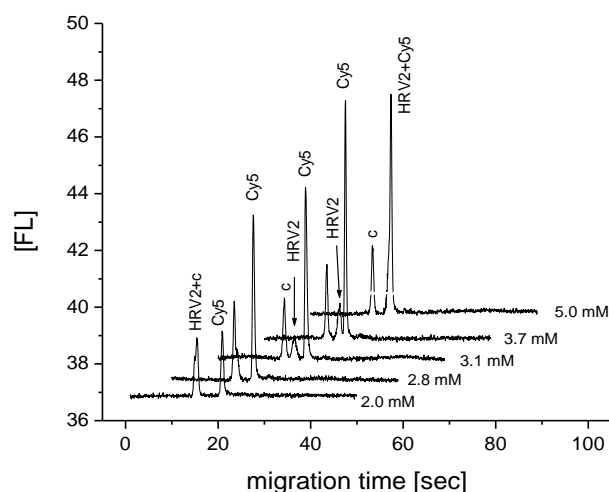


Fig. 21: Electropherograms of Cy5-labeled HRV2 containing samples. BGE was 100 mM sodium borate (pH 8.3) containing SDS at indicated concentrations between 2.0 and 5.0 mM. Samples were analyzed after SEC purification and 1:15 dilution in BGE. Intentionally, a SEC fraction that still contained free dye molecules was employed for analysis. Separations were carried out at 800 V (approx. 19 kV/m), the FL signal was recorded at  $\lambda_{\text{ex}}/\lambda_{\text{em}}$  630/680 nm. c, contaminant. Image taken from [2].

Plotting of the selectivity coefficient between the three sample constituents against the SDS concentration of the BGE (figure 22, taken from [2]) demonstrates that at 3.1 mM SDS concentration baseline separation of the analytes was achieved. A resulting electropherogram can be found in figure 23.

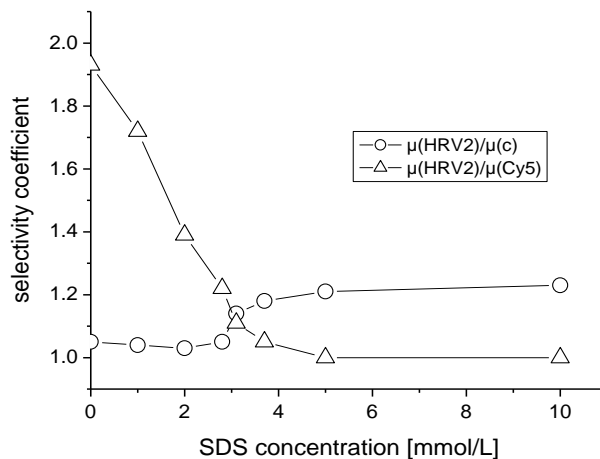


Fig. 22: Selectivity coefficients, i.e. ratio of the total electrophoretic mobilities  $\mu$  between labeled HRV2, Cy5 and the contaminant, c, respectively, as a function of the SDS content of the BGE. Image taken from [2]

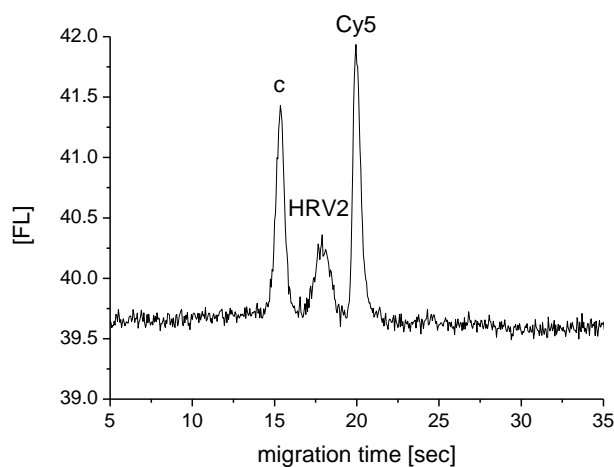


Fig. 23: Electropherogram of Cy5-labeled HRV2, an equally labeled contaminant of the virus preparation and free dye molecules. At 3.1 mM SDS concentration in the BGE, baseline separation of all sample constituents was accomplished. Other chip electrophoresis conditions as with figure 21.

Upon application of our adapted script and with 100 mM sodium borate, pH 8.3 including 3.1 mM SDS as BGE, we were able to assess several analytical questions via chip electrophoresis – peak identification reactions via virus degradation to proteins and RNA followed by proteolytic digestion of proteins, receptor binding experiments with several soluble recombinant receptor fragments derived from the VLDLR as well as temperature



dependant time curves of virus denaturation. However, most interesting for our further scheduled analyses was the fact, that electrophoresis in the chip format allowed for virus analysis in the complete absence of detergents. CE of viruses or subviral particles only yielded reproducible results upon application of surfactants above their critical micellar concentration (CMC) in the capillary format (refer to 2.3.1). Therefore, we were surprised by our chip electrophoretic finding, which we related to the short migration distance of virions on chips when compared to the capillary format. A corresponding electropherogram obtained via chip electrophoresis in the absence of detergents can be found in figure 24 (taken from [1]).

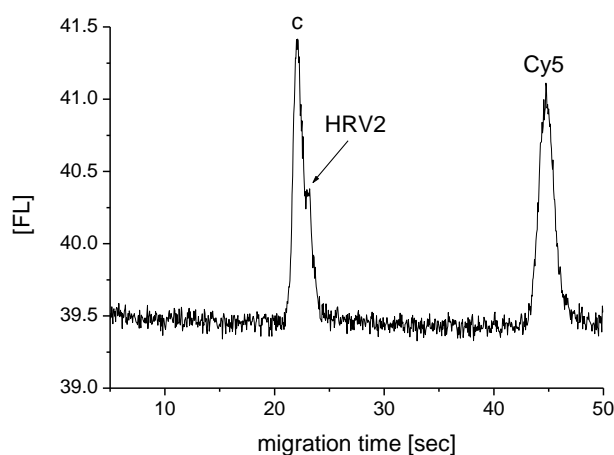


Fig. 24: Electropherogram of Cy5-labeled HRV2, an equally labeled contaminant of the virus preparation and free dye molecules. Upon application of BGE without any detergents labeled HRV2 and the contaminant were comigrating. However, although no baseline separation between sample constituents was accomplished, still electrophoresis in the absence of any surfactants was possible, a very important prerequisite for the analysis of liposomes in our chip electrophoretic system. Other chip electrophoresis conditions as with figure 21. Image taken from [1].

Although no separation between labeled virus and the equally modified contaminant was possible without application of detergents, absence of detergents was a very important prerequisite for the extension of our electrophoretic system to questions concerning virus binding to membranes in the course of cell infection. However, instead of working with living cells, we opted for liposomes as model membranes to mimic the *in vivo* situation. Liposomes are not stable in the presence of detergents. Therefore, receptor mediated attachment of virions to model membranes could previously only be investigated indirectly in CE, i.e. via the disappearance of corresponding peaks (refer to 2.3.3). We suggested that electrophoresis in the chip format would allow for tracing of all constituents of such binding experiments.

### 2.3.3 Capillary Electrophoresis of Liposomes [63, 64]

Liposomes in electrically driven capillary separation methods are mostly employed as part of the separation system itself. Application of liposomes as pseudostationary phase in CE (liposome electrokinetic chromatography, LEKC) constituted an advancement of micellar electrokinetic chromatography (MEKC) introduced by Terabe et al. [65, 66] employing detergents. In LEKC, liposomes are dispersed in the BGE to assess interactions of analytes with membranes mimicking the interaction with living cells. This allowed for instance the development of a model for human drug absorption via the transcellular passive transport route. A variant of LEKC employed only partial filling of a coated capillary with a liposome containing solution [67]. Due to low EOF values and application of uncharged lipids for liposome preparation a non-moving, liposome containing plug was generated through which analytes had to pass in the course of their migration. Alteration of analyte mobility was a result of interaction with lipid vesicles.

In capillary electrochromatography (CEC), liposomes are immobilized as coating on the capillary silica surface and thus employed as stationary phase comparable to LC. Again separation of analytes is based on different partition between the liquid bulk and the stationary liposome phase. Capillary coatings with phospholipids are described as semi-permanent, which implies that, although no liposomes have to be present in the BGE during a run, often coatings have to be regenerated after analysis.

A series of papers also concentrated on liposomes as analytes in CE. The main interest lay in the stability of liposomes and leakage of encapsulated drugs as well as in the homogeneity of liposome formulations concerning their size and mobility. Bilek et al. [68, 69] employed liposomes functionalized for protein binding via implantation of an anchor lipid containing a nitrilotriacetate acid group for complexation of  $\text{Ni}^{2+}$ . His6-tagged proteins were employed for attachment to  $\text{Ni}^{2+}$  on the liposome surface. Such, binding of HRV2 to receptor decorated liposomes could be followed. However, since analysis of HRV2 in the capillary format requires the application of detergents in the BGE (refer to 2.3.1) but since liposome analysis in CE on the other hand also precludes the application of surfactants, resulting adducts were not resolved as CE peak but deduced from the appearance of spikes upon complex formation. Nevertheless, these publications demonstrate the basic principles underlying the work presented in the course of this thesis.

# 3 Results and Discussion

Interaction of human Rhinovirus with cells during early virus infection can be structured into several steps reaching from the receptor mediated endocytosis of virions into host cells to the transfer of viral RNA from the inside of late endosomes through the endosomal membrane to the cytosol of the respective cell (see chapter 2.1). Part of the research in our laboratory concentrates on the development of an *in vitro* system allowing for the discrete targeting of each of these early infection steps employing serotype 2 of HRV as representative. Instead of working with cells, we opted for liposomes as vesicles since they offer the possibility of a well characterized model membrane in terms of lipid composition as well as particle size. For similar reasons we replaced native receptor molecules with recombinant receptor fragments bound via His6-tags to Ni<sup>2+</sup>-ions embedded on the liposome surface. In continuation of previous work (see chapter 2.3) I opted for electrophoresis, both in the capillary as well as in the chip format, to target our analytical questions. My electrophoretic results were further supported by transmission electron microscopy (TEM).

Figure 25 outlines the early steps of the infection pathway of HRV2. Electrophoresis of viral 150S (i in figure 25) as well as subviral 80S particles has already been published extensively (see chapters 2.3.1 – 2.3.2), however, electrophoresis of subviral 135S particles has only been seldomly described. Therefore, the first part of this chapter will be dedicated to findings concerning this latter subviral particle. Receptor mediated attachment of virions to cell surfaces (ii in figure 25) comprises the first key step in virus infection and respective results will be discussed thereafter. Receptor bound virions are then internalized into cells via endocytosis (iii – iv in figure 25). Upon maturation, endosomes undergo changes in the pH of their aqueous interior from neutral to acidic values around pH 5.6. This acidification triggers a series of changes in internalized virions termed virus uncoating (v – vi in figure 25). In the course of this process, the viral RNA is shuttled from the inside of the virus capsid through assumed size selective pores in the endosomal membrane to the cytosol of the infected cell (see chapter 2.1). To investigate the process of pore formation an electrophoresis based leakage assay was developed that will be

described alongside its application in the evaluation of membrane disrupting abilities of HRV2 virions and viral proteins. Finally, viral RNA has entered the cytosol of the infected cell (vii in figure 25) and is ready for viral replication. To monitor the viral RNA transfer across a membrane, the employment of molecular beacons – short single stranded oligonucleotides, which bind specifically to corresponding nucleotide sequences of the viral RNA, thus yielding a fluorescence signal, was suggested. Upon encapsulation of beacons in liposomes inverse endosomes were created, which were intended to follow the viral genome transfer from a position outside of a membrane to the aqueous lumen of a liposomal vesicle. Initial experiments demonstrated comparability of this inverse direction of RNA transfer to the *in vivo* situation. First results in method development for the setup of such inverse endosomes will be presented at the end of this chapter.

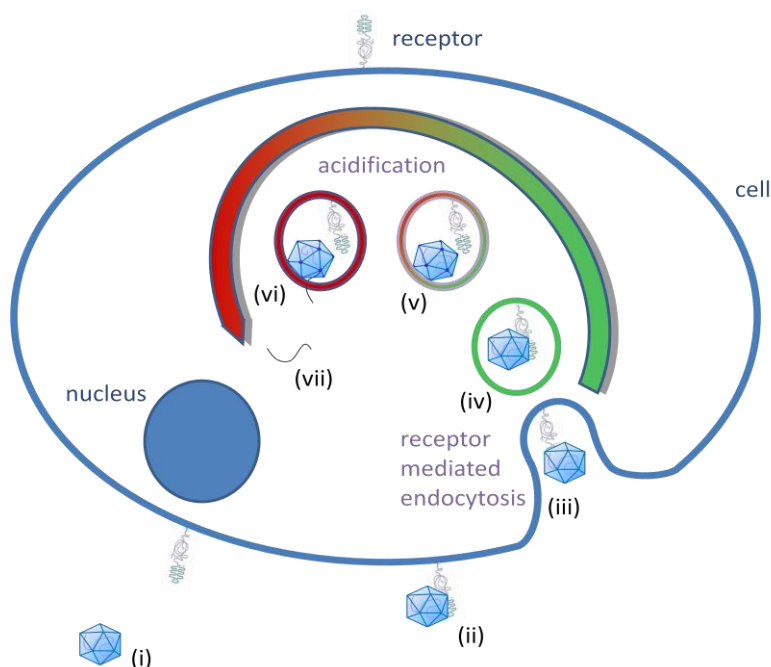


Fig. 25: Interaction of HRV2 virions with cells: free HRV2 (i); HRV2 bound to receptor molecules of the VLDL receptor family on the cell surface (ii); internalization of receptor bound virions (iii); HRV2 in early endosomes (iv); acidification of endosomes triggers virus uncoating (v) which finally leads to the transfer of viral RNA through the plasma membrane (vi) into the cytosol of the infected cell (vii).

Some data presented below, especially resulting publications, were obtained in close cooperation with other authors. Therefore, at the beginning of each subchapter the state of publication as well as the amount of experimental contribution of respective authors to the corresponding publication will be detailed.

### 3.1 Capillary Electrophoresis of Subviral 135S Particles

Publication: Capillary Electrophoresis of 135S Particles of Human Rhinovirus Serotype 2

State of publication: under preparation

Experimental contributing authors:	Victor U. Weiss – 55%
	Gerhard Bilek – 15%
	Angela Pickl-Herk – 25%
	Irene Goesler – 5%

Virions from human Rhinovirus serotype 2 (HRV2) convert in the course of their cell infection from particles sedimenting at 150S to particles sedimenting at 80S (subviral B-particles). 80S particles lack viral protein number 4 (VP4), the innermost capsid protein, and the viral RNA genome. An intermediate of this conversion, a particle including the viral RNA but already lacking VP4 and sedimenting at 135S is also known and termed subviral A-particle. CE of 135S particles was so far only reported once [52]. We report here: (i) A reproducible way of 135S particle preparation; moreover, we could demonstrate the dependence of 135S particle formation on the dilution of the virus stock solution. (ii) We were also able to estimate the stability of 135S particles in free solution. (iii) We confirmed the identity of our obtained subviral species by several means: Electrophoretic mobility, UV-absorption spectra, sucrose density gradient centrifugation, immunaffinity reaction and size exclusion chromatography (SEC). Transmission electron microscopy (TEM) imaging of virions at different stages of virus conversion additionally confirms our CE findings. In such a way, we could clearly distinguish between viral 150S and subviral 135S and 80S particles. (iv) We were able to trace the conversion of 135S to 80S particles after application of additional triggers of virus conversion. Therefore, we could demonstrate that subviral 135S particles are no end points or aborted particles of virus infection but intermediates of the virus uncoating process. The accessibility of subviral 135S particles offers the possibility to target this intermediate of virus uncoating specifically. Thus it is of great importance for further understanding of the viral infection pathway and for elucidating structural intermediates of virus uncoating.

## Analysis of viral 150S and subviral 80S particles

Virus analysis via CE in Thesit containing buffer is known to yield just one peak from two unresolved sample constituents – a contaminant from the virus preparation and the virus itself (see chapter 2.3.1). After heating of such a sample for 10 min to 56.0°C, viral 150S particles are completely converted to subviral 80S particles, lacking VP4 as well as the viral RNA genome [47]. Both species, the intact viral 150S and the subviral 80S particle, migrate similarly in CE, however, they can be sufficiently distinguished via their electrophoretic mobility. For viral 150S particles the electrophoretic net mobility values  $5.7 \times 10^{-9} \text{ m}^2/\text{Vs}$ , for 80S particles  $8.5 \times 10^{-9} \text{ m}^2/\text{Vs}$  [51]. In contrast to 80S particles, intact virions show UV absorption at 260 nm resulting from still encapsulated viral RNA [52].

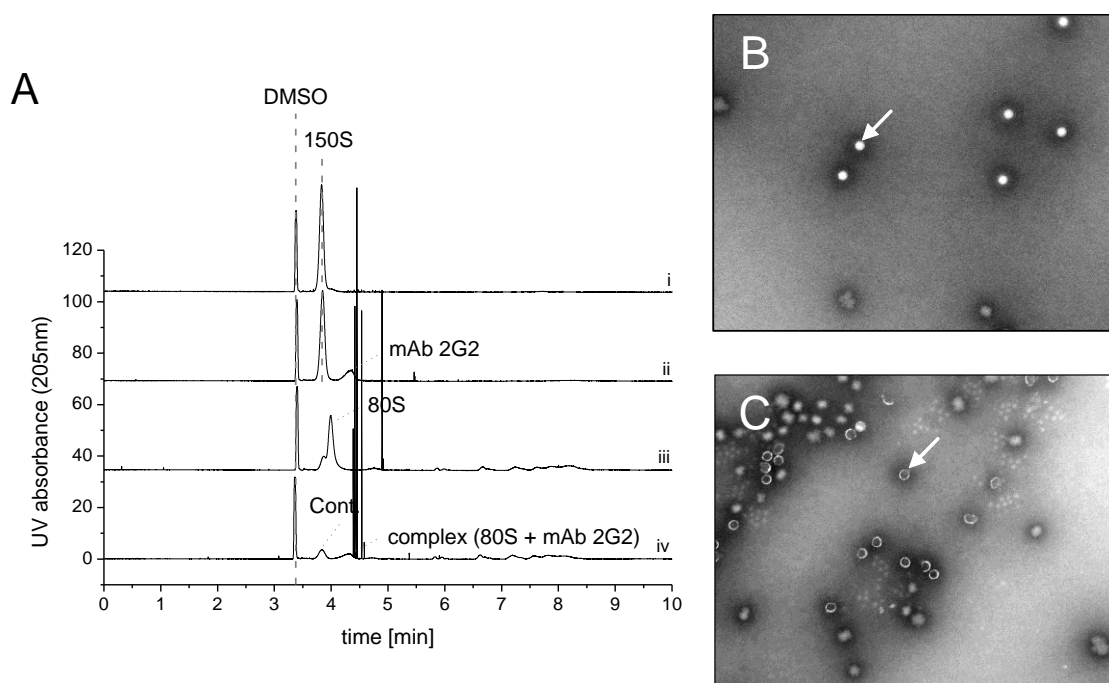


Fig. 26: Analysis of viral 150S and subviral 80S particles. (A): CE of HRV2 150S (i) and 80S (iii) particles and electropherograms obtained upon mixing of virions with monoclonal antibody 2G2 (mAb 2G2) (ii 150S + 2G2; iv 80S + 2G2). Subviral 80S particles react with the antibody in contrast to 150S particles. Additionally, 150S and 80S particles can be differentiated visually as seen from TEM image of 150S particles (B) and TEM image of 80S particles (C). Native virions appear as bright dots, 80S particles as dark areas of uniform density surrounded by bright coronas. Due to pores in the viral capsid (80S particles lack viral protein 4) and the missing viral RNA genome, subviral 80S particles allow readily for negative stain penetration. For CE, the applied field strength valued approx. 42 kV/m at 20.0°C with sodium borate (100 mM boric acid, pH 8.3) containing 10 mM Thesit as BGE. The sample buffer (SB) did not contain any detergents. Capillary: fused silica, 50  $\mu\text{m}$  inner diameter,  $L_{\text{tot}} / L_{\text{eff}} = 60.0 / 51.5 \text{ cm}$ . TEM images were

obtained with phospho-tungsten acid pH 7.3 as contrast medium on glow discharged carbon coated copper grids. Images were taken at a  $8.9 \times 10^4$  fold magnification.

Figure 26 A depicts electropherograms for an HRV2 sample run in Thesit containing BGE. Before heating, virus and contaminant are comigrating (i). However, after thermal denaturation the peak for the subviral 80S particle is partially resolved from the contaminant peak as described above (iii). Viral 150S particles do not react with mAb 2G2 ([57]and ii), whereas subviral 80S particles do (iv). The appearance of spikes after monoclonal antibody addition, demonstrates the precipitating ability of mAb 2G2 for empty viral capsids. We further visualized viral 150S and subviral 80S particles via TEM. Viral 150S particles (figure 26 B) appear as bright dots upon TEM imaging since negative stain cannot penetrate the proteinaceous viral capsid. Subviral 80S particles (figure 26 C), however, have lost VP4 as well as the RNA genome. Upon viral uncoating, pores open at fivefold axes on the capsid surface that allow for negative stain penetration. Therefore, subviral 80S particles show a core of high density surrounded by a bright circle. Cloud shaped particles upon imaging of viral 150S and subviral 80S particles most probably result from denatured virions during the staining process.

The release of RNA from inside of the viral capsid constitutes the critical step of cell infection. Subviral 135S particles are therefore an important intermediate of HRV2 uncoating. Although virions have already started to convert by release of VP4, they still include the viral genome. Therefore, 135S particles allow for investigation of direct mechanisms of RNA release. Subviral 135S particles have been recorded once during CE analysis [52]. However, we could greatly improve the reproducibility of the described formation protocol. We found the formation of 135S particles of HRV2 depending on the dilution of the virus stock solution prior to heat denaturation (10 min heating of virus solution to 56.0°C). We opted for heat denaturation instead of sample acidification in order to minimize matrix effects and additional sample dilution during virus uncoating. First experiments with sample acidification yielded comparable results to the heat denaturation setup (data not shown). Low diluted virus stock solutions mainly yielded 135S particles, whereas higher dilution mainly led to the formation of 80S particles upon virus uncoating. In such a way, conversion of native 150S particles could be directed to either of the two subviral species.

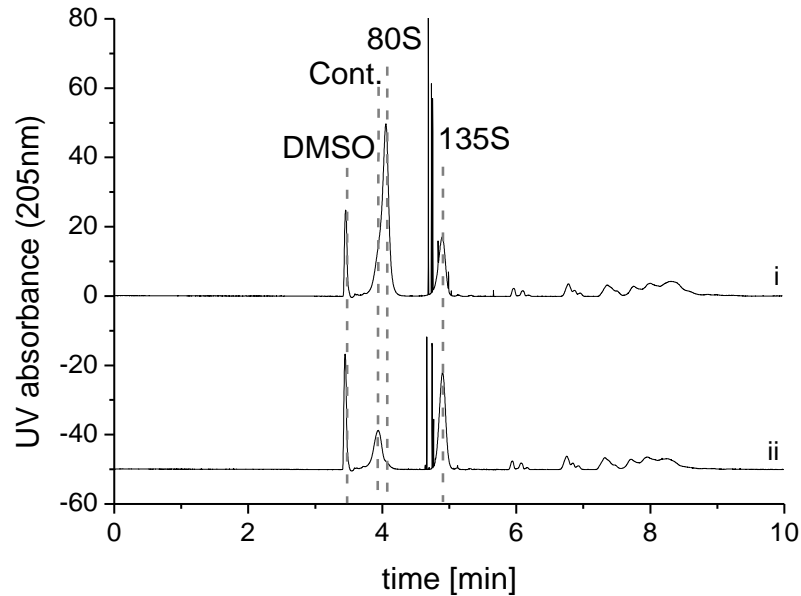


Fig. 27: Electropherograms obtained for HRV2 samples upon heat denaturation (10 min at 56.0°C) at different virus concentrations. At 2.0 mg/mL (1:2 dilution of virus stock) favourably 80S particles are formed (i), whereas at 3.0 mg/mL (3:4 dilution of virus stock) mostly subviral 135S particles can be found (ii). HRV2 was diluted to indicated concentration values in SB prior to heat denaturation. After heating the sample volume was adjusted with SB and intermediate DMSO solution to a final dilution of 1 : 10 for HRV2 and 1 :  $4 \times 10^3$  for DMSO. CE conditions as with figure 26.

Figure 27 shows two sample electropherograms obtained for heat denaturation at different virus concentrations. Whereas heat denaturation of a 2.0 mg/mL HRV2 sample (1:2 dilution of virus stock) preferentially yielded subviral 80S particles migrating with  $8.5 \times 10^{-9} \text{ m}^2/\text{Vs}$  (i), at 3.0 mg/mL HRV2 concentration (3:4 dilution of virus stock) a peak with a migration time of about 4.8 min corresponding to a net mobility of  $17.8 \times 10^{-9} \text{ m}^2/\text{Vs}$  prevailed (ii). A peak with the latter mobility neither corresponds to viral 150S nor subviral 80S particles and was thus suggested to be related to subviral 135S particles. Furthermore, an UV absorption maximum at 260 nm (data not shown) supports our peak identification. Such maxima are only obtained for RNA containing viral species [52]. Spikes recorded at approximately 4.6 min migration time probably result from aggregating hydrophobic subviral particles and / or VP4 molecules in free solution. In a next step we evaluated the applicability of our findings to other HRV2 preparations.



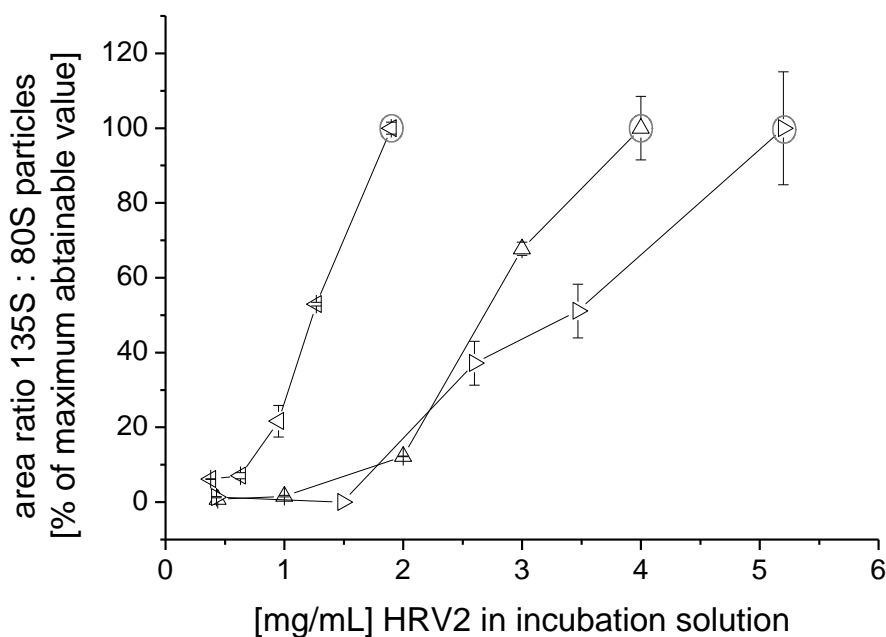


Fig. 28: Concentration dependence of subviral particle formation upon heat denaturation (10 min at 56.0°C) of viral 150S particles for three virus preparations. At low virus concentrations (up to approx. 1.0 mg/mL) mostly 80S particles are formed upon virus conversion, whereas high 135S particle concentrations are obtained for undiluted virus solutions (circled data points). Measurements were at least in duplicate. Data points were obtained by calculating area ratios of the 135S peak : (80S + contaminant) peak bundle. The value obtained for the highest virus concentration for each stock solution was set to 100%, all other ratios were related to respective maximum values.

Figure 28 depicts the dependence of subviral particle formation on the dilution of the virus stock upon heat denaturation. Three preparations with 1.9, 4.0 and 5.2 mg/mL virus concentration were investigated. For calculation of data points, the ratio of the area of the 135S peak to the area of the peak bundle (contaminant and subviral 80S particles) migrating at approximately 4 min runtime was calculated. The ratio obtained for the highest virus concentration for each of the three virus preparations was set to 100%. Ratios obtained for diluted incubation solutions during heat denaturation were then related to the 100% value. Measurements were carried out at least in duplicate for each data point.

It was observed that heat denaturation of undiluted HRV2 solutions always yielded highest amounts of subviral 135S particles. After slight dilution of virus stocks with SB prior to heat denaturation, a reduction of the obtained 135S particle peak was observed and more

80S particles were detected. Yet both subviral species were still found in parallel. However, after dilution of HRV2 stocks to approximately 1.0 mg/mL almost exclusively 80S particles were observed. Influence of the ionic strength of employed buffers on the preferential formation of subviral 80S particles upon heat denaturation of diluted virus stock solutions was negligible (data not shown). For other *picornaviridae* stabilization of virions is known after interaction with short fatty acids such as myristic acid, which is in fact also covalently bound to VP4 [70 – 72] or after interaction with other proteins, for example, albumin [73]. In the case of HRV2 initial experiments neither showed stabilization of subviral 135S particles upon virus pre-incubation with fatty acid suspensions – myristic, palmitic and stearic acid as most abundant fatty acids described as pocket factors with bovine enterovirus (BEV) [74] were tested – nor did the addition of bovine serum albumin (BSA) during heat denaturation increase the amount of obtained subviral 135S particles (data not shown). In fact, preincubation of virions with fatty acid suspensions prior to heat denaturation rather decreased the amount of obtained subviral 135S particles (figure 29).

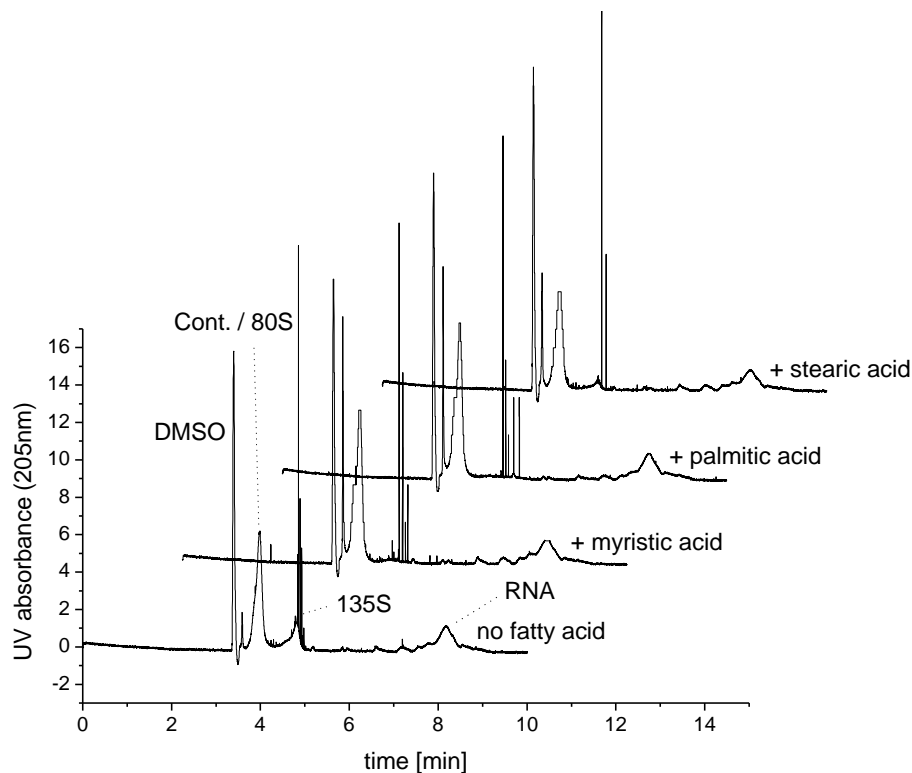


Fig. 29: Decrease in the amount of obtained 135S particles upon heat denaturation (10 min at 56.0°C) of virus solutions pre-incubated with fatty acid suspensions. All three fatty acids tested – myristic, palmitic and stearic acid – lead to a significant lower number of obtained subviral 135S particles than the control diluted in plain SB. HRV2 was diluted 1:2 in SB or SB / fatty acid

suspension and incubated for 1 hour on ice prior to heat denaturation. After virus conversion samples were further diluted with SB and DMSO to a final dilution of 1:15 for virus and  $1 : 4 \times 10^3$  for DMSO. CE conditions as with figure 26.

We therefore suggest that addition of fatty acids to virus solutions during heat denaturation hinders the interaction of viral capsids with other components of the incubation solution. In fact, we found that the contaminant of the virus preparation or rather the area ratio VP1 / contaminant, when analyzing samples in SDS containing BGE, was significant for the amount of obtained subviral 135S particles during heat denaturation. The lower the ratio VP1 / contaminant, the higher was the amount of obtained subviral 135S particles. The contaminant from virus preparations thus seems to stabilize 135S particles but could so far not be identified.

After conversion of native virions, subviral 135S particles remain stable after dilution to lower analyte concentrations for CE analysis in Thesit containing BGE. Even after one week storage of diluted samples at 4.0°C still approximately 80 % of the initial amount of 135S particles were found in solution (data not shown). This slow conversion of subviral 135S to 80S particles might be explained by accessibility of the viral RNA genome to RNases through pores in the 135S particle (missing VP4 capsid protein) or by simple RNA diffusion through such pores. However, our findings allow for preparation of subviral 135S particles of HRV2 at fairly high concentrations and stability, both criteria being important prerequisites for investigation of this virus uncoating intermediate via TEM, cryo TEM and X-Ray crystallography.

### **Identification of subviral 135S particles**

Several characteristics of subviral 135S particles besides their electrophoretic mobility and UV absorption can be employed for their identification:

(i) Originally, subviral 135S particles were defined via their sedimentation characteristic. Therefore, we subjected a sample containing viral as well as subviral particles to sedimentation in a 10 - 40 w/w% sucrose gradient. After collection of 20 fractions we

subjected samples to CE employing a Thesit containing BGE. Indeed, when we plotted the peak area ratio between the respective virus species and DMSO as internal standard, we found that our putative 135S particles sediment slower than viral 150S particles, i.e. were found in lower numbered fractions from sucrose gradient centrifugation (figure 30).

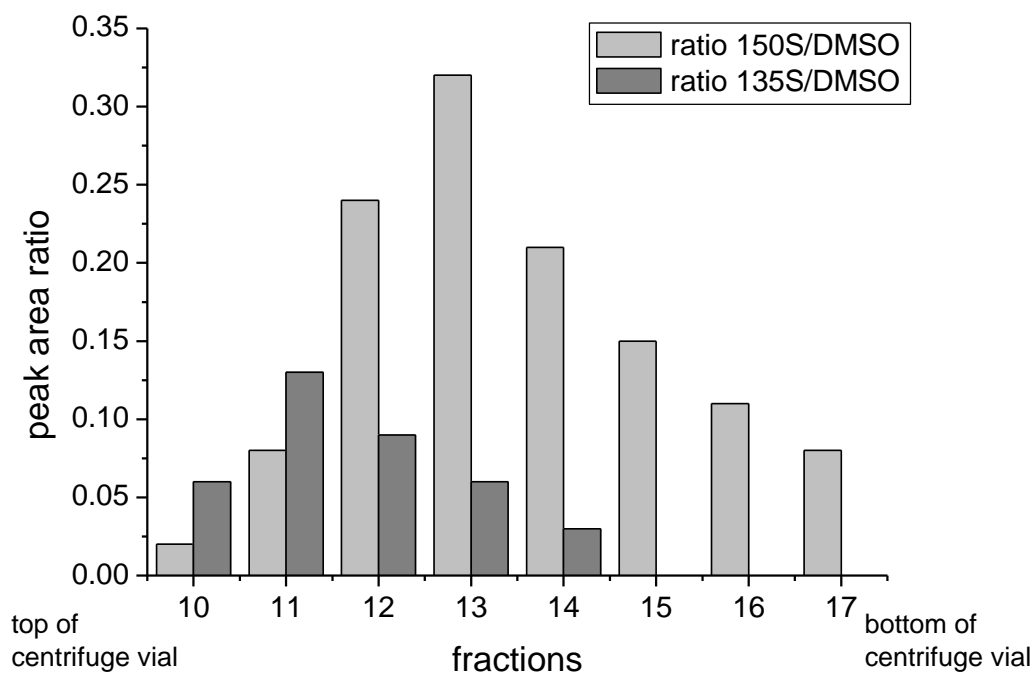


Fig. 30: Sedimentation of 150S viral and 135S subviral particles in a 10 - 40 w/w% sucrose gradient. Plotted are peak area ratios between the respective viral or subviral species and DMSO as internal standard. It is apparent that the apex for the 135S / DMSO curve can be found in fractions corresponding to higher positions in the vial (lower index in the figure) than the apex for the 150S / DMSO curve. This signifies that subviral 135S particles sediment slower than intact virions.

(ii) We suggested reactivity of monoclonal antibody 2G2 with 135S particles. Such an immunaffinity reaction had been shown to work with 80S particles but not with intact virions ([57] and Fig. 26). Figure 31 depicts the resulting electropherograms of 135S particle containing samples before and after addition of mAb 2G2. The respective peak at approximately 4.8 min disappeared from the electropherogram with a concomitant appearance of a large number of spikes from resulting aggregates between mAb 2G2 and subviral 135S particles which demonstrates mAb binding.

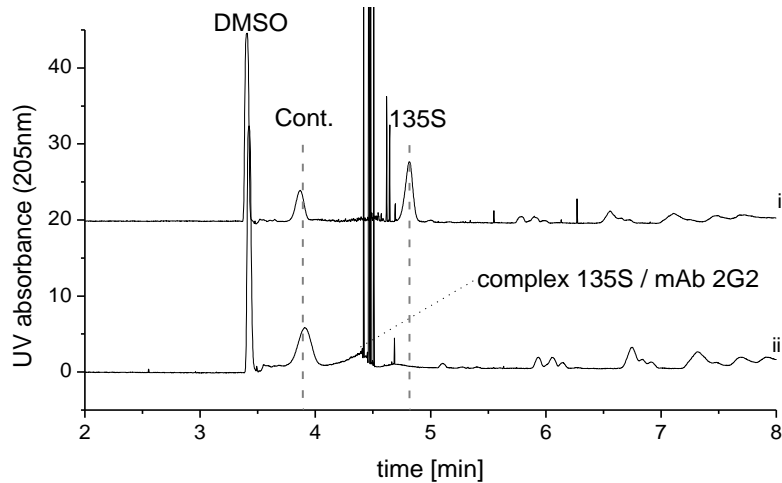


Fig. 31: CE of HRV2 subviral 135S particles (i) and an electropherogram obtained upon mixing of 135S particles with mAb 2G2 (ii). Incubation of subviral 135S particles with aggregating mAb 2G2 results in the disappearance of the peak obtained for 135S particles with the concomitant appearance of a large number of spikes (similar to mAb 2G2 precipitating subviral 80S particles). CE conditions as with figure 26.

(iii) SEC allows separation of low molecular mass material from large moieties like virions and subviral particles. When we applied a sample with putative subviral 135S particles to a spin SEC followed by CE analysis, we found the corresponding peak with the mobility of  $17.8 \times 10^{-9} \text{ m}^2/\text{Vs}$  (putative 135S particles) in the void volume (figure 32).

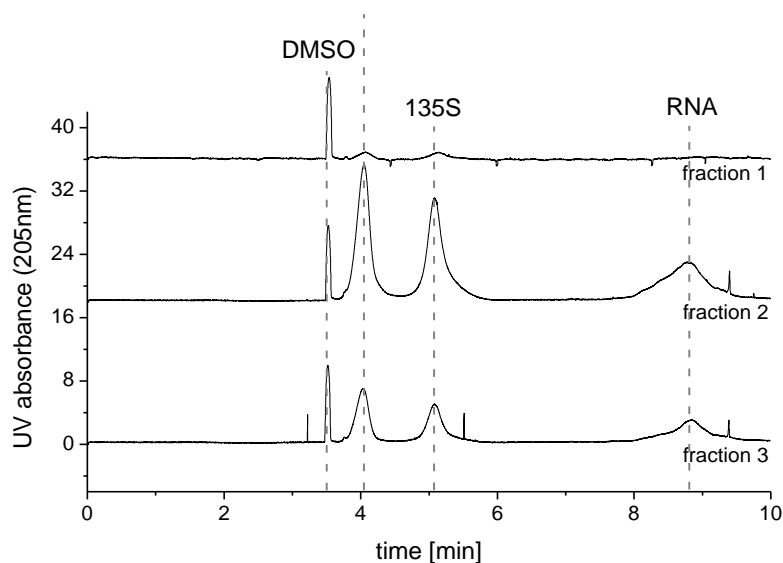


Fig. 32: CE results of spin SEC fractions (7.0  $\mu\text{L}$  fraction volume each). Fraction 2 comprised the main fraction for subviral particles. Coelution of putative 135S particles with other subviral

particles and the contaminant of the virus preparation was observed. Therefore, it was concluded that the peak recorded at approx. 5.1 min corresponded to the large biological assembly of a subviral particle. CE conditions as with figure 26.

Furthermore, coelution of putative 135S particles with 80S particles, released RNA and the contaminant of the virus preparation was observed, which allowed estimation of the size of the corresponding particle as comparable to other subviral species. It is of note that via SEC we could greatly diminish the level of spikes previously obtained for unpurified subviral 135S particle samples. Upon heating (10 min at 56.0°C) of the main 135S particle containing SEC fraction (number 2) and subsection to CE analysis in SDS containing BGE, we detected the absence of one of the four peaks related to viral proteins (figure 33). We thus reasoned this peak to correspond to VP4 which is missing in 135S particle samples. From the sum of our carried out experiments we could conclude that we were able to target subviral 135S particles specifically.

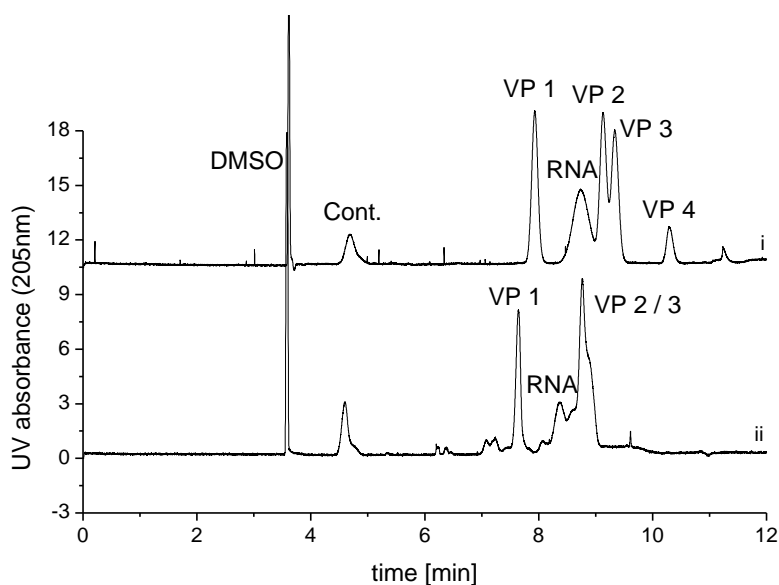


Fig. 33: Electropherograms of virus containing samples in SDS buffer before (i) and after (ii) 135S preparation and spin SEC. Heating (10 min at 56.0°C) of virus samples in SDS containing BGE before SEC yields 4 peaks for the viral proteins (VP 1 – 4) and a peak for the viral RNA. However, likewise treatment of virus samples after 135S preparation and SEC yields only 3 peaks of viral proteins, the peak for VP4 is missing. Furthermore, RNA is already slightly degraded resulting in several small underlying peaks. Different migration times between trace i and ii resulted from slightly varying EOF values. BGE included 10 mM SDS instead of Thesit, other CE conditions as with figure 26.

## Conversion of subviral 135S to 80S particles

Upon further heating of 135S particles to 56.0°C a gradual conversion of 135S to 80S subviral particles can be observed. Figure 34 depicts the resulting electropherograms of additional 4 min heating steps. Additional heating resulted in a decrease of the 135S particle peak with a concomitant increase of the peak for 80S particles. Also the appearance of spikes, which were recorded frequently for 135S particle samples, greatly diminished upon further heating. After 12 min of additional sample heating, subviral 135S particles almost quantitatively converted to 80S particles. Therefore, we could demonstrate that subviral 135S particles are no artificial end points or aborted particles in the course of virus infection, but can be further transformed to subviral 80S particles *in vitro*.

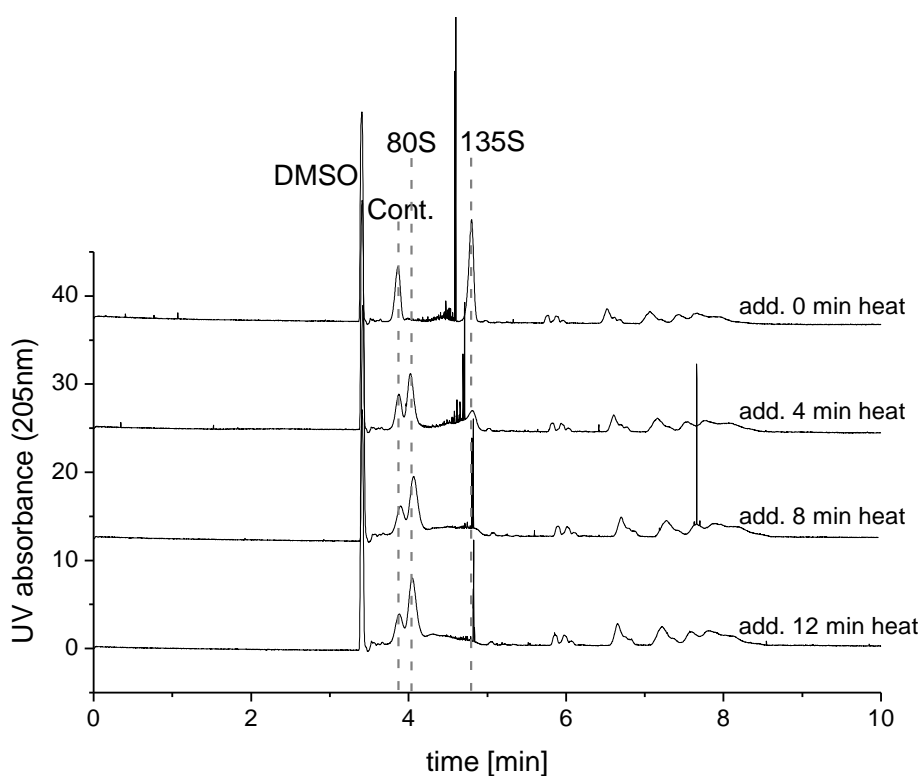


Fig. 34: Conversion of subviral 135S to 80S particles induced via additional sample heating to 56.0°C. Samples were analyzed after 4 min incubation steps at elevated temperature. Electropherograms obtained after additional heating steps are depicted from top to bottom. The peak obtained for the subviral 135S particles migrating at approximately 4.8 min disappears with the concomitant appearance of the peak for subviral 80S particles migrating at approximately 4.0 min. CE conditions as with figure 26.

### Negative stain TEM imaging of 135S particles

TEM imaging of subviral 135S particles showed intermediates of the virus uncoating process. Whereas viral 150S particles appear as bright dots of uniform density and subviral 80S particles as bright coronas with stained centers, 135S particles appear differently (figure 35). The interior of the virus capsid shows considerably more contrast than intact virions and is as well surrounded by a corona. The grainy texture of the interior of 135S particles is in good accordance with the theory of virus uncoating: Subviral 135S particles have lost already the innermost viral capsid protein but still include the RNA genome. Therefore, due to lacking VP4 and conformational change of the other viral proteins in the course of pore formation in the viral capsid, contrast medium of TEM imaging can access the virus interior. However, due to still encapsulated viral RNA, the stain cannot fill the complete interior of particles as for completely empty subviral 80S particles.

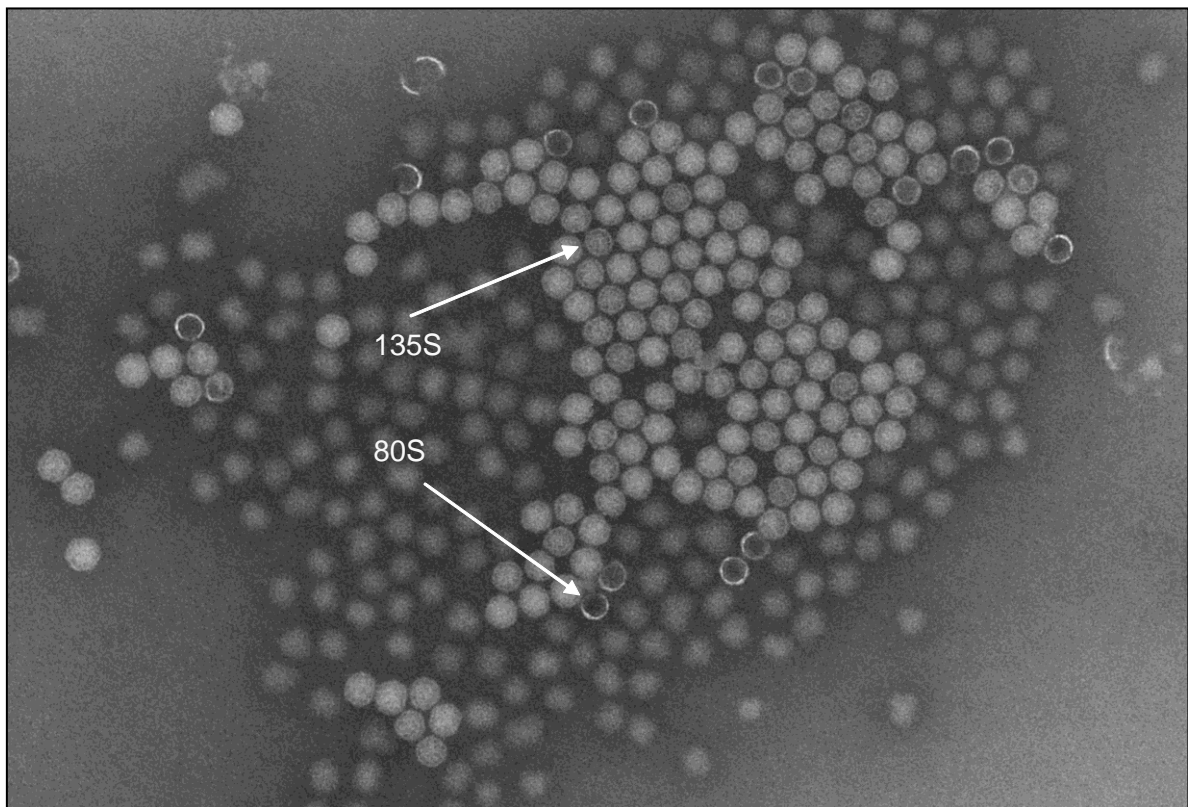


Fig. 35: TEM image of subviral 135S particles. The intact viral capsid of 150S particles does not allow for stain penetration into the virus lumen. Subviral 135S particles have expelled the innermost capsid protein VP4 and have undergone already structural changes of the virus capsid. Therefore, they are more accessible to stain than intact virions. However, subviral 135S particles are stained to a less extent than empty 80S capsids, which no longer encapsulate the viral RNA genome and allow therefore even better for stain penetration. TEM imaging as with figure 1.



## Conclusion

Conversion of native HRV2 virions sedimenting at 150S to subviral particles can be achieved *in vitro* either through acidification or through heat denaturation. For the latter we demonstrated the conversion to subviral 135S particles in detail. Depending on the dilution of virus stock uncoating intermediates can be targeted specifically: Heating of HRV2 samples of low virus content preferentially yields subviral 80S particles that have lost VP4 of the viral capsid as well as the viral genome. Heating of less diluted HRV2 samples allows for targeting of subviral 135S particles. Subviral 135S particles have lost already VP4 but still include the viral RNA genome. Through additional triggers of virus conversion we could demonstrate that subviral 135S particles are no artificial end points or aborted particles in the course of virus infection, but can be further transformed to subviral 80S particles. Additionally, we carried out several experiments for identification and confirmation of the 135S species besides CE analysis – UV absorption, sucrose density centrifugation, immunoaffinity reaction and spin SEC. Finally, we visualized this transitional step of virus uncoating via TEM. Specific targeting of subviral 135S particles as intermediates of the uncoating process is of importance for further understanding of the infection pathway. We describe the generation of a well defined starting material for structural elucidation techniques.

## Experimental Section

**Chemicals:** Boric acid (99.99%), sodium dodecyl sulphate (SDS of reagent plus grade), His-select® Nickel Affinity Gel (suspension in 30% ethanol / H<sub>2</sub>O), and the three fatty acids – myristic (99%), palmitic (99%) and stearic (98.5%) acid – were purchased from Sigma Aldrich (Steinheim, Germany). Fatty acids were suspended in SB at 21 mM via extensive vortexing and ultrasonication. Larger debris was removed via spinning (10sec at 100 rcf) on a table top centrifuge (model 5415D, Eppendorf, Hamburg, Germany). Sodium hydroxide (pellets pure) was from E. Merck (Darmstadt, Germany) and Sephadex G-50 (DNA grade) from Amersham Bioscience (Little Chalfont, England). Sucrose (D(+)-Saccharose) was from Carl Roth (Karlsruhe, Germany). Thesit (Polyethylene glycol dodecyl ether; membrane research grade) and DMSO (*p.a.*) were from Fluka (Buchs, Switzerland). A 1:200 dilution of DMSO in water was employed as intermediate DMSO stock. Phospho-tungsten acid, 2% in water, pH 7.3 was employed as negative stain for TEM imaging. Water was bidistilled from a quartz apparatus.

**Biological Material:** HRV2 was produced and its purity and concentration assessed as described [8, 46]. Three preparations in sodium borate (50 mM boric acid, *ad* pH 7.4 via sodium hydroxide) with

concentrations of approx. 1.9 mg/mL, 4.0 mg/mL and 5.2 mg/mL virus were employed. All three HRV2 preparations were used for recording of the concentration dependence of subviral particle formation upon heat denaturation. The HRV2 preparation with 1.9 mg/mL was employed as well for experiments concerning the influence of fatty acids on subviral 135S formation, the HRV2 preparation with 5.2 mg/mL for sucrose gradient separation. All other measurements were carried out with the 4.0 mg/mL HRV2 preparation. Monoclonal antibody 2G2 (mAb 2G2) was prepared in 50 mM Tris, pH 8.0 at a concentration of 9.0 mg/mL.

**Instrumentation:** CE analyses were carried out on two 3D CE instruments (Agilent, Waldbronn, Germany) in parallel. Fused silica capillaries (50  $\mu\text{m}$  inner diameter, 375  $\mu\text{m}$  outer diameter) were from Polymicro (Phoenix, USA), obtained via Optronis (Kehl, Germany). Both capillaries measured 60.0 cm in total with a respective effective length of 51.5 cm. Electrophoresis was carried out in positive polarity mode at  $2.5 \times 10^4$  V. The cassettes of the instruments were cooled to 20.0°C, samples were injected by application of pressure (50 mbar for 9 sec). Analytes were detected via their UV absorption at 205 nm and 260 nm, respectively. Sodium borate (100 mM boric acid adjusted to pH 8.3 via 3 M sodium hydroxide solution) was employed as sample buffer (SB), the BGE additionally contained 10 mM Thesit as detergent. For virus denaturation to viral proteins and RNA, SDS instead of Thesit was employed as surfactant, as well at 10 mM. For spin SEC experiments, SB was diluted to 50 mM boric acid concentration ( $\frac{1}{2}$  SB). SB and BGEs were filtered through syringe filters (CA membrane, 0.20 $\mu\text{m}$  from Minisart obtained via Wagner&Munz, Vienna, Austria) and spun (1 min at 400 rcf). Before each run, the capillary was flushed for 2 min with BGE for preconditioning. Postconditioning was carried out via flushing of the capillary for 2 min with 1 M sodium hydroxide solution and bidistilled water. TEM imaging was carried out on a Morgani 268 Transmission Electron Microscope (FEI Tecnai, Eindhoven, The Netherlands) employing a Morada CCD camera at  $8.9 \times 10^4$  fold magnification. Sucrose gradient centrifugation was done on a Beckman L7 ultracentrifuge employing a SW50.1 rotor at  $4.5 \times 10^4$  rpm for 35 min at 4.0°C.

**Procedures:** Heat denaturation of HRV2 was performed in a water bath at 56.0°C for 10 min. Storage solution of His-select® Nickel Affinity Gel was replaced by  $\frac{1}{2}$  SB. Spin SEC was carried out on an Eppendorf table top centrifuge employing spin X filters (CA membrane, 0.45  $\mu\text{m}$  from Corning obtained via Sigma Aldrich, Schnellendorf, Germany). Filter inlets were filled with Sephadex G-50 swelled in  $\frac{1}{2}$  SB and the column was dried via spinning. Four  $\mu\text{L}$  of heat denatured HRV2 were mixed with 1.5  $\mu\text{L}$  of a recombinant soluble receptor fragment of the very-low-density-lipoprotein receptor (MBP-V33333 at 5.5 mg/mL in 20 mM Tris-HCl, pH 7.5, 150 mM NaCl, 20 mM  $\text{CaCl}_2$ ) and with 1.5  $\mu\text{L}$  of His-select® Nickel Affinity Gel (in  $\frac{1}{2}$  SB). Incubation of virions was 1 hour on ice with receptor fragments followed by 15 min incubation with Nickel Affinity Gel. The receptor fragment is known to bind intact viral capsids [10, 58, 75] and was grafted with a His6-tag at its C- terminus, allowing for binding of free valences of  $\text{Ni}^{2+}$  ions. Upon application of 7.0  $\mu\text{L}$  of the analyte solution to a spin SEC column followed by sample elution via spinning (30 sec at 800 rcf), gel bound (via receptor molecules) viral 150S particles remained on the filter inlet. The spin SEC column was flushed with 7.0  $\mu\text{L}$   $\frac{1}{2}$  SB 3 times consecutively via spinning (30 sec at 800 rcf) and the respective fractions were collected.

For TEM imaging spin SEC was carried out with 4.8  $\mu\text{L}$  of a heat denaturated virus sample via spinning (30 sec at 800 rcf). The column was flushed with 5.0  $\mu\text{L}$  SB 8 times consecutively via spinning (30 sec at 800 rcf) and the respective fractions were collected and analyzed on CE. TEM imaging of 135S particles was carried out by combining fractions 4 and 5 of spin SEC and dilution of the resulting solution 1:25 in SB. Glow discharged (20 mA, 30 sec) carbon coated copper grids were employed for imaging with 2 % phosphotungsten acid pH 7.3 as contrast medium. Four  $\mu\text{L}$  of each sample were applied to a grid for 1 min, washed and stained for 1 min. For sucrose gradient centrifugation 4.8 mL of a 10 - 40 [w/w%] sucrose gradient in  $\frac{1}{2}$  SB were prepared in 13 x 51 mm Beckman Ultraclear<sup>TM</sup> centrifuge tubes. 16.0  $\mu\text{L}$  HRV2 stock was heat denaturated and 8.0  $\mu\text{L}$  of native virions were added. This mix of viral and subviral particles was stored over night at 4.0°C. Twenty  $\mu\text{L}$  of the viral / subviral particle mix were subjected to sucrose gradient centrifugation. 240  $\mu\text{L}$  fractions were collected from the top of the gradient and the protein content of the fractions was assessed via a Nanodrop ND-1000 spectrophotometer (PEQLAB, Erlangen, Germany). UV / Vis absorption was assessed at 225 and 260 nm in parallel. 30  $\mu\text{L}$  of fractions showing highest protein content were subjected to spin SEC prior to CE analysis after addition of DMSO as neutral EOF marker. Peak area ratios between the respective viral or subviral species and DMSO as internal standard were calculated.

**Sample preparation:** For analysis of 150S and 80S particles the HRV2 stock was diluted 1:13 in DMSO containing sample buffer; an aliquot of this dilution was heat denaturated. Heated and unheated aliquots of such HRV2 dilutions were mixed with SB yielding samples of 150S viral or 80S subviral particles. In parallel, this mixing step was carried out with mAb 2G2 stock. The final HRV2 concentration valued 24.0 nM, mAb 2G2 was applied in roughly 30.0 fold molar excess. The final DMSO dilution valued 1:2.0 x 10<sup>3</sup>. Incubation of viral particles with mAb 2G2 was carried out for 10 min at ambient temperature. Sample preparation of native 150S viral particles for TEM imaging was accomplished after 1:100 fold dilution of the virus stock in SB. Heat denaturation of such a stock produced 80S particles for TEM imaging.

For analysis of the concentration dependence of subviral particle formation, HRV2 stocks were diluted with SB to respective concentration values and heat denaturated. Before analysis, the sample volume was adjusted with SB and DMSO to a final 1 : 10 virus and a 1 : 4.0 x 10<sup>3</sup> DMSO dilution.

For experiments concerning the influence of fatty acids with different alkyl chain lengths on the formation of subviral 135S particles, HRV2 stock was diluted 1:2 in SB or SB / fatty acid suspensions prior to heat denaturation. After virus conversion, samples were further diluted with SB and DMSO to a final dilution of 1:15 for virus and 1 : 4 x 10<sup>3</sup> for DMSO.

For analysis of spin SEC fractions, samples were diluted 1 : 2 in  $\frac{1}{2}$  SB containing DMSO to a final DMSO dilution of 1 : 4.0 x 10<sup>3</sup>.

For complete denaturation of 150S particles to viral proteins and RNA, HRV2 was diluted 1 : 20 in SDS containing BGE including 1 :  $4.0 \times 10^3$  DMSO and heat denaturated. Subviral 135S particles of spin SEC fraction 2 were heat denaturated after 3 : 7 dilution in  $\frac{1}{2}$  SB additionally containing DMSO (final dilution 1 :  $4.7 \times 10^3$ ) and SDS (final concentration 8.5 mM)

Other 135S particle containing samples were obtained after dilution of the 4.0 mg/mL HRV2 stock to 3.3 mg/mL virus content with SB followed by heat denaturation. CE was carried out after further dilution of this 135S particle incubation solution with SB including DMSO and for some aliquots mAb 2G2 as well. The HRV2 content of samples valued 27.3 nM, mAb 2G2 was employed in approximately 31.0 fold molar excess. The final DMSO dilution factor in samples valued  $2.0 \times 10^3$ . For tracing the conversion of subviral 135S to 80S particles, a sample prepared in such a way (without mAb 2G2) was heated in a water bath at 56.0°C. CE was carried out after 4 min heating steps.

## 3.2 Receptor Mediated Attachment of Virions to Liposomes

Publication: Mimicking virus attachment to host cells employing liposomes: Analysis by chip electrophoresis

State of publication: published in Electrophoresis 2009, 30, 2123 – 2128

Experimental contributing authors: Victor U. Weiss – 55%

Gerhard Bilek – 30%

Angela Pickl-Herk – 15%

Victor U. Weiss  
 Gerhard Bilek  
 Angela Pickl-Herk  
 Dieter Blaas\*  
 Ernst Kenndler

Max F. Perutz Laboratories,  
 Medical University of Vienna,  
 Vienna Biocenter (VBC), Vienna,  
 Austria

Received February 20, 2009  
 Revised March 24, 2009  
 Accepted March 25, 2009

## Research Article

# Mimicking virus attachment to host cells employing liposomes: Analysis by chip electrophoresis

Electrophoresis on a chip increasingly replaces electrophoresis in the capillary format because of its speed and containment of the sample within a disposable cartridge. In this paper we demonstrate its utility in the analysis of the interaction between a virus and a liposome-anchored receptor, mimicking viral attachment to host cells. This became possible because detergents, obligatory constituents of the BGE for capillary electrophoretic separation of the virus, were not necessary in the chip format. Separations were carried out in sodium borate buffer, pH 8.3. Liposomes and virus were both labeled for laser-induced fluorescence detection at  $\lambda_{\text{ex}}/\lambda_{\text{em}}$  630/680 nm. Free virus and virus-receptor complexes were resolved from virus attached to receptor-decorated liposomes in the absence of additives or sieving matrices within about 30 s on commercially available microfluidic chips.

### Keywords:

Chip electrophoresis / Fluorescence labeling / Human rhinovirus / Liposome / Very-low-density lipoprotein receptor  
 DOI 10.1002/elps.200900108

## 1 Introduction

Human rhinoviruses (HRVs), main causative agents of the common cold, bind different cell surface receptors for infection. HRV2 belongs to the minor group of HRVs that recognize members of the low-density lipoprotein receptor family [1]. The ligand-binding domain of these receptors is composed of various numbers of modules of about 40 amino acid residues in length and arranged in tandem that differently contribute to ligand binding [2]. In order to better understand the structural basis of ligand recognition, recombinant concatemers of module 3 of the very-low-density lipoprotein receptor (VLDLR) have been used in a

number of studies [3–5]. As a result, it is now clear that up to five modules within a single receptor molecule can attach to five icosahedral-symmetry-related binding sites around one vertex of the viral capsid [6, 7].

Attachment of viruses to cells can be mimicked *in vitro* by using receptor-carrying liposomes [8, 9]. In previous work we used electrophoresis in coated fused-silica capillaries to monitor this process. Attachment of HRV2 to fluorescent unilamellar liposomes decorated with maltose-binding protein (MBP)-V33333, a his<sub>6</sub>-tagged receptor consisting of five repeats of module 3 of human VLDLR and expressed as a fusion with MBP, resulted either in a shift of the liposome peak or in its disappearance; concomitantly, a large number of spikes were observed, which we attributed to aggregates [10].

Detergents proved essential in preventing aggregation of viral particles in CE with fused-silica capillaries, independent of whether bare or coated [11]. However, work with liposomes precludes the use of surfactants. A solution to this problem was our finding that chip electrophoresis rendered neat virus peaks even in the absence of detergents for reasons that are not fully clear to us. We assume that it might be related to the much shorter residence time in the chip compared with the capillary. However, we first used chip electrophoresis for the analysis of complex formation of virus with different soluble concatemers of module 3 [12, 13]. In the present paper the recombinant

**Correspondence:** Professor Ernst Kenndler, Max F. Perutz Laboratories, Medical University of Vienna, Inst. Med. Biochem., Vienna Biocenter (VBC), Dr. Bohr Gasse 9/3, A-1030 Vienna, Austria

**E-mail:** ernst.kenndler@univie.ac.at

**Fax:** +43-1-4277-9616

**Abbreviations:** **DOGS-NTA**, 1,2-dioleoyl-*sn*-glycero-3-[*N*-(5-amino-1-carboxypentyl) iminodiacetic acid)succinyl] (nickel salt); **FL**, fluorescence; **HRV**, human rhinovirus; **MBP**, maltose-binding protein; **PEG750PE**, 1,2-distearoyl-*sn*-glycero-3-phosphoethanolamine-*N*-[methoxy (polyethylene-glycol)-750] (ammonium salt); **POPC**, 1-palmitoyl-2-oleoyl-*sn*-glycero-3-phosphocholine; **spin SEC**, spin size exclusion chromatography; **v-r**, virus-receptor; **v-r-l**, virus-receptor-liposome; **VLDLR**, very-low-density lipoprotein receptor

\*Additional corresponding author: Professor Dieter Blaas  
 E-mail: dieter.blaas@medunivie.ac.at

his<sub>6</sub>-tagged MBP-V3333 molecules were attached to the membrane *via* 1,2-dioleoyl-*sn*-glycero-3-[(*N*-(5-amino-1-carboxypentyl) iminodiacetic acid)succinyl] (nickel salt) (DOGS-NTA). In order to follow the binding of the virus to the membrane, we then employed fluorescence (FL) detection of both virus and liposomes. For this purpose virus was labeled within its protein coat with the amine-reactive dye Cy5, whereas liposomes were visualized *via* encapsulation of Atto 637 (free acid form) in their aqueous core. We here demonstrate the utility of chip electrophoresis for the assessment of the interaction of virus with receptor-decorated liposomes.

## 2 Materials and methods

### 2.1 Chemicals

Sephadex G50 (DNA grade) and Cy5 were obtained from Amersham Bioscience (Little Chalfont, England). Cy5 was dissolved in DMSO (>99.9%, Sigma Aldrich, Steinheim, Germany) to yield a 25 mM stock solution. Atto 637 (in free acid form) was obtained from Fluka (Buchs, Switzerland). Boric acid (99.99%) was from Sigma Aldrich. Sodium hydroxide (>97%) was from E. Merck (Darmstadt, Germany). Water was doubly distilled from a quartz apparatus. 1-Palmitoyl-2-oleoyl-*sn*-glycero-3-phosphocholine (POPC), 1,2-distearoyl-*sn*-glycero-3-phosphoethanolamine-*N*-[methoxy (polyethyleneglycol)-750] (ammonium salt) (PEG750PE) and DOGS-NTA were from Avanti Lipids (Alabaster, AL, USA) and purchased *via* Instruchemie (Delfzijl, The Netherlands). DOGS-NTA was already loaded with nickel ions upon delivery and was incorporated into liposomes as such.

### 2.2 Biological materials

Preparation and purification of HRV2 and assessment of purity and concentration were carried out as described previously [14, 15]. A 5  $\mu$ L aliquot of HRV2 at 9.5 mg/mL (1.1  $\mu$ M) in 50 mM sodium borate, pH 7.4 was employed in all chip electrophoresis experiments. The model receptor consisted of four copies of ligand-binding module 3 of human VLDLR arranged in tandem; it was fused to MBP at its N-terminus and carried a his<sub>6</sub>-tag at its C-terminus (MBP-V3333) [4]. The working solution was at 2.0 mg/mL (32  $\mu$ M) in TBSC buffer (20 mM Tris-HCl, 150 mM NaCl, 20 mM CaCl<sub>2</sub>, pH 7.5).

### 2.3 Instrumentation

Chip electrophoresis was carried out on the Agilent 2100 Bioanalyzer system applying commercially available DNA chips (Agilent Technologies, Waldbronn, Germany). DNA chips, produced from soda lime glass, allow analysis of up to

12 samples *per* chip. Analytes were monitored *via* FL, employing both excitation wavelengths of the instrument produced by a light-emitting diode ( $\lambda_{\text{max}} = 470$  nm) and a red laser ( $\lambda_{\text{max}} = 630$  nm); chips were thermostated to 30°C during analysis. Data were collected with the Agilent 2100 Expert software. Prior to use BGE and sample buffer were centrifuged for 10 min on a tabletop centrifuge (5415D, Eppendorf, Hamburg, Germany). The same centrifuge was employed for spin size exclusion chromatography (spin SEC).

### 2.4 Buffers

Electrophoretic separations were carried out in 100 mM boric acid adjusted to pH 8.3 with 3 M NaOH. BGE was prepared daily to attain the EOF values around  $5 \times 10^{-8}$  m<sup>2</sup>/Vs. BGE was diluted with bidistilled water to 80 mM boric acid concentration (sample buffer; BGE0.8) and to 50 mM boric acid concentration (labeling buffer; BGE0.5).

### 2.5 Chip handling

DNA chips were handled as described previously [12, 13]. In short, chip channels were filled with 12  $\mu$ L BGE on the Chip Priming Station by the application of pressure (20 s, 1 mL syringe volume, upper syringe clip position, position C of the base plate) from the BGE outlet well. Twelve microliters of Cy5 containing sample buffer (62.5 nM dye concentration) were applied to the ladder well for adjustment of the instrument optics and 12  $\mu$ L BGE to the remaining two wells marked "G". Six microliters of the samples were applied to the remaining wells. After the removal of the chip, electrodes were cleaned with the Electrode Cleaning Chip (filled with 380  $\mu$ L doubly distilled water). The script (defining all operational steps of the chip analysis) that is normally employed for DNA analysis was modified to positive polarity mode for both sample injection to the separation channel and electrophoretic analysis. The injection voltage was set to 1300 V, the separation voltage to 800 V (approx. 19 kV/m).

### 2.6 Production of multilamellar vesicles

Lyophilized lipids were dissolved in chloroform at 10 mM each prior to mixing in a round-bottom flask in the molar ratio of POPC:PEG750PE:DOGS-NTA = 18:1:1. Chloroform was added to about 3.0 mL; the solvent was evaporated and the resulting lipid film was dried for at least 3 h under a stream of nitrogen. The dry film was hydrated in 1.7 mL BGE0.5 or BGE0.5 containing 11  $\mu$ M Atto 637 (free acid form) to obtain FL liposomes. The flask was rotated at room temperature for at least another 3 h and vortexed several times. The multilamellar vesicle suspension was kept overnight at 4°C for maturation and either extruded to produce large unilamellar vesicles or stored at -40°C.

Assuming that all lipids were incorporated into liposomes, the calculated total lipid concentration was 7.1 mM including, 0.4 mM DOGS-NTA for unstained liposomes, and 5.9 mM, including 0.3 mM DOGS-NTA for FL liposomes.

## 2.7 Extrusion

To produce vesicles of defined size, the multilamellar vesicle suspension was sequentially extruded through two overlaid polycarbonate filters with pore sizes of 400, 200 and 100 nm by using a Mini-Extruder (Avanti Lipids) placed on a heating block pre-warmed to 50°C. The suspension was passed 35 times through each couple of filters [16, 17].

## 2.8 Virus labeling

HRV2 was labeled by mixing 5  $\mu$ L virus stock with 4.5  $\mu$ L BGE0.5 and 0.5  $\mu$ L 25 mM Cy5 in DMSO (approximate  $2.2 \times 10^3$ -fold molar excess of dye over virus). Incubation was carried out overnight under light protection at ambient temperature. Low-molecular-weight material was removed from the labeled virus on spin columns; filters from Corning Spin-X centrifuge tubes (cellulose acetate membrane, pore size 0.45  $\mu$ m, obtained from Sigma Aldrich) were filled with Sephadex G50 swelled in BGE0.5 (slurry corresponding to 900  $\mu$ L settled material in total, applied consecutively in two 450  $\mu$ L portions). The column was spun dry on a table-top centrifuge; the labeling mix was applied and the elution was started *via* spinning for 1 min at 800 rcf. The column was washed with 20  $\mu$ L of BGE0.5 *via* spinning (1 min, 800 rcf) and the total recovered eluate (30  $\mu$ L) was subjected to the same procedure on a fresh spin column (washing with 15  $\mu$ L). The final main fraction contained 5.25 pmoles (*i.e.* 115 nM) HRV2. Only 6% of the total virus remained on the columns and was recovered upon additional washings with 20  $\mu$ L buffer, each.

## 2.9 Liposome purification

Non-encapsulated Atto 637 was removed from the FL-labeled liposomes *via* spin SEC on G50 Sephadex columns as above, but equilibrated in bidistilled water. Ten microliters of liposome suspension were applied followed by elution at 800 rcf (1 min). The column was then rinsed with 20  $\mu$ L BGE0.5 (1 min, 800 rcf) and the total eluted material was collected.

## 2.10 Sample preparation for chip electrophoresis

Cy5-labeled HRV2 was diluted 1:21, the receptor stock solution 1:9 and the liposomes 1:10.5, all with BGE0.8. Note that FL-labeled liposomes were about 3.6 times less concentrated. Atto 495 was added as fluorescent EOF

marker ( $\lambda_{\text{ex}} = 495$  nm; 3.0  $\mu$ M final concentration). The final concentration of labeled HRV2 was 5.6 nM with the receptor being present in approximately 50-fold molar excess (based on a stoichiometry of 12 receptor molecules binding one virion). The DOGS-NTA in the outer liposomal membrane was in excess over receptor between 1.3- (labeled liposomes) and 5.4-fold (unlabeled liposomes). Samples were prepared by mixing constituents in the sequence receptor, liposomes and labeled HRV2—followed by 20 min incubation at ambient temperature under light protection.

## 3 Results and discussion

The experimental conditions were selected such as to enable recording of free virus as well as receptor-decorated liposomes and to obtain clear indications for virus attachment to the vesicles. The present chip electrophoresis setup relies on FL detection; therefore, the aqueous core of the liposomes was filled with Atto 637 ( $\lambda_{\text{ex}} = 635$  nm) and the virus was rendered fluorescent by reaction of Cy5 ( $\lambda_{\text{ex}} = 649$  nm) with the capsid proteins. This allowed for monitoring within the instrument-specific 630 nm channel.

It is evident that separation is governed by the mobility of the analytes and that of the EOF, whereby the mobility of the liposomes might depend on their size (and certainly on their composition) and that of the virus is affected by the chemical modification of its capsid upon labeling [18]. Moreover, the mobility of virus and liposomes presumably changes upon reaction with receptor fragments. Electrophoresis in the micro-device has the invaluable advantage that no detergent is needed (which would most probably disintegrate the liposomes). However, in general its separation performance is lower than that of the classical capillary format.

### 3.1 Liposomes

The employed liposomes consisted of POPC, PEG750PE and DOGS-NTA in 18:1:1 molar ratio and were extruded consecutively through filters of 400, 200 and 100 nm pore size. Samples representative of the corresponding size ranges taken after each extrusion step were analyzed by chip electrophoresis (Fig. 1). When measuring at the apex of the peaks, the largest vesicles (400 nm size) exhibited a clearly longer migration time when compared with the smaller ones (200 and 100 nm) that were barely distinguishable. Note that longer migration times correspond to higher electrophoretic mobility, as the anionic particles are swept by the EOF toward the cathodic end of the channel. The liposomes with smaller diameter were apparently more homogenous, as they gave narrower peaks. Signal fluctuations within the sample zones of the larger-sized liposomes most likely result from many slightly different species. Atto 637 was not completely removed by spin SEC; however, it did not interfere as it was sufficiently resolved from the



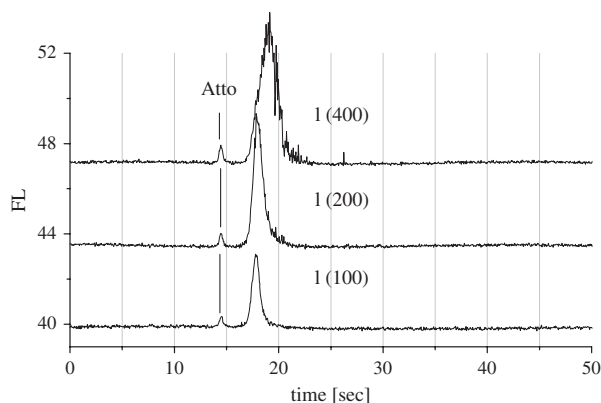


**Figure 1.** Chip electrophoresis of liposomes, l, from the same preparation but serially extruded through filters with 400, 200 and 100 nm pore size. The liposomes were FL labeled by inclusion of an aqueous solution of Atto 637 into the vesicle core. Total lipid concentration approximately 190  $\mu\text{M}$ . BGE, 100 mM boric acid adjusted to pH 8.3 with 3 M NaOH. Sample buffer was BGE diluted to 80 mM boric acid concentration. Separations were carried out at 800 V (approx. 19 kV/m). FL signal recorded at  $\lambda_{\text{ex}}/\lambda_{\text{em}}$  630/680 nm (arbitrary units).

liposome peaks. The reproducibility of the migration times, expressed by the standard deviation of the mean as determined on three different days by using five different chips (two samples *per* chip, ten samples in total) was 2.1%.

### 3.2 Virus–receptor–liposome complex

For the following binding experiments liposomes extruded through 200 nm pore size filters were used. To allow for decoration with his<sub>6</sub>-tagged receptors, liposomes were made to contain about 5% DOGS-NTA. In the present work we used MBP-V3333, a receptor fragment consisting of four repeats of module 3 of human VLDLR arranged in tandem and expressed with MBP at its N-terminus and a his<sub>6</sub>-tag at its C-terminus. Figure 2A shows the electropherogram of Atto 637-filled liposomes (l), Fig. 2B that of liposomes decorated with MBP-V3333 receptor (l+r). Binding of the receptor *via* its his<sub>6</sub>-tag to the DOGS-NTA in the membrane does not significantly change the migration behavior of the liposomes. However, a significantly different electropherogram was obtained after incubation with virus (Fig. 2C). Assuming a final lipid concentration of 190  $\mu\text{M}$  with 4.8  $\mu\text{M}$  of DOGS-NTA being accessible at the outer leaflet, the molar excess of the DOGS-NTA groups over receptor was 1.3-fold (see Section 2). However, even when the DOGS-NTA-groups in the membrane are in excess over the his<sub>6</sub>-tags, receptor binding is not expected to be quantitative because the dissociation constant is in the 10<sup>-6</sup> M range [19], which is within the same order as the analyte concentrations. Therefore, a peak attributed to virus bound to soluble receptor fragments, indicated as virus–receptor complex (v–r) was recorded as well (Fig. 2C). It has a slightly longer migration time than the peak ascribed to a contaminant, c, present in all virus preparations and also becoming labeled with amino-

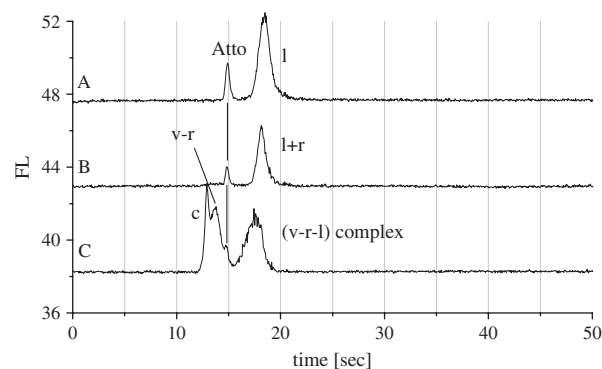


**Figure 2.** Chip electrophoresis of FL liposomes, l, upon incubation with receptor, r, and Cy5-labeled HRV2, v. (A) Atto 637-labeled liposomes, (B) Liposomes as in (A) after decoration with receptor; (C) Electropherogram obtained after incubation of the receptor-decorated liposomes with HRV2 resulting in binding of virus (v–r–l complex). Sample buffer, BGE, separation conditions and FL detection as with Fig. 1; c, contaminant of the virus preparation.

reactive dyes [20]. The liposome peak is shifted to a shorter migration time with concomitant zone broadening. This peak corresponds to the DOGS-NTA-doped liposomes, decorated with receptor and carrying receptor-attached virus (v–r–l). There is an increase in noise, which probably reflects heterogeneous species, either liposomes carrying various numbers of virions or liposomes aggregated *via* bridging, mediated by single or multiple virions.

To explicitly demonstrate the attachment of labeled HRV2 to our receptor-decorated model membrane, we repeated our experiments with unlabeled liposomes. This approach allowed us to follow exclusively the signal of labeled HRV2. Figure 3A depicts an electropherogram of labeled HRV2 that comigrates with the contaminant c (v+c). Incubation of the virus with MBP-V3333 yields a peak with increased migration time corresponding to (v–r), see Fig. 3B. After incubation of v–r with unlabeled liposomes (Fig. 3C), a third peak, identical to (v–r–l) in Fig. 2 was seen together with excess of v–r. Not only the position but also the apparent noisiness of the peaks was identical upon application of stained and unstained liposomes (compare Figs. 2C and 3C). However, for unstained liposomes the employed total lipid concentration for complex formation was about 3.6 times higher than in experiments with FL-labeled vesicles. Therefore, the ratio between DOGS-NTA-groups and his<sub>6</sub>-tagged receptors was about 5.4 as compared with the ratio of 1.3 in the experiment shown in Fig. 2. As a consequence, less free v–r were recorded. This suggests that v–r complexes do not dissociate significantly from the liposomes during electrophoresis.

### 3.3 Is HRV–liposome binding specific?

In order to exclude direct interaction between virus and liposomes in the absence of receptor, virus and DOGS-NTA-doped liposomes were incubated. Figure 4 shows that virus (and the contaminant, v+c) and liposomes (l) migrate

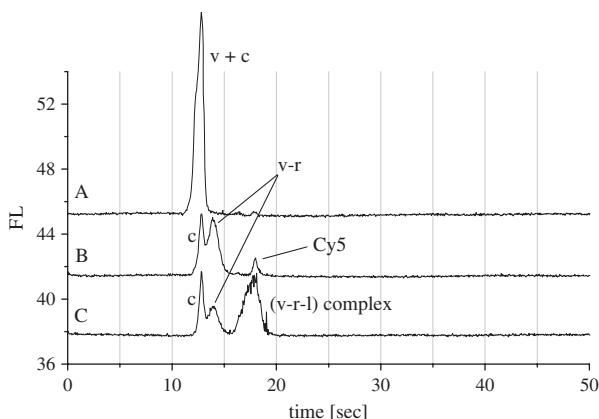


**Figure 3.** Shift of the labeled HRV2 peak upon subsequent incubation with receptor and unlabeled liposomes. Electropherogram of (A) HRV2 comigrating with the contaminant of the virus preparation; (B) upon incubation with soluble receptor fragments; (C) after incubation of (B) with liposomes. Sample buffer, BGE, separation conditions and FL detection as with Fig. 1; c, contaminant resulting from the virus preparation; small excess of Cy5 is also detected.

identically regardless of whether analyzed separately (A and B) or as a mixture (C). Taken together, these results prove that specific interaction between receptor-decorated liposomes and virus can be monitored by chip electrophoresis in very short times.

#### 4 Concluding remarks

Chip electrophoresis was employed to study the early steps in viral infection by using a liposome-based system. Liposomes as model membranes and a rhinovirus were detected on-chip upon FL labeling. The electrophoretic separation was carried out in a buffer solution without detergent; this is a clear advantage over CE where such additives are mandatory for reproducible analysis of virus. However, detergents disrupt liposomes. Only the conditions of chip electrophoresis allowed for the preservation of the components and the analysis of both components and their interaction products. Liposomes were functionalized *via* incorporation of DOGS-NTA, allowing for decoration with soluble his<sub>6</sub>-tagged recombinant receptor fragments. Receptor-carrying liposomes, in turn, were able to specifically bind HRV2. The individual analytes and liposome-bound virus appear as baseline-resolved peaks in the electropherograms; the latter is clearly distinguished from the peaks of their constituents.

This analytic system constitutes a starting point for the investigation of the early infection steps of non-enveloped viruses, which are still not fully understood. These include interactions of the viral capsid with a receptor anchored in a lipid membrane followed by the transfer of the viral genome into the cytosol. Indeed, we are currently investigating RNA release into receptor-decorated liposomes on acidification of within late endosomes. Furthermore, we are in the process of comparing the receptor-binding parameters of the mono-

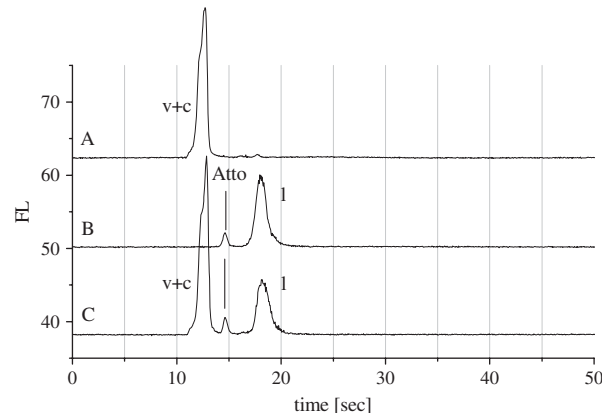


**Figure 4.** Binding of HRV2 to liposomes depends on the receptor. Electropherograms obtained for (A) HRV2, (B) liposomes and (C) for both analytes after incubation in the absence of receptor. Concentrations as in Fig. 2 and separation conditions as in Fig. 1.

nitrilo-triacetate lipid used in this report with a Tris-nitrilo-triacetate lipid in order to limit dissociation of the receptor from the liposome membrane. These findings will be the subjects of forthcoming publications. Collectively, using a HRV as a model system, our experiments set the stage to make the first step in this process accessible to rapid analysis by chip electrophoresis.

*This work was supported by the Austrian Science Foundation (Project P19365). The authors thank Agilent Technologies GmbH, Waldbronn, for support and Irene Goesler for virus preparation.*

*The authors have declared no conflict of interest.*

#### 5 References

- [1] Vlasak, M., Roivainen, M., Reithmayer, M., Goesler, I., Laine, P., Snyers, L., Hovi, T. *et al.*, *J. Virol.* 2005, **79**, 7389–7395.
- [2] Blacklow, S. C., *Curr. Opin. Struct. Biol.* 2007, **17**, 419–426.
- [3] Konecni, T., Kremser, L., Snyers, L., Rankl, C., Kilar, F., Kenndler, E., Blaas, D., *FEBS Lett.* 2004, **568**, 99–104.
- [4] Moser, R., Snyers, L., Wruss, J., Angulo, J., Peters, H., Peters, T., Blaas, D., *Virology* 2005, **338**, 259–269.
- [5] Wruss, J., Runzler, D., Steiger, C., Chiba, P., Köhler, G., Blaas, D., *Biochemistry* 2007, **46**, 6331–6339.
- [6] Verdaguer, N., Fita, I., Reithmayer, M., Moser, R., Blaas, D., *Nat. Struct. Mol. Biol.* 2004, **11**, 429–434.
- [7] Querol-Audi, J., Konecni, T., Pous, J., Carugo, O., Fita, I., Verdaguer, N., Blaas, D., *FEBS Lett.* 2009, **583**, 235–240.
- [8] Bubeck, D., Filman, D. J., Hogle, J. M., *Nat. Struct. Mol. Biol.* 2005, **12**, 615–618.
- [9] Bilek, G., Kremser, L., Blaas, D., Kenndler, E., *Electrophoresis* 2006, **27**, 3999–4007.
- [10] Bilek, G., Kremser, L., Wruss, J., Blaas, D., Kenndler, E., *Anal. Chem.* 2007, **79**, 1620–1625.

- [11] Kremser, L., Blaas, D., Kenndler, E., *Electrophoresis* 2004, 25, 2282–2291.
- [12] Weiss, V. U., Kolivoska, V., Kremser, L., Gas, B., Blaas, D., Kenndler, E., *J. Chromatogr. B* 2007, 860, 173–179.
- [13] Kolivoska, V., Weiss, V. U., Kremser, L., Gas, B., Blaas, D., Kenndler, E., *Electrophoresis* 2007, 28, 4734–4740.
- [14] Okun, V. M., Ronacher, B., Blaas, D., Kenndler, E., *Anal. Chem.* 1999, 71, 2028–2032.
- [15] Hewat, E. A., Neumann, E., Conway, J. F., Moser, R., Ronacher, B., Marlovits, T. C., Blaas, D., *EMBO J.* 2000, 19, 6317–6325.
- [16] Patty, P. J., Frisken, B. J., *Biophys. J.* 2003, 85, 996–1004.
- [17] Hope, M. J., Nayar, R., Mayer, L. D., Cullis, P. R., in: Gregoriadis, G. (Ed.), *Liposome Technology*, 2nd Edn., vol. 1, CRC Press, Boca Raton, FL, 1993, pp. 124–139.
- [18] Kremser, L., Petsch, M., Blaas, D., Kenndler, E., *Anal. Chem.* 2004, 76, 7360–7365.
- [19] Dorn, I. T., Neumaier, K. R., Tampe, R., *J. Am. Chem. Soc.* 1998, 120, 2753–2763.
- [20] Okun, V., Ronacher, B., Blaas, D., Kenndler, E., *Anal. Chem.* 2000, 72, 2553–2558.

Publication: Chip electrophoretic characterization of liposomes with biological lipid composition: Coming closer to a model for viral infection

State of publication: in press at Electrophoresis journal; elps.200900382.R1

Experimental contributing authors: Victor U. Weiss – 30%

Gerhard Bilek – 55%

Angela Pickl-Herk – 15%

Gerhard Bilek  
Victor U. Weiss  
Angela Pickl-Herk  
Dieter Blaas  
Ernst Kenndler

# Chip electrophoretic characterization of liposomes with biological lipid composition:

## Coming closer to a model for viral infection

*Max F. Perutz  
Laboratories, Medical  
University of Vienna,  
Vienna Biocenter (VBC),  
Vienna, Austria*

**Abbreviations:** **Ch**, Cholesterol; **DOGS-NTA**, 1,2-Dioleoyl-sn-Glycero-3-[(N-(5-amino-1-carboxypentyl)iminodiacetic acid)succinyl] (nickel salt); **FL**, fluorescence; **HRV**, human rhinovirus; **LDLR**, low-density lipoprotein receptor; **LUV**, large unilamellar vesicle; **NBD-PC**, 1-Oleoyl-2-[12-[(7-nitro-2-1,3-benzoxadiazol-4-yl)amino]dodecanoyl]-sn-Glycero-3-Phosphocholine; **n-phl**, “non-physiological” liposomes; **PE**, L- $\alpha$ -Phosphatidylethanolamine; **PEG750PE**, 1,2-Distearoyl-sn-Glycero-3-Phosphoethanolamine-N-[Methoxy(Polyethyleneglycol)-750]; **phl**, “physiological” liposomes; **POPC**, 1-Palmitoyl-2-Oleoyl-sn-Glycero-3-Phosphocholine; **SM**, Sphingomyelin; **VLDLR**, very-low-density lipoprotein receptor.

**Keywords:** HRV; chip electrophoresis; liposome; receptor; DOGS-NTA

**Correspondence:** Prof. Ernst Kenndler, Prof. Dieter Blaas, Max F. Perutz Laboratories, Medical University of Vienna, Inst. Med. Biochem., Center for Mol. Biol., Vienna Biocenter (VBC), Dr. Bohr Gasse 9/3, A-1030 Vienna, Austria

e-mail: [ernst.kenndler@univie.ac.at](mailto:ernst.kenndler@univie.ac.at), [dieter.blaas@medunivie.ac.at](mailto:dieter.blaas@medunivie.ac.at)

Tel: +43 1 4277 61635

Fax: +43 1 4277 9616

## Abstract

In first attempts at elucidating the transfer of the RNA genome of a human rhinovirus through lipid membranes *in vitro* we made use of liposomes decorated with recombinant receptors. This model system was characterized previously by capillary electrophoresis but suffered from the requirement for inclusion of polyethylene glycol-modified lipids for reliable separations [Weiss *et al.* (2009) *Electrophoresis*, 30,2123-2128]. We here report the analysis of liposomes with a lipid composition much more similar to that of biological lipid bilayers. We found that vesicles containing and lacking this non-physiologic lipid differ significantly in their electrophoretic mobility (by factor 2) although the concentration of charge-bearing lipids in their bilayers is the same. We demonstrate that binding of a human rhinovirus to the latter liposomes decorated with a cognate receptor can be analyzed via electrophoresis on microchips; we support our results with transmission electron microscopy.

# 1 Introduction

A keystone in viral infection is the transfer of the viral genome from the virion into the host cell. In the case of non-enveloped viruses entering via receptor-mediated endocytosis, this is achieved either by disruption of vesicular membranes or by transferring the nucleic acid through a pore. Human rhinoviruses (HRVs), main causative agents of the common cold, are valuable models for the study of these processes because they are well characterized and different HRV types appear to exploit either of these mechanisms depending on the receptor used. HRV2, a minor group virus binds members of the low-density lipoprotein receptor (LDLR) family and is taken up via clathrin-mediated endocytosis. The low pH environment of late endosomes then triggers the structural conversion of the virions into subviral particles that is accompanied by the transfer of the RNA through the vesicular membrane [1]. The latter step is only poorly understood; hence, there is a strong demand for an *in vitro* system allowing for a detailed dissection of this process.

In a first step towards this goal we established a liposome system where recombinant His6-tagged derivatives of a cognate receptor, the very-low density lipoprotein receptor (VLDLR), were attached to the liposomes via NTA-lipids in the presence of Ni-ions. Virus can be bound to these receptors and conformational modifications be triggered by incubation at low pH. However, the versatility of the system was compromised by the requirement to include polyethylene-modified lipids to allow for analysis of the liposomes by capillary electrophoresis [2]. Assuming that the same applied for chip electrophoresis, earlier work was done with liposomes (henceforth called “non-physiologic liposomes”; *n-phl*) made of 90 % POPC, 5 % PEG750PE and 5.0 % DOGS-NTA (see list of abbreviations), which is a highly non-physiologic composition [3] (Table 1). The liposomes dealt with in the present communication have a significantly reduced POPC content and PE, SM and Ch were incorporated into the lipid bilayer. Ch and SM affect membrane fluidity and allow for raft formation; PEG750PE, which is not present in natural membranes, was omitted. DOGS-NTA was maintained in order to enable decoration with receptor fragments. In addition, filling the vesicle core with an aqueous solution of a FL dye, as previously employed for

detection, was replaced by inclusion of NBD-PC, a fluorescent lipid, into the membrane. The implementation of the FL lipid was done in order to enable a more reproducible way of vesicle labeling. Using this labeling method, one could apply liposomes without purification steps to separate free dye material. Such purification steps were necessary for the previous labeling method where soluble dye molecules had been encapsulated in the liposomal lumen. Moreover, encapsulated dye always tends to leak out to some extent from the liposomal compartment, whereas lipid-labeled dyes stay permanently in the membrane. Overall, the membrane composition was similar to that commonly employed in experimental membrane fusion and in studies of virus interaction with membranes [4-8]. Liposomes with this more physiologic composition we here term “physiologic liposomes” (*p<sub>hl</sub>*).

We describe the use of a microdevice for the electrophoretic characterization of *p<sub>hl</sub>* in comparison to *n-p<sub>hl</sub>* and the tracking of *p<sub>hl</sub>* carrying recombinant receptors and HRV2. The system enables, by default, parallel detection in two fluorescence channels. As found in previous work with chip electrophoresis [9, 10] and in agreement with a recent paper dealing with *n-p<sub>hl</sub>* [3], aggregate formation of viruses was absent in chip electrophoresis even when detergents were omitted. This is important because detergents usually render liposomes unstable. We here demonstrate that virus attachment to liposomes of a lipid composition closely matching that of plasma membranes can be reliably and rapidly analyzed by electrophoresis on microchips; the nature of the analytes separated by chip electrophoresis was confirmed by electron microscopy.



## 2 Experimental Section

### 2.1 Chemicals

Lipids were from Avanti Lipids (Alabaster, US) and purchased via Instruchemie (Delfzijl, Netherlands). *1-Palmitoyl-2-Oleoyl-sn-Glycero-3-Phosphocholine* (POPC), *L- $\alpha$ -Phosphatidylethanolamine*, Transphosphatidylated (PE) from chicken egg, Sphingomyelin (SM), Cholesterol >98% (Ch), *1,2-Distearoyl-sn-Glycero-3-Phosphoethanolamine-N-[Methoxy(Polyethylene glycol)-750] (Ammonium Salt)* (PEG750PE), *1,2-Dioleoyl-sn-Glycero-3-[(N-(5-amino-1-carboxypentyl)iminodiacetic acid)succinyl] (nickel salt)* (DOGS-NTA), and *1-Oleoyl-2-[12-[(7-nitro-2-1,3-benzoxadiazol-4-yl)amino]dodecanoyl]-sn-Glycero-3-Phosphocholine* (NBD PC) were used.

Boric acid (99.00%) and DMSO (>99.9%) were from Sigma Aldrich (Steinheim, Germany). Cy5 was purchased from Amersham Bioscience (Little Chalfont, England) and dissolved in DMSO to a final concentration of 25 mM. Sephadex G50 (DNA grade) was also from Amersham Bioscience. The free acid form of Atto 495 (Fluka, Buchs, Switzerland) was used as mobility marker. Tris(hydroxymethyl)-aminomethan (Tris, ultrapure grade) was purchased from Applichem (Darmstadt, Germany) and NaOH pellets (>97%) from E. Merck (Darmstadt, Germany).

### 2.2 Biological material

HRV2 was prepared, purified and its concentration determined as described [11, 12]. For chip electrophoresis a virus preparation at 9.5 mg/mL and for TEM imaging a preparation with 5.5 mg/mL was used (both in 50 mM sodium borate, pH 7.4). A recombinant receptor derived from the very-low-density lipoprotein receptor (VLDLR) was employed for liposome decoration. It consisted of 4 tandem repeats of module 3 (V3), a maltose binding protein (MBP) at its N-

terminus and a His6-tag at its C-terminus [13]. A stock solution at 2.0 mg/mL in TBSC buffer (20 mM Tris-HCl, pH 7.5, 150 mM NaCl, 20 mM CaCl<sub>2</sub>) was used.

### **2.3 Instrumentation**

Sample analysis on commercially available soda lime glass chips (DNA chips from Agilent Technologies, Waldbronn, Germany) was carried out on the Agilent 2100 Bioanalyzer system as previously described [9, 10]. Chip electrophoresis employed positive polarity mode for electrophoretic sample injection into the separation channel as well as for analysis itself, i.e. migration was towards the cathode at 1300 V for injection and 800 V (approx. 19 kV/m) for separation. The background electrolyte (BGE) was 100 mM boric acid adjusted to pH 8.3 with 3 M NaOH. It was freshly prepared daily to attain EOF values of around  $55 \times 10^{-9}$  m<sup>2</sup>/Vs. BGE diluted with bidistilled water to 80 mM boric acid concentration was used as sample buffer and diluted to 50 mM concentration as labeling buffer and for swelling of Sephadex G50. Fluorescent analytes were detected by employing both excitation wavelengths of the instrument (maximum  $\lambda_{ex}$  at 470 nm and 630 nm, respectively). For imaging, a Morgani 268 transmission electron microscope (FEI Tecnai, Eindhoven, The Netherlands) was employed.

### **2.4 Liposome Production**

The preparation of multi-lamellar liposome and their extrusion to large unilamellar vesicles (LUVs) with a diameter of 200 nm was as previously described [14-16]. In addition to the previously described lipid composition [3], LUVs with a more biological composition (“physiologic liposomes”, phl), similar to that given in [4-8], were fabricated. They consisted of POPC : PE : SM : Ch : DOGS-NTA : NBD-PC at a molar ratio of 1 : 1 : 1 : 1.5 : 0.5 : 0.05. If not indicated otherwise, liposomes were hydrated in 50mM Tris-HCl buffer (pH 8.0) giving a total lipid concentration of about 7.8 mM. In few cases hydration was carried out in 50 mM borate buffer, pH 8.3.

## 2.5 Virus labeling

Five  $\mu\text{L}$  of HRV2 stock solution were diluted to 9.5  $\mu\text{L}$  with labeling buffer before addition of 0.5  $\mu\text{L}$  Cy5 at 25 mM in DMSO ( $2.2 \times 10^3$  fold molar excess of dye over virus during labeling). Incubation was for 18 hrs at ambient temperature in the dark. Low molecular mass material was removed via spin size exclusion chromatography (spin SEC) on Sephadex G50 as described [3]. Cy5 labeled virus at approximately 115 nM was obtained.

## 2.6 Sample preparation for chip electrophoresis

Purified Cy5 labeled HRV2 was diluted 1:21, the receptor stock solution 1:9 and liposomes 1:10.5 all in sample buffer. Atto 495 was included as fluorescent EOF marker ( $\lambda_{\text{ex}}$  at 495 nm) at a final concentration of approximately 3  $\mu\text{M}$ . Fluorescence labeled virus at 5.6 nM was thus incubated with an approximately 640 fold molar excess of soluble receptor fragments. DOGS-NTA lipid was present at 10 fold molar excess over receptor molecules. Incubation was carried out at ambient temperature under light protection for approximately 20 min.

## 2.7 Transmission electron microscopy

Liposomes were diluted 1:20 (0.4 mM total lipid concentration) for imaging. HRV2 was diluted 1:100 (6.4 nM final virus concentration). Liposome-attached virus was obtained by mixing receptor-decorated liposomes (10  $\mu\text{L}$  liposome stock with 1  $\mu\text{L}$  of receptor stock resulting in a 120 fold molar excess of receptor over DOGS-NTA lipid; incubation at ambient temperature for 20 min) with HRV2 (10  $\mu\text{L}$  of a 1:50 dilution; incubation at ambient temperature for 20 min). After incubation, the liposome/virus/receptor mixture was brought to 200  $\mu\text{L}$ . To assess non specific attachment 1  $\mu\text{L}$  liposome stock was incubated with 1  $\mu\text{L}$  of a 1:50 dilution of the HRV2 stock for 20 min at ambient temperature, and the mixture was brought to 20  $\mu\text{L}$ . All dilutions were carried out in 50 mM Tris-HCl buffer, pH 8.0. Carbon coated copper grids were glow discharged at 20 mA for 30 s. Four  $\mu\text{L}$  sample was applied to a grid for 1 min, washed and negatively stained

with 2 % phosphotungstic acid (pH 7.3) for 1 min. Photographs were taken at  $5.6 \times 10^4$  fold magnification using a Morada CCD camera.

## 3 Results and Discussion

### 3.1 Chip electrophoresis of liposomes of different composition

We endeavored to compose liposomes, which come closer to the composition of biological membranes. However, membranes are very heterogeneous with regard to their lipid-ratios. Therefore, one representative composition was chosen, which met best the lipid compositions given in literature [4-8]. In previous work we found that *n-phl* consisting of 90% POPC, 5% PEG750PE and 5% DOGS-NTA migrate as anions in CE [3]; note that both PEG750PE and Ni-loaded DOGS-NTA possess a negative charge at the pH of the BGE (see Table 1). PEG750PE contains a single charged phosphate group; the Ni-loaded DOGS-NTA has also one negative charge in excess because of the 3 anionic acetate moieties from which only two are compensated by the  $\text{Ni}^{2+}$  ion. From the electropherogram shown in Figure 1, upper trace, it can be seen that these *n-phl* are recorded at the detector with a relatively short migration time, closely after the peak of residual Atto 637. The vesicles are carried to the detector at the cathodic end of the channel by the EOF, which has a mobility of about  $55 [10^{-9} \text{ m}^2 \text{ V}^{-1} \text{ s}^{-1}]$ . Concerning the electrophoretic mobility of the anionic vesicles an apparent trend is found on the particle size. The 200 nm diameter particles as shown in Figure 1 have an average mobility of  $19.2 [10^{-9} \text{ m}^2 \text{ V}^{-1} \text{ s}^{-1}]$  (Table 2). The EOF mobility was obtained from Atto 495, which is zwitterionic at pH 8.3 and thus migrates as a neutral substance. The distribution of the mobility of the vesicles which are migrating in the electrophoretic peak is derived from the span covering plus/minus three times the standard deviation of the peak around the maximum. It values  $4.2 [10^{-9} \text{ m}^2 \text{ V}^{-1} \text{ s}^{-1}]$  which means that around 99% of the liposome species have a mobility between  $17.1$  and  $21.3 [10^{-9} \text{ m}^2 \text{ V}^{-1} \text{ s}^{-1}]$ .

The average mobility is slightly larger ( $20.2 [10^{-9} \text{ m}^2 \text{ V}^{-1} \text{ s}^{-1}]$ ) for *n-phl* of the same composition, but 400 nm in size, and slightly smaller for 100 nm sized vesicles ( $18.4 [10^{-9} \text{ m}^2 \text{ V}^{-1} \text{ s}^{-1}]$ ). However, there is no statistically significant difference in the average mobilities if we consider their standard deviations (*n* is 12 or 10, respectively). The mobility distribution of the vesicle peaks differs slightly between the species (see Table 2): the smaller particles have a smaller span (absolute and relative) than the 400 nm vesicles; it seems that their population is more homogeneous with respect to the mobility.

Relating the negative charge of the vesicle to individual anionic lipids in the bilayer seems an oversimplification if we consider the mobility of liposomes with the same size of 400 nm, but with a lower concentration of the charged lipids. We have measured the mobility of liposomes without DOGS-NTA, consisting of 95% POPC and 5% PEG750PE. Although these liposomes contained only half of the anionic lipids (5% instead of 10%), their mobility increased slightly to  $21.2 [10^{-9} \text{ m}^2 \text{ V}^{-1} \text{ s}^{-1}]$  instead of decreasing. It should be pointed out that even bilayers consisting of only POPC are negatively charged, although the lipid is zwitterionic and thus formally neutral. This demonstrates that for such vesicles the relation of charge properties of the electric double layer, zeta potential, and mobility is complex.

An electropherogram of *phl* is shown in Figure 1, lower trace. A very broad peak appears at about twice the migration time of the *n-phl* peak. At first sight it appears that *phl* are much more heterogeneous than *n-phl*. However, a closer view on the mobility and its distribution (Table 2) leads to the conclusion that (i) the mean electrophoretic mobility of the *phl* is by a factor of 2 larger than that of the *n-phl*, with an average of  $40.0 [10^{-9} \text{ m}^2 \text{ V}^{-1} \text{ s}^{-1}]$  (taken from the peak apex). This is surprising because the percentage of negatively charged lipids in the vesicles (around 10%, originating from DOGS-NTA and NBD-PC) is the same. This result again shows that the simple addition of formal charges of the individual lipids in the bilayer is not appropriate to explain the electrophoretic properties of the vesicles. (ii) Although the *phl* migrate as a very broad peak in the electropherogram, their mobility distribution, as given by the span (Table 2) is even lower in absolute units ( $1.8 [10^{-9} \text{ m}^2 \text{ V}^{-1} \text{ s}^{-1}]$ ) as compared to the *n-phl*. The population is also more homogeneous, as the mobility of more than 99% of the species varies only within 5% around the

average. For practical reasons the following experiments were carried out with liposomes prepared in Tris-HCl, pH 8.0 buffer; the liposomes with the same composition, but hydrated in sodium borate, pH 8.3, exhibited a similarly high mobility (average mobility is  $35.8 [10^{-9} \text{ m}^2 \text{ V}^{-1} \text{ s}^{-1}]$ , standard deviation  $0.9 [10^{-9} \text{ m}^2 \text{ V}^{-1} \text{ s}^{-1}]$ ). This indicates that the lipid composition governs the electrophoretic behaviour.

### 3.2 Analysis of the receptor-mediated binding of virus to liposomes

Inclusion of DOGS-NTA in the lipid bilayer creates an anchor for attachment of recombinant receptor fragments via their His<sub>6</sub>-tag (most likely with 1:1 stoichiometry). The applicability of this approach has been successfully demonstrated previously [17]; here we investigated whether receptor decoration of *pfl* can also be tracked via chip electrophoresis. Note that the POPC content was reduced from 90% to about 20%, that PE and SM are now constituents with about 20% each, and that Ch (at about 30%) was included. Labeling of the vesicles previously carried out by incorporation of a soluble dye into the aqueous vesicle core is here substituted by incorporation of a fluorescent lipid in the bilayer. The drastic changes in membrane composition have no influence on decoration of the liposome with the receptor. This can be seen from the shift of the liposome peak towards a shorter migration time (compare Figure 2 upper and middle trace). Note that only liposomes are detected as they contain the fluorescent nitro-benzoxadiazol-4-yl amino group.

The large shift of the *pfl* peak from 42 to 30 sec migration time results from attachment of the receptor. It is interesting that this is caused by the much smaller reduction of the electrophoretic mobility by roughly 10% (from  $(-)40 [10^{-9} \text{ m}^2 \text{ V}^{-1} \text{ s}^{-1}]$  to about  $(-)35 [10^{-9} \text{ m}^2 \text{ V}^{-1} \text{ s}^{-1}]$ ). The much more pronounced effect on the migration time is the result of the relation between the analyte mobility and that of the counter-directed EOF, which is around  $(+)55 [10^{-9} \text{ m}^2 \text{ V}^{-1} \text{ s}^{-1}]$ . Therefore the resulting apparent mobility of the analyte (which determines the migration time) of around  $55-40=(+)15 [10^{-9} \text{ m}^2 \text{ V}^{-1} \text{ s}^{-1}]$  is increased to around  $55-35=(+)20 [10^{-9} \text{ m}^2 \text{ V}^{-1} \text{ s}^{-1}]$ ; this leads to the observed significant change of the migration time.

Note that interaction of the uncharged His<sub>6</sub> with DOGS-NTA does not change the overall charge as the former replaces two water molecules from the latter (see the structural formula given in Table 1). However, the receptor adds 39 formal negative charges (90 aspartic and glutamic acid versus 51 arginine and lysine residues). Indeed, the free receptor fragment migrates as anion at pH 8.3 with a mobility of about 20 [10<sup>-9</sup> m<sup>2</sup> V<sup>-1</sup> s<sup>-1</sup>], which is much lower than the mobility of the bare liposome. Taken together, it is plausible that liposomes carrying receptor fragments exhibit a mobility between that of the components.

Incubation of the receptor-decorated liposomes with virus (*v*) results in the electropherogram shown in Figure 2, lower trace. A marginal further shift of the peak maximum to a shorter migration time is observed. As the virus is not detectable, there is no proof for assembly between virus and receptor-decorated liposome. Therefore, HRV2 was FL labeled with Cy5, which has an excitation wavelength of 630 nm.

The electropherogram recorded at  $\lambda_{\text{ex}}$  630 nm is presented in Figure 3. The upper trace shows the signal obtained from the labeled virus taken as reference. Due to the absence of any detergent in the BGE, virus (*v*) and a contaminant, which is always present in the virus preparations, are migrating unresolved as a neat peak with about 12 s migration time. Upon incubation of the virus with receptor (*r*) the peak of the resulting complex shifts to a slightly longer migration time, with improved resolution from the (unchanged) contaminant peak (Figure 3, middle trace). Finally, the formation of the assembly between virus, receptor and liposome (*phl*) can be clearly seen from the electropherogram of the incubation mixture of these three constituents (Figure 3, lower trace). The peak of this (*v+r+phl*) assembly has the same migration time and shape than that obtained with the blue laser (compare with Figure 2, lower trace).

To assess the specificity of the interaction, virus was also mixed with bare liposomes and analyzed. Comparison of the electropherograms of the virus alone (Figure 4, upper trace) with that obtained from an incubation mixture of liposomes with virus in the absence of receptors (Figure 4, lower trace) shows that the virus peak remains completely unchanged. This proves that the virus only binds to receptor decorated liposomes.

### 3.3 Transmission electron microscopy

Virus binding to receptor-decorated liposomes was also assessed via electron microscopy. Figure 5 shows pictures of *pfl*, virus, assemblies resulting from mixing receptor-decorated *pfl* with virus, and a mixture of bare liposomes (lacking receptor) with virus, respectively. Samples corresponding to those analyzed in the Figures 2-4 were applied to glow-discharged carbon coated copper grids and negatively stained with 2% phosphotungstic acid, pH 7.3. Liposomes appear as circular density with diameters ranging from about 50 nm to 200 nm (Fig. 5A). Due to adsorption and dehydration as part of sample preparation, they are not perfectly round. The image confirms that extrusion leads to a size distribution with a maximum diameter of 200 nm, limited by the pore size of the polycarbonate filter. HRV2 is shown in Figure 5B. The particles are well dispersed and not aggregated. Figure 5C shows receptor-decorated liposomes after incubation with virus. The virions are no longer distributed randomly but are preferentially seen attached to liposomes and only few free virus particles are detected. To again confirm the specificity of the interaction, virus was incubated with bare liposomes (Fig. 5D). Liposomes and virus particles are randomly distributed and no virions are attached to the lipid vesicles. This confirms that the virus does not interact with the membrane *per se* but depends on the receptor for attachment. These findings support our results obtained by chip electrophoresis.

It can be further seen that liposomes with attached viral particles appear to have somewhat changed their shape. This is because a virion can bind several receptor-molecules and thus is able to bind a number of nickel-complexing lipids (DOGS-NTA). This results either in the virion-mediated aggregation between liposomes or a slight engulfment of the virus particle in the lipid membrane. Concerning the latter phenomenon, DOGS-NTA lipids most probably enrich at the position of virus binding and thus the membrane can bend around receptor-bound virus. Both effects can contribute to a slight change in the liposome appearance upon receptor-mediated virus binding.



## 4 Conclusion

Liposomes with a composition similar to that of native cell membranes were made (termed *phl*). They were labeled by incorporating a FL lipid into the bilayer. To allow for binding of a His<sub>6</sub>-tagged viral receptor a Ni-NTA lipid was included. We demonstrate that such liposomes can be electrophoresed on a chip and migrate with a mobility much larger than that of liposomes with a high content of POPC and PEG750PE (termed *n-phl*). The *phl* deliver a broad peak at a longer migration time which is a consequence of the smaller difference between the EOF mobility and that of the vesicles. Despite the broader peak, these liposomes are more homogeneous in terms of the mobility of the vesicle population than *n-phl*.

Binding of FL labeled virus to these receptor decorated liposomes was assessed by chip electrophoresis with FL detection at  $\lambda_{\text{ex}}$  470 nm (liposomes) and at  $\lambda_{\text{ex}}$  630 nm (virus). Virus binding to the liposomes was dependent on the presence of the receptor. This was confirmed by electron microscopy.

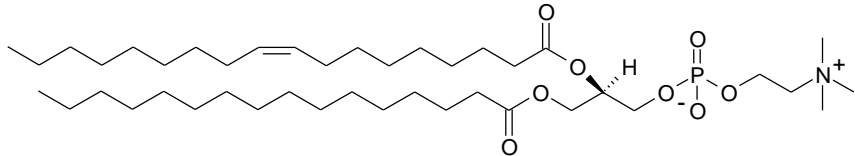
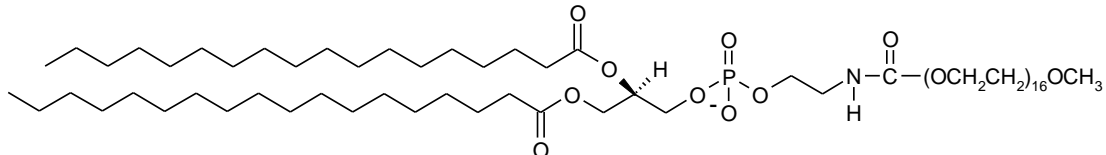
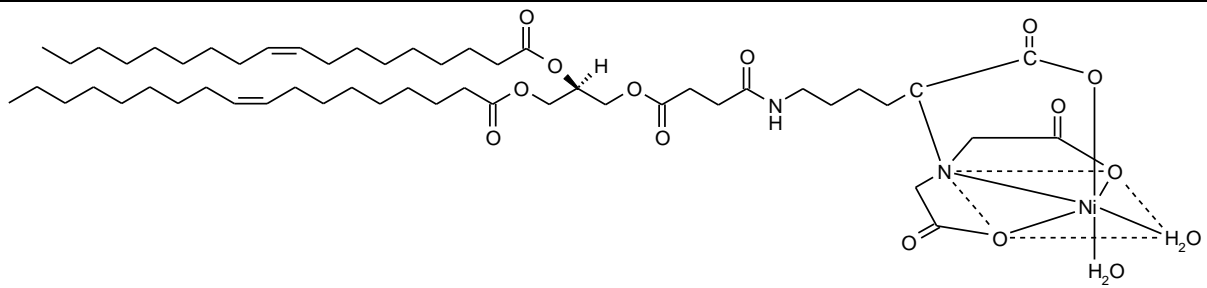
### Acknowledgement

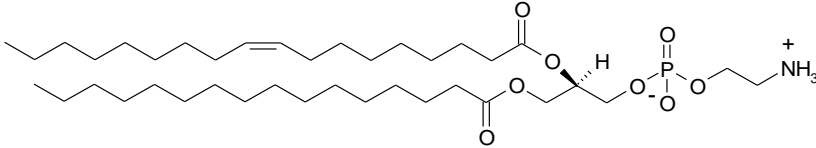
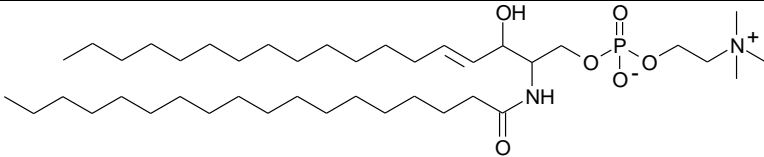
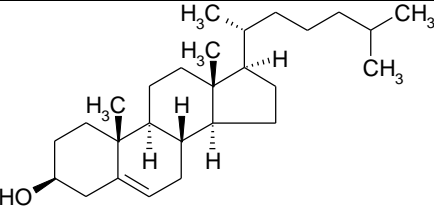
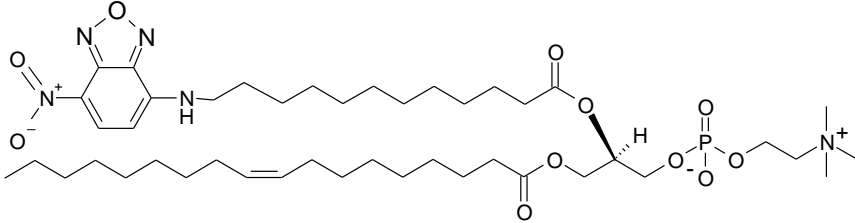
This work was supported by the Austrian Science Foundation (Project P19365). The authors thank Agilent Technologies GmbH, Waldbronn, for support, Irene Goesler for virus preparation, Guenter Resch and Marlene Brandstetter for help with electron microscopy.

## References

- [1] Fuchs, R., Blaas, D. (Eds.), *Human rhinovirus cell entry and uncoating*, World Scientific and Imperial College Press 2008.
- [2] Wiedmer, S. K., Shimmo, R., *Electrophoresis* 2009, 30, S240-S257.
- [3] Weiss, V. U., Bilek, G., Pickl-Herk, A., Blaas, D., Kenndler, E., *Electrophoresis* 2009, 30, 2123-2128.
- [4] White, J., Helenius, A., *Proceedings of the National Academy of Sciences of the United States of America* 1980, 77, 3273-3277.
- [5] Wubbolts, R., Leckie, R. S., Veenhuizen, P. T., Schwarzmann, G., Mobius, W., Hoernschemeyer, J., Slot, J. W., Geuze, H. J., Stoorvogel, W., *J Biol Chem* 2003, 278, 10963-10972.
- [6] Kobayashi, T., Beuchat, M. H., Chevallier, J., Makino, A., Mayran, N., Escola, J. M., Lebrand, C., Cosson, P., Gruenberg, J., *J Biol Chem* 2002, 277, 32157-32164.
- [7] Evans, W. H., Hardison, W. G., *Biochem J* 1985, 232, 33-36.
- [8] Alberts, B., Johnson, A., Lewis, J., Raff, M., Roberts, K., Walter, P., *GS Garland Science* 2002, 589-590.
- [9] Kolivoska, V., Weiss, V. U., Kremser, L., Gas, B., Blaas, D., Kenndler, E., *Electrophoresis* 2007, 28, 4734-4740.
- [10] Weiss, V. U., Kolivoska, V., Kremser, L., Gas, B., Blaas, D., Kenndler, E., *J. Chromatogr.B* 2007, 860, 173-179.
- [11] Hewat, E. A., Neumann, E., Conway, J. F., Moser, R., Ronacher, B., Marlovits, T. C., Blaas, D., *Embo J* 2000, 19, 6317-6325.
- [12] Okun, V. M., Blaas, D., Kenndler, E., *Anal Chem* 1999, 71, 4480-4485.
- [13] Moser, R., Snyers, L., Wruss, J., Angulo, J., Peters, H., Peters, T., Blaas, D., *Virology* 2005, 338, 259-269.
- [14] Torchilin, V., Weissig, V., *Oxford University Press* 2003, 1-8.
- [15] Hope, M. J., R. Nayar, L. D. Mayer, Cullis, P. R., *Liposome Technology, 2nd ed* 1993, 124-139.
- [16] Patty, P. J., Frisken, B. J., *Biophys J* 2003, 85, 996-1004.
- [17] Bilek, G., Kremser, L., Blaas, D., Kenndler, E., *Electrophoresis* 2006, 27, 3999-4007.

**Table 1.** Lipid constituents of the liposomes investigated.

	Abbreviation	Content (mol%)	Structural formula	Formal Charge
<i>n-phl</i> <sup>a)</sup>	POPC	90.0 (95.0)		0
	PEG750PE	5.0 (5.0)		-1
	DOGS-NTA	5.0 (0)		-1
<i>phl</i> <sup>b)</sup>	POPC	19.8		0

	PE	19.8		0
	SM	19.8		0
	Ch	29.7		0
	DOGS-NTA	9.9		-1
	NBD-PC	1.0		-1

<sup>a)</sup> *n-phl*: “non-physiologic” liposomes; <sup>b)</sup> *phl*: “physiologic” liposomes

**Table 2** Electrophoretic mobility distribution of liposomes with different composition, size or buffer used during their preparation.

Mobility, standard deviation and mobility span in [ $10^{-9} \text{ m}^2 \text{ V}^{-1} \text{ s}^{-1}$ ]. The span covers species within  $\pm 3$  times the standard deviation of the electrophoretic peak.

Liposome	Size, nm	Average Mobility	Standard deviation	n	RSD%	Span
POPC:PEG750PE <sup>a) 1)</sup>	400	21.2	0.5	12	2.4	3.0
POPC:NTA:PEG750PE <sup>b) 1)</sup>	400	20.2	1.0	10	5.0	6.0
POPC:NTA:PEG750PE <sup>b) 1)</sup>	200	19.2	0.7	10	3.6	4.2
POPC:NTA:PEG750PE <sup>b) 1)</sup>	100	18.4	0.7	10	3.8	4.2
POPC:PE:SM:Ch:DOGS-NTA:NBD-PC <sup>c) 1)</sup>	200	35.8	0.9	5	2.5	5.4
POPC:PE:SM:Ch:DOGS-NTA:NBD-PC <sup>c) 2)</sup>	200	40.0	0.3	5	0.8	1.8

<sup>a)</sup> 19:1; <sup>b)</sup> 18:1:1; <sup>c)</sup> 1:1:1:1.5:0.5:0.05. molar ratio; <sup>1)</sup> liposomes prepared in 50 mM boric acid adjusted to pH 8.3 with NaOH; <sup>2)</sup> liposomes prepared in 50 mM Tris-HCl buffer, pH 8.0

## Figure Legends

**Figure 1.** Chip electrophoresis of liposomes with different membrane composition. Upper trace: non-physiologic liposomes (*n-phl*), 200 nm diameter, the free acid form of Atto 637 was encapsulated for detection at  $\lambda_{\text{ex}}/\lambda_{\text{em}}$  630/680 nm. Total lipid concentration: 190  $\mu\text{M}$  [3]. Lower trace: physiologic liposomes (*phl*), 200 nm diameter, membrane labeled with NBD-PC for detection at  $\lambda_{\text{ex}}/\lambda_{\text{em}}$  470/525nm. Total lipid concentration: 740  $\mu\text{M}$ . Separation conditions: soda lime glass chip, BGE: 100 mM boric acid, adjusted to pH 8.3 with NaOH. Sample buffer: BGE diluted with bidistilled water to 80 mM boric acid concentration. Separation voltage: 800 V (approx. 19 kV/m).

**Figure 2.** Attachment of FL labeled virus (*v*) to physiologic liposomes (*phl*) via a VLDL-receptor derivative (*r*). Detection of liposomes at  $\lambda_{\text{ex}} = 470$  nm; Cy5 labeled virus is not detectable at this wavelength. Atto 495 was employed as EOF marker. Sample components: 5.6 nM FL labeled HRV2; 640 fold molar excess of receptor over virus; 10 fold molar excess of accessible DOGS-NTA lipid over receptor; total lipid concentration in the samples 740 $\mu\text{M}$ . BGE, sample buffer and separation conditions as in Figure 1.

**Figure 3.** Binding of FL labeled virus (*v*) to physiologic liposomes (*phl*) via a recombinant receptor derivative (*r*) detected at  $\lambda_{\text{ex}} = 630$  nm. Labeled liposomes are not detectable at this wavelength. Other conditions as in Figure 1. Cont., contaminant in the virus preparation.

**Figure 4.** Attachment of HRV2 to liposomes depends on the receptor. Upper trace: virus. Lower trace: incubation mixture of virus (*v*) and bare *phl* in the absence of receptor. Concentration of analytes as in Figure 2, BGE, sample buffer and separation conditions as in Fig. 1. Detection at  $\lambda_{\text{ex}} = 630$  nm.

**Figure 5.** Virus binding to liposomes depends on the receptor. TEM images of liposomes (A); HRV2 (B); a mixture of virus and receptor-decorated liposomes (C); a mixture of virus and bare liposomes (D). Samples were adsorbed to glow-discharged carbon coated copper grids and negatively stained with 2% phosphotungstic acid, pH 7.3. Images were taken at a  $5.6 \times 10^4$  fold magnification. Size bar = 100 nm

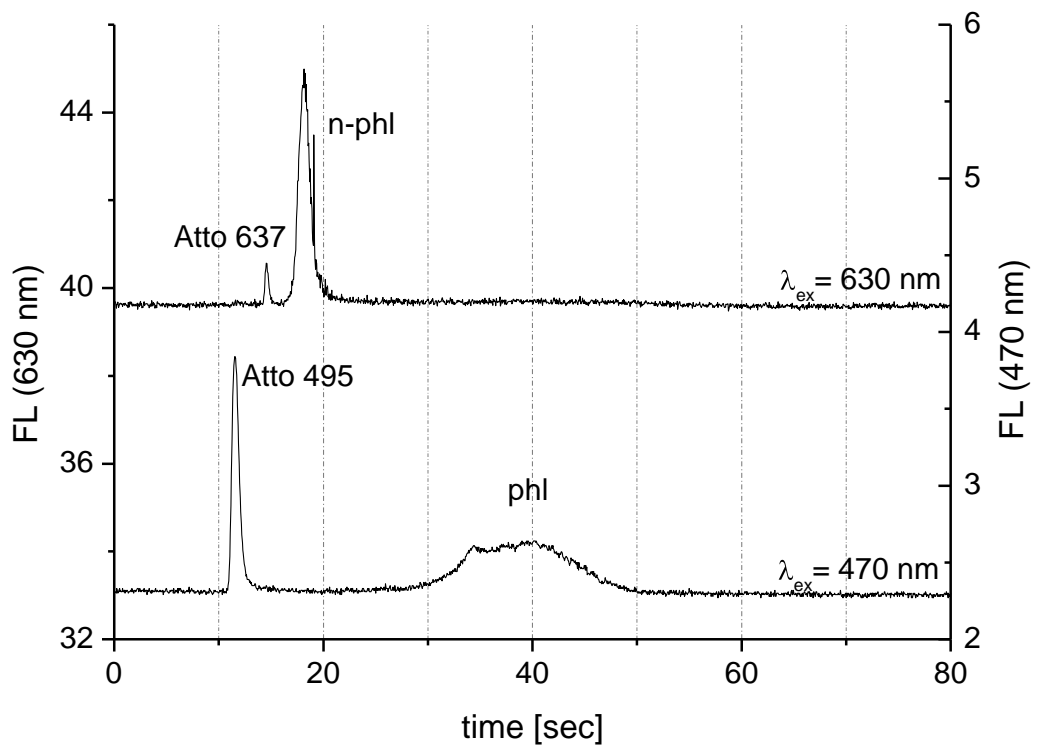
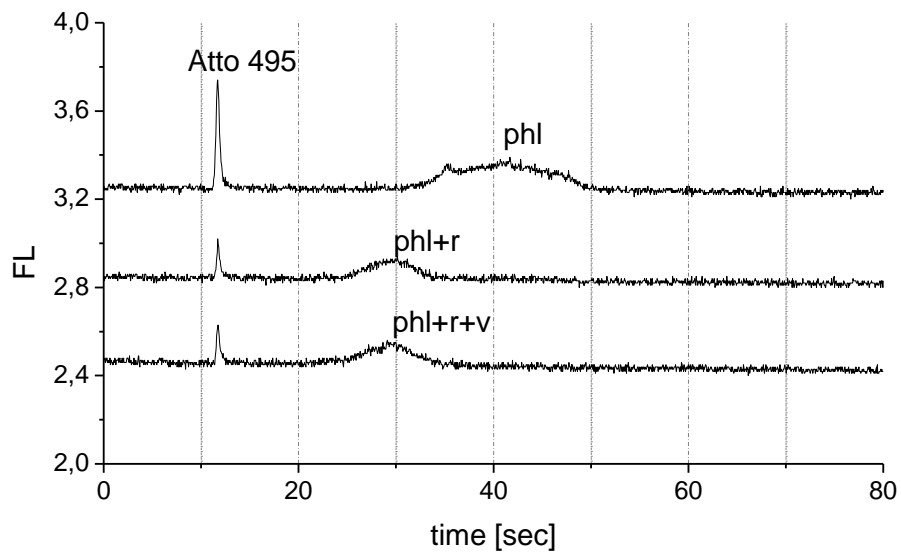
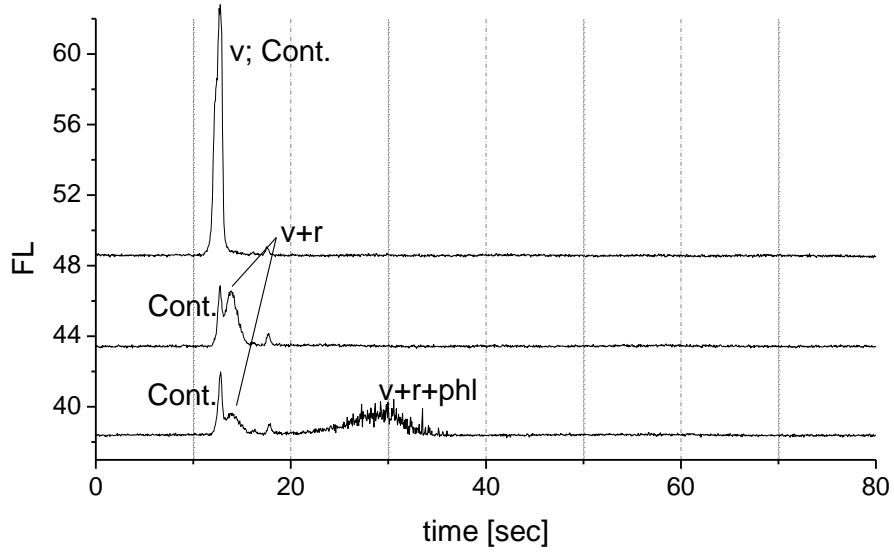


Figure 1.



**Figure 2.**





**Figure 3.**

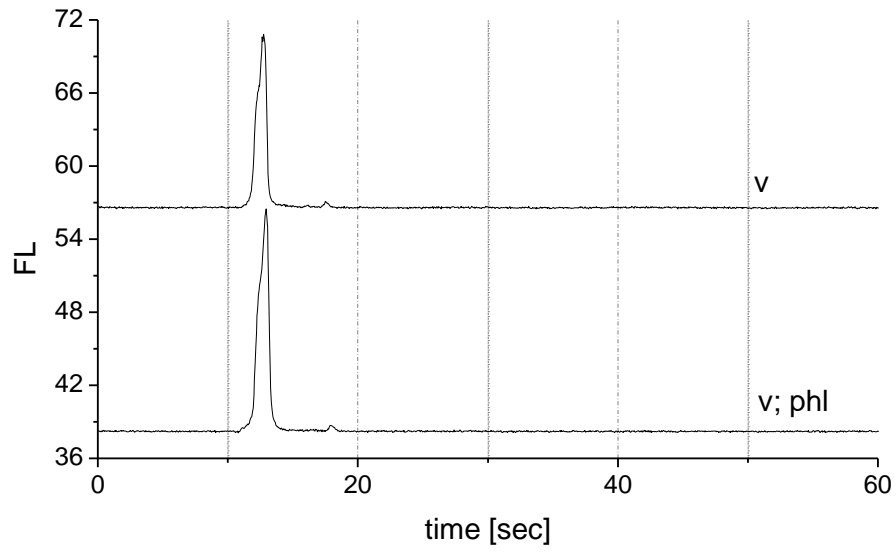


**Figure 4.**

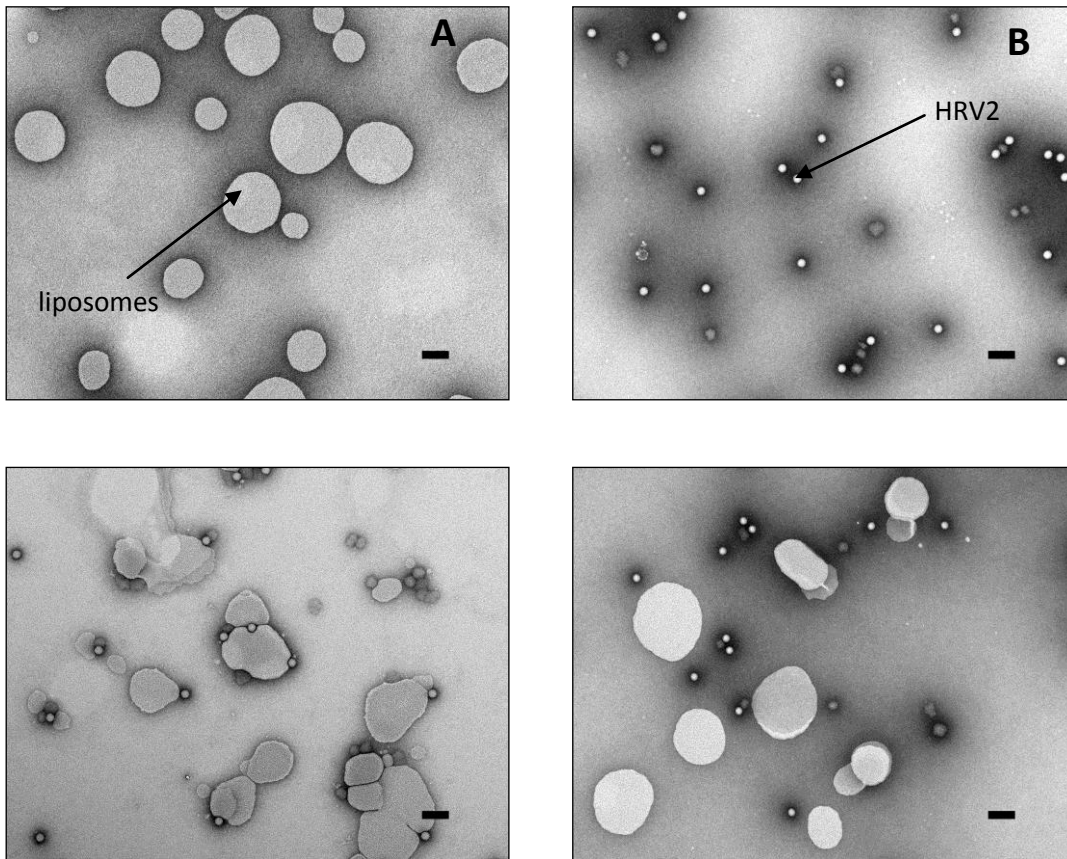


**Figure 5.**

### 3.3 Determination of Leakage from Lipid Vesicles via Electrophoresis

Various leakage assays are reported in literature, for instance based on de-quenching effects upon release of a fluorophore like calcein previously encapsulated at self-quenching concentrations inside liposomes [e.g. 76], or based on encapsulation of a fluorophore / quencher pair (ANTS/DPX) followed by the release of both molecules upon membrane permeabilization [e.g. 77, 78] or based on separation of  $Tb^{3+}$  and dipicolinic acid (DPA) via a membrane [e.g. 79 – 81]. In those leakage assays permeabilization of the respective membranes causes an increase in fluorescence, either by a drop in the fluorophore concentration below its self-quenching level, by high dilution of a fluorophore / quencher solution upon its release from liposomes or by complex formation between two previously separated molecules. However, all these described leakage assays also exhibit drawbacks. In the case of encapsulated fluorophores at self quenching levels already partial leakage of fluorophore molecules from inside of liposomes might be sufficient to obtain a disproportionally high fluorescence response, since the fluorophore concentration inside the lipid vesicles has already dropped below self-quenching values. In the case of leakage assays that rely on interaction between two different molecules, like for instance the fluorophore / quencher pair ANTS/DPX, preferential leakage of one molecule over the other was reported [78] and leakage assays have to be corrected for that effect.

In previous experiments we opted for unilamellar liposomes as model membrane encapsulating a fluorescent dye (Atto 637, free acid form). Application of our samples to Agilent 2100 Bioanalyzer DNA chips allowed for electrophoretic baseline separation of free and still encapsulated dye (as demonstrated in 3.2). Therefore, it was reasoned that chip electrophoresis allows for tracking of both dye contingents during leakage experiments – still encapsulated and already released fluorophores. The degree of leakage caused by peptides and viral proteins could thus be regarded as the ratio between the area of the liposome peak ( $A_{Liposome}^{Leak}$ ) and the area of the free dye peak ( $A_{Dye}^{Leak}$ ). This obtained value was further corrected for unspecific liposome leakage by relating the original ratio ( $A_{Liposome}^{Leak} : A_{Dye}^{Leak}$ ) to an average ratio  $\tilde{A}$  of two blank ratios ( $A_{Liposome}^{Blank} : A_{Dye}^{Blank}$ ) measured in the absence of membrane disrupting agents at the beginning and at the end of each respective chip. Therefore, leakage could be expressed in

terms of intact liposomes as ratio of ( $A_{\text{Liposome}}^{\text{Leak}} : A_{\text{Dye}}^{\text{Leak}}$ ) to  $\tilde{A}$ . Data points were finally obtained as average values of at least four measurements from two independent chips.

Several peptides are known to induce leakage of model membranes. Two of those peptides, GALA [82, 83] and the 24 amino acid long N-terminus of the HRV2 viral capsid protein VP1 [76], were chosen as positive controls for our chip based liposome leakage assay. On the other hand Insulin Chain A and a peptide of the HRV2 viral capsid protein 2 (VP2) termed 8F5 antigen were chosen as negative controls. A series of resulting electropherograms obtained for GALA induced leakage is presented in figure 36. An increase in the first peak (the free dye) as well as a concomitant decrease of the second peak (the liposomes encapsulating dye molecules) is observable with increasing peptide concentrations.

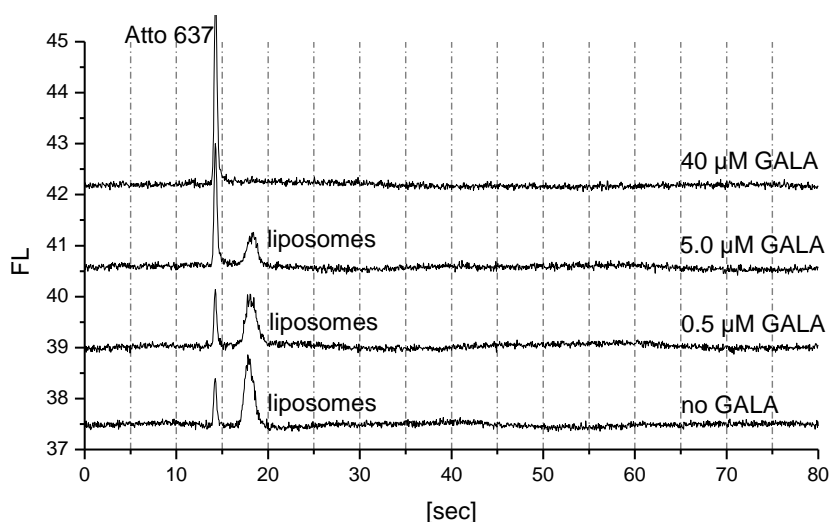


Fig. 36: Electropherograms obtained for liposomes pre-treated with increasing GALA concentrations, a leakage inducing peptide. An increase of the peak for the free dye as well as a concomitant decrease of the peak for the encapsulated dye upon incubation with GALA is observable.

The resulting leakage curves for tested peptides are presented in figure 37. It is of note that for the N-terminus of VP1 problems with the protein stock solution were experienced. In fact, already for very low concentrations milky solutions were obtained, probably due to aggregating peptide fragments. Therefore, leakage experiments were repeated with a

slightly modified VP1-N peptide. Addition of six lysines increased the water solubility of the N-terminal peptide dramatically which was also reflected in the obtained leakage curve: Already at 1 mM concentration the modified VP1-N peptide lead to complete liposome leakage, whereas at that concentration for the original peptide still roughly 90 % of all liposomes remained intact.

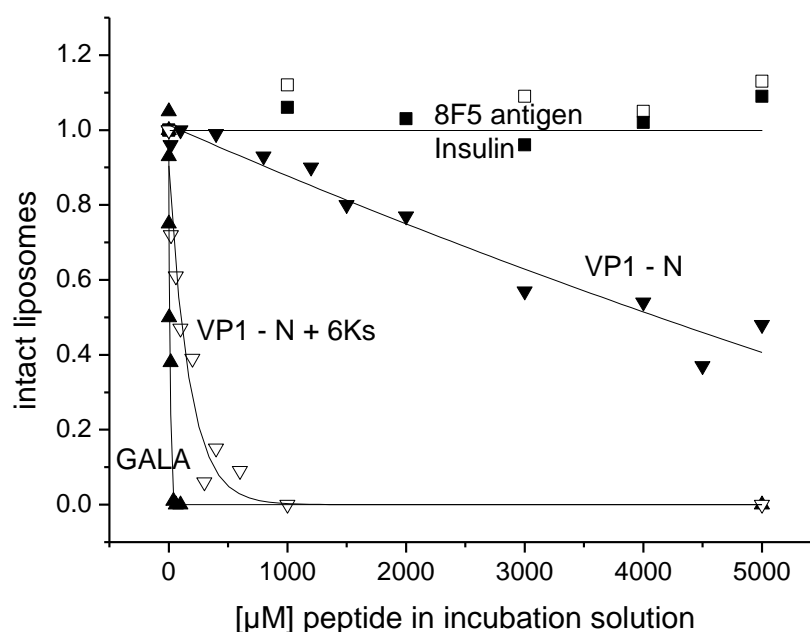


Fig. 37: Liposome leakage obtained for various peptides. Insulin and 8F5 antigen were employed as negative controls, GALA and the N-terminal peptide of VP1 as positive controls. Leakage was calculated as described in the text.

For the future we plan to record TEM images of lipid vesicles treated with our control peptides followed by statistic analysis of the obtained liposomes. We suggest that phosphotungsten acid, the contrast medium for TEM imaging, can enter permeabilized liposomes, i.e. liposomes exhibiting pores in their lipid bilayer. Such, we want to support our chip electrophoretic results.

### Experimental Section

**Chemicals:** Boric acid (99.99%) was purchased from Sigma Aldrich (Steinheim, Germany), sodium hydroxide (pellets pure) and sodium acetate trihydrate (ACS grade) were both from E. Merck (Darmstadt, Germany). Atto 495 in its free acid form (Atto Tec, Siegen, Germany) was obtained from Sigma Aldrich as

well. Sephadex G50 (DNA grade) and Cy5 were from Amersham Bioscience (Little Chalfont, England). Cy5 was dissolved in DMSO to obtain a 25 mM stock solution. DMSO (p.a.) and acetic acid (99%) were from Fluka (Buchs, Switzerland). Water was of Millipore grade. Lipids were as described (refer to 3.2) for *n-phls* and obtained from Avanti Lipids (Alabaster, AL, USA) via InstruChemie (Delfzijl, The Netherlands). Liposomes (90% POPC, 5% PEG750, 5% Ni-NTA; encapsulating 11 μM Atto 637, free acid form; in 50 mM sodium borate, pH 8.3; extrusion to 200 nm diameter) were prepared as detailed (refer to 3.2) and purified via spin SEC on the day of analysis (Sephadex G50 swelled in 50 mM sodium acetate buffer, pH 5.0; lipid concentration after SEC at approx. 1.96 mM). The peptides GALA (WEAALAEALAEALAEHLAEALAEALEALAA), VP1-N (NPVENYIDEVLNEVLVVPNINSSN) and VP-N + 6Ks (NPVENYIDEVLNEVLVVPNINSSNKKKKKK) were from GenScript (Piscataway, US); the peptide 8F5 antigen (VKAETRLNPDLQPTE) was from Pi Chem (Graz, Austria). Insulin chain A (ammonium salt from bovine pancreas, HPLC grade) was obtained from Sigma Aldrich.

**Instrumentation:** Chip electrophoretic leakage assays were carried out on Agilent 2100 Bioanalyzer employing DNA chips (Agilent Technologies, Waldbronn, Germany). Modifications in chip handling and analysis were as described (refer to 3.2). 100 mM sodium borate, pH 8.3 was employed as BGE.

**Sample preparation:** Leakage assays of peptides were carried out with 10 mM stocks of the investigated proteins solved in 50 mM sodium acetate buffer, pH 5.0. Starting from those stocks several lower concentrated protein stocks in the same buffer were prepared. Constant liposome sample volumes (1.5 μL after SEC) were mixed with respective protein solutions and the total volume was adjusted via 50 mM sodium acetate buffer, pH 5.0 to 3.0 μL, if necessary. For preparation of blank samples, liposomes were mixed with plain sodium acetate buffer. Incubation was carried out under light protection for 15 min at ambient temperature. Samples were re-neutralized with 12.0 μL of 80 mM sodium borate, pH 8.3 additionally containing approx. 3.8 μM Atto 495 as EOF marker.

**Data analysis:** Samples were analyzed twice on each of two independent DNA chips and the degree of leakage was calculated as ratio between peak areas of encapsulated and free dye related to an average ratio measured in the absence of any membrane permeabilizing agents.

### 3.4 Investigation of Membrane Disrupting Abilities of HRV2

After development of a chip based electrophoretic leakage assay (refer to 3.3) membrane disrupting abilities of intact HRV2 virions were assessed. Transfer of viral RNA through the endosomal membrane in the course of virus infection is either related to membrane disruption or to pore formation in the lipid bilayer. However, in the case of HRV2 the latter case was presumed (refer to 2.1.1). Literature further emphasizes membrane disrupting abilities of VP1 [76] and VP4 [84]. Therefore, I took interest in leakage from lipid vesicles caused by intact virions at different pH values. Furthermore, the degree of leakage caused by subviral particles as well as the role of receptor molecules in the leakage process was investigated.

A first experimental approach targeted leakage from lipid vesicles via intact virions of HRV2 at different pH values in the absence of receptor molecules. pH values were adjusted via 50 mM sodium acetate according to table 1. Samples were reneutralized via 80 mM sodium borate, pH 8.3 before chip electrophoresis. A surface fitted to resulting data points displays the interaction of virions with liposomes at different pH values and is presented in figure 38 for visualization of overall results (for presentation of individual data points refer to figure 39). As expected, especially for acidic pH values < 6.0 interaction of HRV2 with liposomes was found. No such interaction could be found for neutral pH values.

Acidification via 50 mM sodium acetate at indicated pH	pH value of incubation solution		pH value of reneutralized solution
5.0	5.1	Reneutralization via 80 mM sodium borate pH 8.3	8.0
5.3	5.5		8.1
5.6	5.9		8.2
5.7	6.6		8.3
5.8	7.1		8.3

Table 1: pH values during chip electrophoretic leakage assays employing intact virions.



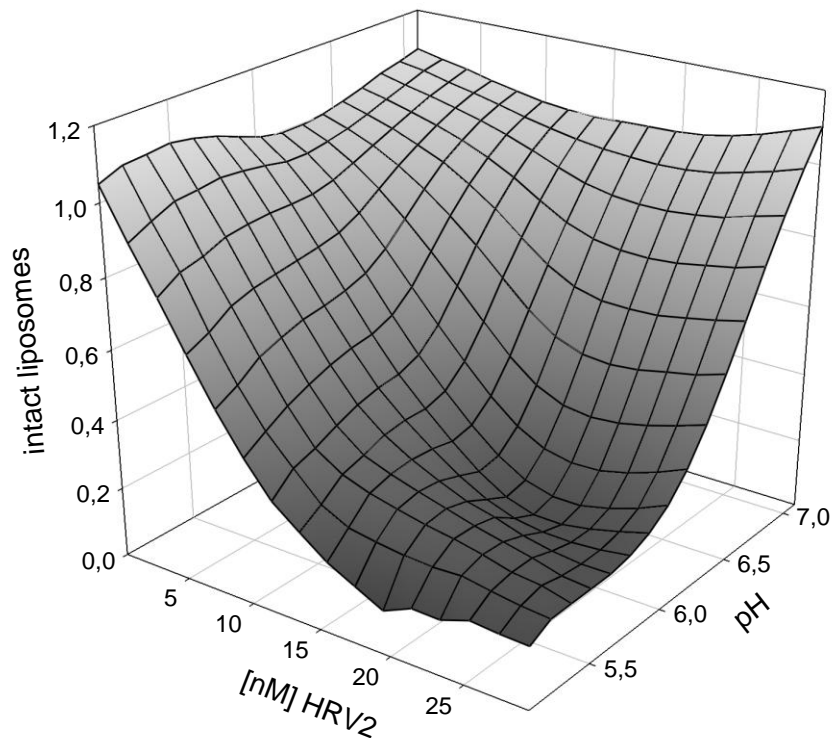


Fig. 38: Fitted surface based on data points obtained for chip electrophoretic leakage assays employing intact HRV2 virions as disrupting agents for lipid membranes at different pH values for visualization of overall results. Data points were obtained as peak area ratio between still encapsulated and already released dye and related to blank measurements (refer to 3.3).

In the course of chip electrophoretic leakage assays several problems related with leakage caused by intact virions occurred:

- (i) At virus concentrations of 5 nM (approx. 10 fold molar excess of virions over liposomal particles) and higher often spikes were recorded. Such results were assumed to be related to liposomes bridged together via hydrophobic viral intermediates.
- (ii) In contrast to electropherograms obtained for leakage induced by GALA (figure 36), leakage induced by HRV2 virions never resulted in a prominent increase in the area recorded for the free dye as concomitant effect for the decrease in the liposome signal.

- (iii) Even for incubation of virus / liposome mixtures at pH 5.1 no complete leakage of liposomes was detected. Seemingly, upon completed virus uncoating, subviral particles detached again from the liposome surface no longer allowing for leakage of dye molecules from lipid vesicles. Also, MVVs (refer to 2.1.2) might be responsible for incomplete leakage. Upon membrane disruption via HRV2, still some liposomes remained intact, which were previously encapsulated by other lipid membranes and could thus not be targeted by virions in the course of their uncoating.

Nevertheless, the pH and concentration dependence of virus interaction with liposomes could be assessed via chip electrophoretic leakage assays. Figure 39 highlights these features. Interaction between liposomes and virions is only detectable at sufficiently low pH values and sufficiently high virus concentrations (measured at a calculated constant liposome concentration of approximately 0.5 nM). No virus / liposome interaction is detectable if one of these requirements is not met. These findings are in excellent accordance with results following the viral RNA transfer through plasma membranes via encapsulated RT-PCR kits (Bilek, G. et al., results under publication). Processing of transferred viral RNA was only detected in the case of complete shielding of encapsulated kits in the liposome interior from the employed external matrix. However, this shielding could only be accomplished for sufficiently low virus concentrations. Corresponding virus concentrations did not result in liposome leakage in chip electrophoretic experiments.

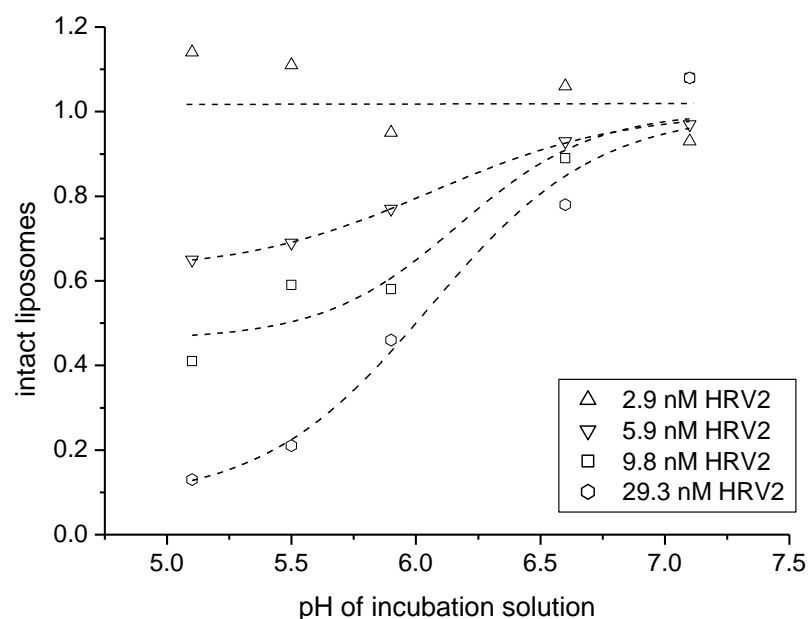


Fig. 39: Interaction between liposomes and HRV2 virions is dependent on sufficiently low pH values and sufficiently high virus concentrations (measured at a constant liposomes concentration

of approximately 0.5 nM). If one of these requirements is not met, no virus / liposome interaction is detectable. Virus / liposome interaction was assessed via chip electrophoretic leakage assays as described (refer to 3.3).

Interaction of liposomes and virions is also conclusive from liposome mobility data obtained from measurements at pH 5.1 incubation (figure 40). Recorded was the mobility shift of the liposome peak upon incubation with different virus concentrations measured at a constant liposome concentration of approx. 0.5 nM. This mobility shift was related to the peak of non encapsulated Atto 637 as internal standard. Interestingly, a decline in the mobility difference of liposomes and the internal standard with increasing virus concentrations was detectable. It resulted from viral modifications (either subviral capsids adherent to or viral proteins anchored in the lipid membrane) of the liposome surface. Investigation of the effect of higher virus concentrations on liposome mobility was limited because of spike formation and finite concentrations of virus stock solutions.

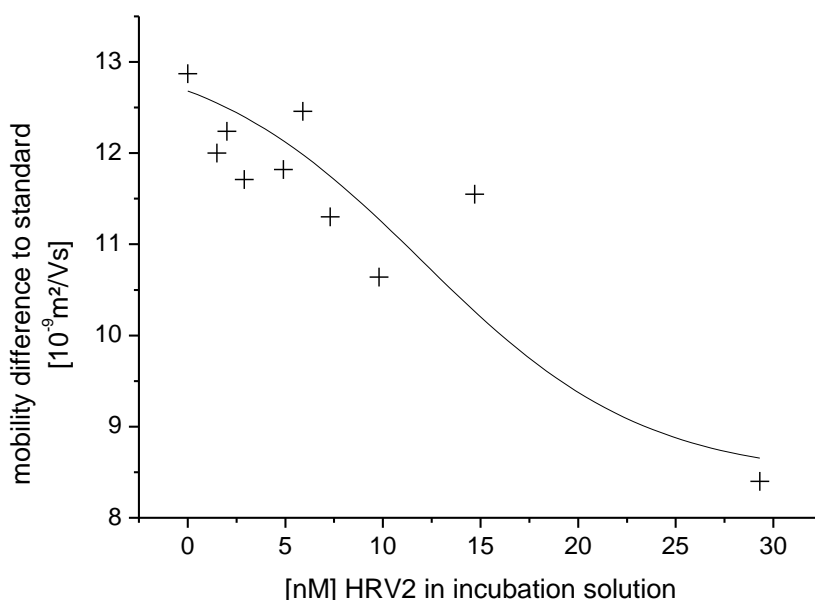


Fig. 40: Mobility shift of liposome peak upon its modification via subviral particles or viral proteins. Recorded was the mobility shift of the liposome signal related to free Atto 637 as internal standard. Chip electrophoretic leakage assays were carried out with intact virions and incubation at pH 5.1.

Following experiments dealt with leakage caused by subviral particles. Therefore virions were acidified to pH 5.1 before liposomes were introduced to the samples. Chip electrophoretic leakage assays were carried out as described (refer to 3.3). From the resulting curves (figure 41) it was concluded that spatial proximity of virions to membranes during the viral uncoating process was essential to observe leakage from lipid vesicles.

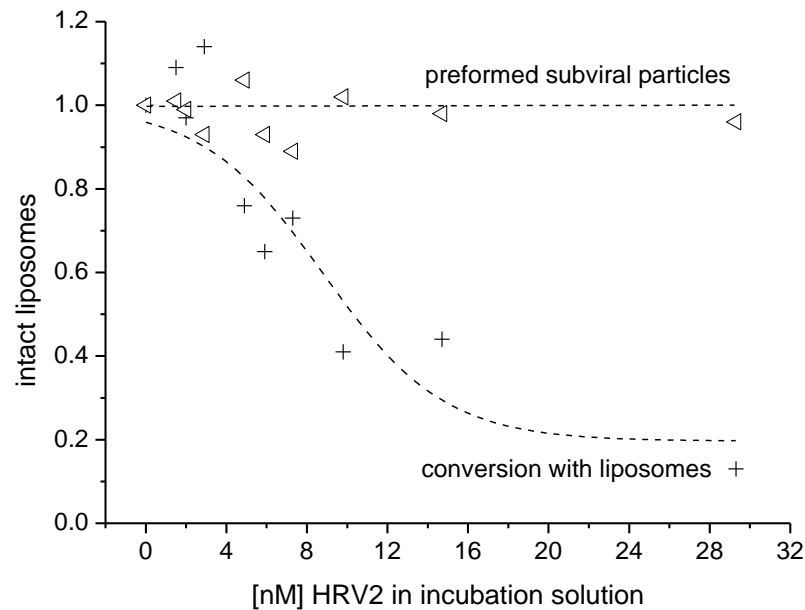


Fig. 41: Comparison of leakage induced via viral and preformed subviral particles upon incubation with liposomes at pH 5.1. Clearly no leakage is detectable for incubation with preformed subviral particles, whereas for virus conversion in the presence of liposomes a high amount of leakage is detected. Data points resulted from chip electrophoretic leakage assays (refer to 3.3).

Finally, also the contribution of receptor mediation to liposome leakage was assessed. Chip electrophoretic leakage experiments were carried out after incubation of liposomes with two different recombinant soluble receptor fragments. Receptor decoration was followed by virus attachment to receptor decorated membranes and acidification of obtained assemblies to pH 5.1 (for characterization of assemblies refer to 3.2). Two different receptor fragments were employed exhibiting different binding strengths to HRV2 virions, respectively. Those receptor fragments were derived from the cellular receptor VLDLR, which is supposed to facilitate HRV2 endocytosis (refer to 2.1.1). VLDLR consists of 8 binding domains from which the third binds strongest to binding sites around the fivefold axis on the viral capsid. According to the viral icosahedral symmetry up to five receptor

domains are able to bind simultaneously to star-shaped dome sites on the capsid. A recombinant soluble receptor consisting of five binding domains number 3 of the VLDLR arranged in tandem (MBP-V33333) therefore exhibits strongest binding affinity to the virus surface [75]. It was therefore chosen as one receptor fragment for the experimental setup. On the other hand a recombinant receptor derived from domains 1 – 3 of VLDLR (MBP - V123) was investigated as well. This receptor fragment exhibited lower binding affinity to virions than MBP-V33333. Figure 42 depicts the resulting leakage curves.

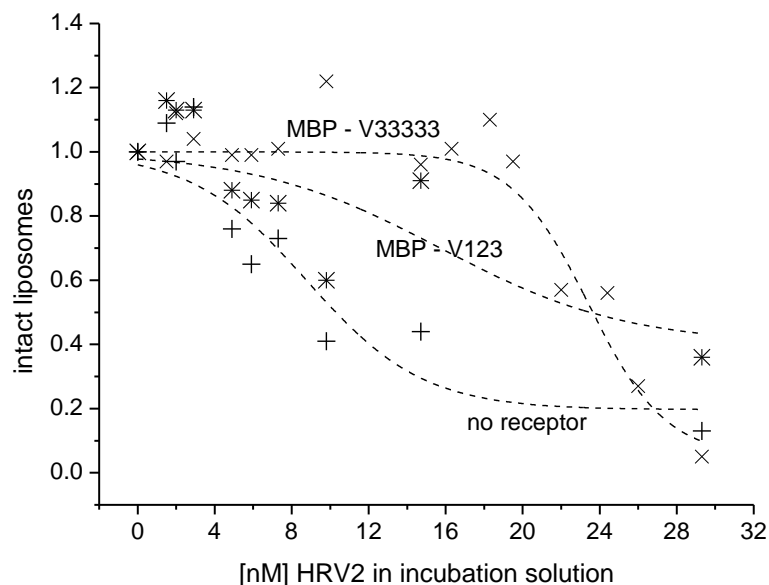


Fig 42: Contribution of receptor mediation to virus induced liposome leakage detected via chip electrophoresis. Upon application of soluble receptor fragments for virus / receptor / liposome adduct formation followed by acidification of obtained mixtures a shift in the obtained leakage curves to higher virus concentrations was observed. This shift probably resulted from receptor molecules in free solution stabilizing virions during the uncoating process. Interestingly, receptor fragments could not be attached completely to liposome surfaces albeit a molar excess of  $\text{Ni}^{2+}$  over His6-tags as observed already for the formation of receptor mediated assemblies (refer to 3.2).

Interestingly, upon acidification of a virus / liposome adduct mediated via MBP-V33333 (liposome concentration approx. 0.5 nM; receptor concentration approx. 6.3  $\mu\text{M}$ ; virus concentration as indicated) leakage was shifted to higher virus concentrations than in the absence of receptor mediation. Also, at high virus concentrations, less intact liposomes were obtained upon receptor mediation. Furthermore, also the drop in a curve fitted to the data points obtained for leakage upon receptor mediation was limited to a smaller virus concentration window. It was thus concluded that:

- (i) Not all receptor molecules were attached to Ni<sup>2+</sup> although Ni<sup>2+</sup> loaded lipid was employed in molar excess over receptor molecules. This result, though unexpected, is in good accordance with data presented under 3.2, where receptor mediated adduct formation between virions and liposomes was investigated in detail. In the course of these experiments it was observed as well that binding of His6 tagged receptor fragments to Ni<sup>2+</sup> loaded liposome surfaces was not complete (as deduced from recorded peaks for virus / receptor complexes even in the presence of liposomes). Also with these experiments Ni<sup>2+</sup> had been employed in molar excess.
- (ii) Receptor molecules not bound to liposome surfaces but present in free solution do not facilitate virus interactions with membranes but additionally stabilize virions against uncoating [7]. This effect explains the shift to higher virus levels recorded in liposome leakage assays.
- (iii) The importance of receptor mediation for the transfer of viral RNA through membranes can be deduced from faster dropping leakage curves as well as from lower levels of intact liposomes upon carrying out leakage experiments under receptor mediation. As soon as the ratio between virions and recombinant receptor fragments is such that virus capsids are no longer stabilized but conditions allow for virus uncoating (virus concentrations of 20 nM or higher), dye leakage from liposomes is recorded for a comparatively narrow virus concentration window. However, it was reported that *in vivo* at acidic pH conditions of virus uncoating (around pH 5.6) the virus / receptor complex had already dissociated (refer to 2.1.1). We therefore suppose that the importance of receptor mediation does not lie with the transfer process itself, but with the arrangement of spatial proximity between virions and membranes before the actual uncoating process.
- (iv) As expected, application of a receptor with lower affinity to virions (MBP-V123) in the course of the formation of receptor mediated virus / liposome adducts yielded intermediate leakage results in between those with receptor mediation via MBP-V33333 and those without receptor mediation.

Similar to leakage results in the absence of recombinant receptor fragments (refer to figures 38 – 39) again problems upon application of higher virus concentrations were experienced. In such electropherograms often spikes are recorded. In contrast to results without receptor mediation, however, the respective virus concentrations causing leakage from liposomes were shifted to higher values (depending on receptor affinity to virions and virus / receptor ratio).

As for the non-receptor mediated case, data obtained from dye leakage experiments upon receptor mediation can be supported by liposome mobility data (figure 43). Depicted is the resulting curve for mediation via MBP-V33333 and acidification to pH 5.1. At low virus concentrations (up to approx. 2 nM HRV2) the recorded liposome mobility related to the mobility of released dye as internal marker changes strongest. After reaching a plateau in the mobility difference between liposomes and the marker (approx. 2 - 10 nM HRV2), the mobility difference is again decreasing upon application of higher virus concentration (10 nM or higher HRV2 content). These findings can be explained by fairly stable virus / receptor conditions at the liposome surface for a HRV2 concentration window of approx. 2 - 10 nM. Increasing the HRV2 concentration even further leads to a decrease in the receptor / virus ratio at the liposome surface. This in turn leads to a decline in liposomal mobility. In fact, comparison of liposome mobility shifts reveals that for high virus content shifts in liposome mobility slowly resemble, regardless of receptor mediation (figure 44). This can be explained by the decline of the number of receptor molecules compared to the number of virus particles.

Interestingly, upon mediation via MBP-V33333, virus induced leakage from liposomes was only recorded for virus concentrations of 20 nM or higher, although mobility data suggests saturation of virions with recombinant receptor fragments at the liposome surface already for virus concentrations of approx. 10 nM. It seems as if in the virus concentration window between 10 and 20 nM still enough receptor fragments are present in solution to allow for additional virus stabilization against pH induced uncoating. However, the number of receptor molecules per virion is constantly declining. Below a threshold of receptor fragments per virion, no additional stabilization against virus uncoating is possible yielding dye leakage from liposomes.

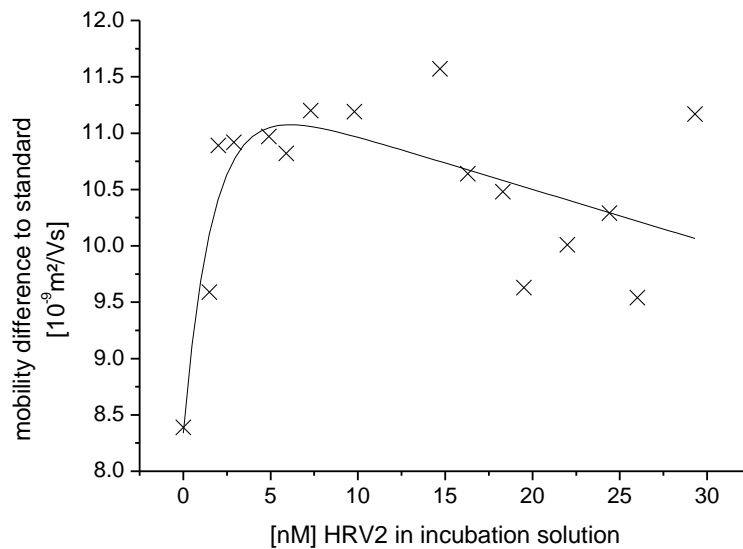


Fig. 43: Interaction of virions with liposomes upon receptor mediation is accessible from mobility data. Depicted are results for MBP-V33333 mediation and acidification to pH 5.1. For virus concentrations up to approximately 2 nM a high shift in liposome mobility was recorded corresponding to the formation of receptor mediated virus / liposome complexes. The mobility shift then reaches a plateau (from 2 nM to approximately 10 nM virus concentration) which can be explained by a still sufficiently high number of recombinant receptor fragments in solution to allow for maintenance of virus / receptor conditions at liposome surfaces. At higher virus concentrations these conditions can no longer be maintained, the ration between receptor molecules and virus particles on the liposome surface decreases which in turn leads to a decrease of the liposomal mobility shift.

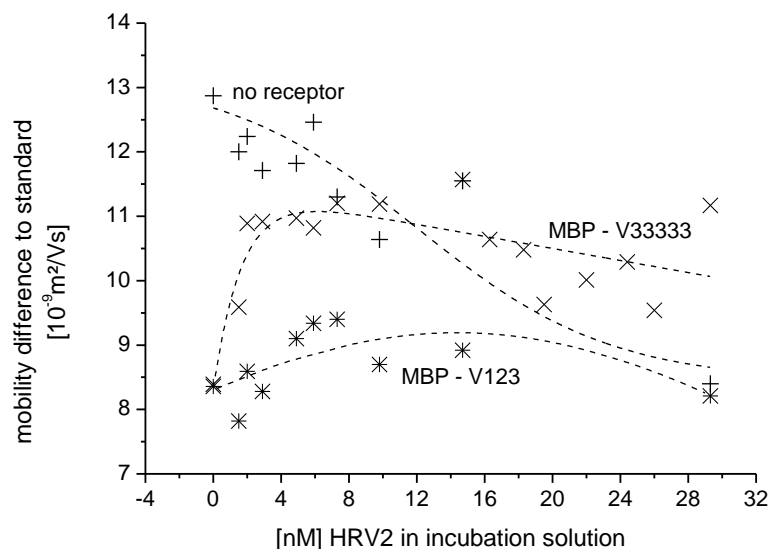


Fig. 44: Comparison of liposome mobility curves upon virus induced liposomal leakage. For high virus concentrations mobility curves start to slowly resemble regardless of receptor mediation because the ratio between recombinant receptor fragments and virus particles on the liposome surface declines.



As an overall result of these experiments one can conclude that a very important goal for future experiments lies in a better attachment of receptor molecules to the liposome surface. This effect might either be obtained by application of other Ni<sup>2+</sup> chelating lipids in the liposome surface (for instance application of tris-nitrilotriacetate groups instead of mono-nitrilotriacetate moieties) or by application of native receptor molecules incorporated into the liposomal membrane.

## Experimental Section

**Chemicals:** Boric acid (99.99%) was obtained from Sigma Aldrich (Steinheim, Germany), sodium hydroxide (pellets pure) and sodium acetate trihydrate (ACS grade) were from E. Merck (Darmstadt, Germany). Atto 495 in its free acid form was from Atto Tec (Siegen, Germany) and obtained as well from Sigma Aldrich. Acetic acid (99%) and DMSO (*p.a.*) were from Fluka (Buchs, Switzerland). Sephadex G50 (DNA grade) and Cy5 were from Amersham Bioscience (Little Chalfont, England). Cy5 was dissolved in DMSO to obtain a 25 mM stock solution. Water was of Millipore grade. Lipids were as described (refer to 3.2) for *n-phl* and obtained from Avanti Lipids (Alabaster, AL, USA) *via* Instruchemie (Delfzyl, The Netherlands). Liposomes (90% POPC, 5% PEG750, 5% Ni-NTA; encapsulating 11 μM Atto 637, free acid form; in 50 mM sodium borate, pH 8.3; extrusion to 200 nm diameter) were prepared as described (refer to 3.2) and purified via spin SEC on the day of analysis (Sephadex G50 swelled in 20 mM sodium borate buffer, pH 8.3; lipid concentration after SEC at approx. 2.94 mM).

**Biological Material:** Production of HRV2 as well as assessment of its purity and concentration was as described [8, 46]. An aliquot of 5.4 mg/mL in 50 mM sodium borate, pH 7.4 was employed for experiments. It was diluted to 2.2 mg/mL virus concentration with Millipore water prior to further dilution steps in 20 mM sodium borate, pH 8.3. Recombinant receptor fragments of the VLDLR were in 20 mM Tris-HCl, pH 7.5, 150 mM NaCl and 10 mM CaCl<sub>2</sub> [75]. One receptor consisted of five receptor domains number 3 arranged in tandem V33333, another of the first three receptor binding domains V123. Both recombinant receptors were fused to His6-tags at their C- and to MBP at their N-termini. MBP-V33333 was at 5.5 mg/mL and MBP-V123 at 8.0 mg/mL. MBP-V123 was diluted to 4.8 mg/mL in its storage buffer prior to application.

**Instrumentation:** HRV2 mediated dye leakage from liposomes was investigated as described (refer to 3.3). Upon relating the peak area of the free dye to the area of liposomes in case of leakage and upon relating this ratio again to an average from blank measurements sometimes values of 150% or higher were calculated (because of recorded spikes). However, these values (corresponding to 150% of intact liposomes upon application of leakage conditions or higher) were not considered for calculation of average values for intact liposomes under such investigated incubation conditions.

**Sample preparation:** SEC purified liposomes were receptor decorated at ambient temperature for 10 min. Alternatively, for experiments in the absence of recombinant receptor molecules, receptor storage buffer was employed. Receptor decorated liposomes were incubated with virus dilutions in 20 mM sodium borate, pH 8.3 again at ambient temperature for 10 min. Receptor mediated adducts (2.3  $\mu$ L) were acidified with 50 mM sodium acetate buffer (2.9  $\mu$ L) at different pH values for incubation at 5.1 - 7.1, respectively (ambient temperature, 15 min). Such, SEC purified liposomes were diluted 1:4, receptor stock 1:13, HRV2 in 20 mM sodium borate, pH 8.3, 3:26 for application in the incubation solution. Incubation solutions were reneutralized with 10.4  $\mu$ L of 80 mM sodium borate, pH 8.3 prior to chip electrophoretic analysis. For formation of subviral particles in the absence of lipid membranes the mixing order of sample constituents was adapted. Virus was acidified (10 min, ambient temperature) before addition of a liposomes/receptor storage buffer mix was carried out. Subviral particles were incubated with lipid membranes for 15 min at ambient temperature.

**Data analysis:** Leakage was calculated as described (refer to 3.3). Mobility differences to the free dye peak were related to the middle of the liposomal signal. Because of recorded spikes mobility calculations with the apex of the liposomal peak did not seem reasonable. Apparent mobility values for both sample constituents were calculated and the mobility difference was plotted.

## 3.5 RNA Transfer of HRV2 through Membranes

State of publication: experimental phase

Contributing authors: Victor U. Weiss – 60%

Gerhard Bilek – 25%

Xavier Subirats – 15%

### Introduction and Molecular Beacon Design

Molecular beacons (MBs) are short single stranded oligonucleotides forming an intramolecular hairpin structure consisting of a stem and a loop region. Upon modification of the oligonucleotide arms with a corresponding fluorophore / quencher pair, MBs are functionalized as FL hybridization probes [e.g. 85 – 91]. The closed hairpin structure of beacons leads to spatial proximity of the fluorophore / quencher pair, which in turn renders the beacon non-fluorescent. According to the mode of quenching, FL is either quenched via direct energy transfer to the quencher that dissipates energy as heat or via fluorescence resonance energy transfer (FRET). In the latter case emitted light of the fluorophore leads to FL excitation of the quencher [88]. Emitted FL is thus shifted to longer wavelengths. Upon specific binding of the loop region to a corresponding target sequence, the MB undergoes a conformational change to an energetically more favourable intermolecular duplex strand. The hairpin structure of the beacon is thus severed and the spatial proximity of the fluorophore / quencher pair lost; FL is reported to occur instantaneously even for incubation at room temperature. For our experiments we developed an MB specifically targeting the HRV2 RNA genome. Upon encapsulation of molecular beacons in liposomes, we intended to follow the viral RNA genome transfer through membranes. The genome of several other viruses has already been targeted successfully in living cells upon application of MBs [92 – 94]. However, application of MBs *in vivo* often leads to problems because of MB digestion resulting in a high FL background. Furthermore, cellular ionic conditions tend to lead to false positive responses [89, 90]. Therefore, in order to circumvent those problems and also to concentrate on the viral RNA transfer itself through membranes, we opted for the well defined membrane conditions of our liposomal model system. We

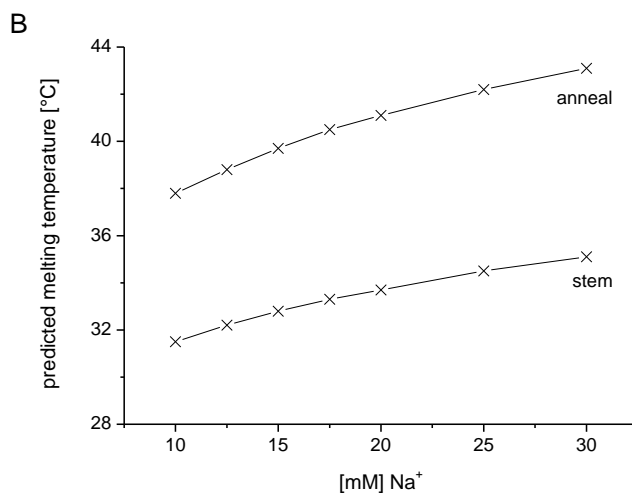
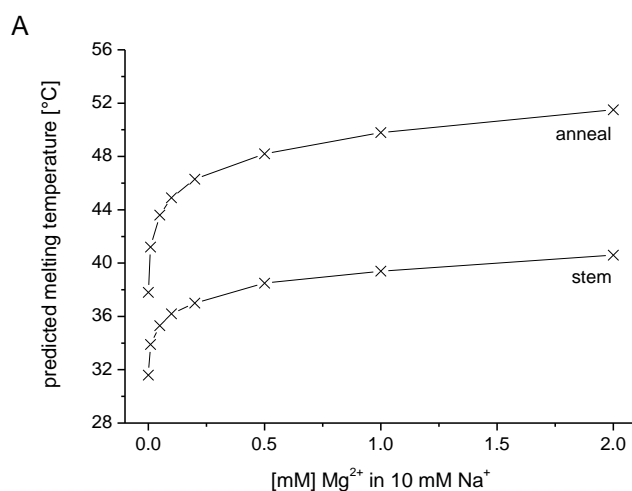
intended to employ chip electrophoresis to detect FL liposomes, i.e. viral genome transfer through membranes reported via MBs. Although CE of beacons has already been reported [95], previous work was based on UV detection and solely concentrated on MB hybridization to short oligonucleotide target sequences. To my knowledge, neither has viral RNA been targeted previously via MBs in CE, nor was the RNA transfer through membranes targeted itself in an analytical electrophoresis setup.

In the course of the MB design process several aspects have to be considered:

- (i) The oligonucleotide target region of the beacon loop has to be accessible for hybridisation, i.e. not highly structured [96, 97]. Therefore, we opted in our experimental setup for targeting of a loop region in the internal ribosomal entry site (IRES) of the HRV2 genome. This IRES sequence has already been predicted in our laboratory as single stranded RNA region via computational folding programs.
- (ii) Loop and stem regions of MBs have to be adjusted in nucleotide number and base content such, that formation of an intramolecular hairpin structure is energetically possible under the anticipated experimental conditions in free solution. However, formation of a duplex strand with the target sequence has to be energetically favoured over intramolecular hybridization. This requires the annealing temperature of the beacon loop to the target sequence to exceed the melting temperature of the stem region. Such, slightly increased temperatures lead to open hairpin structures that are still able to hybridize to target oligonucleotides. Annealing and melting temperatures can be estimated in several ways [98]. One approximation for short oligonucleotides (up to approx. 15 nucleotides) estimates the contribution of each AT base pair with 2.0°C and of each GC pair with 4.0°C to the oligonucleotide melting temperature. Another way of estimating the melting temperature is based on the GC percentage of the nucleotide sequence. This method is proposed for long oligonucleotide sequences. The nearest-neighbour model finally considers thermodynamic data of neighbouring base pairs upon estimation of melting temperatures. The

Rensselaer bioinformatics web server of Michael Zuker [99 – 101] offers the opportunity of online prediction of melting and annealing temperatures of oligonucleotide sequences as well as prediction of oligonucleotide folding to thermodynamically stable structures.

- (iii) Computational approaches [101] can be employed for prediction of MB melting and annealing temperatures dependencies on various parameters. For instance buffer ionic strength (expressed via the concentration of the monovalent cation  $\text{Na}^+$ ) [89] as well as the  $\text{Mg}^{2+}$  content [87] of the buffer solution and the oligonucleotide concentration itself were found to influence melting and annealing temperatures of molecular beacons. Figure 45 demonstrates these dependencies. In short, it can be concluded that higher concentrations of monovalent cations,  $\text{Mg}^{2+}$  or oligonucleotides increase beacon melting and annealing temperatures:



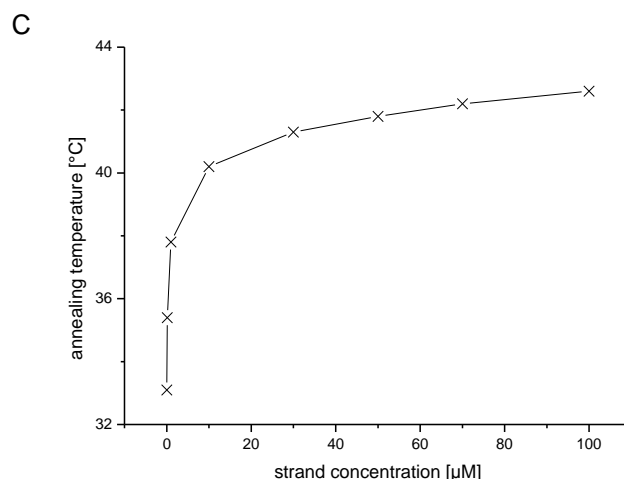


Fig. 45: Predicted stem melting and loop annealing temperatures [99 – 101] for an exemplary molecular beacon of the design `acgcTTTTTTTTTTTTTTTTTTTTTTTTTTTTTgcgt`. Depicted are dependencies on  $[Mg^{2+}]$  (A) at constant  $[Na^+]$  of 10 mM (this value corresponds approximately to 70 mM sodium borate, pH 8.3) and dependencies on  $[Na^+]$  (B) in the absence of  $Mg^{2+}$ . Calculations were carried out via the  $T_M$  server for stem melting and via the 2-state hybridization server for annealing temperatures. Annealing was calculated to an oligonucleotide consisting of 60 A at 1  $\mu M$  total oligomer concentration (probe and target sequence together, half of the given strand concentration value is assigned to each sequence, respectively). (C) relates computed annealing temperatures to the total concentration of oligonucleotides present in the sample solution. Calculations were carried out for constant  $[Na^+]$  at 10 mM in the absence of  $Mg^{2+}$  for annealing to a 60 A oligonucleotide.

- (iv) Proximal G-bases additionally quench attached fluorophore molecules [102].
- (v) The length of the loop region influences the relative position of the modified arms of the MB stem upon hybridization to the target sequence. For probe lengths of 13, 25 or 35 nucleotides both arms were found to form a *trans*-position upon binding to the target sequence [87]. *Trans*-position of MB arms in the opened state is important because of increased spatial distance between fluorophore and quencher leading to a maximum FL signal upon probe binding.

In accordance with the considerations detailed above, we designed a molecular beacon targeting the IRES region of the HRV2 genome (figure 46). We opted for a 5 nucleotide stem flanking a 25 nucleotide loop region. FL modification was carried out at the 5' end

proximal to an A base. The beacon was modified via carboxyfluorescein (FAM) for FL in-batch measurements and via Cy5 for CE because of higher detection sensitivity of the corresponding laser. The 3' end was modified via a Black Hole Quencher (BHQ), respectively. The stem melting temperature was predicted to 48.4°C, the annealing temperature to 52.7°C in 10 mM Na<sup>+</sup> including 0.5 mM Mg<sup>2+</sup> (corresponding to 70 mM sodium borate, pH 8.3, 0.5 mM MgCl<sub>2</sub>) at 0.5 μM total oligonucleotide concentration. These values corresponded to a free energy of -1.3 kcal/mol for closed hairpin structure and -19.0 kcal/mol for the hybridized beacon [101]. Annealing to a HRV2 genome sequence of 64 nucleotides including the IRES even resulted in a predicted temperature of 58.8°C (free energy of -21.0 kcal/mol). In the latter case additional interactions of the beacon stem with nucleotide regions flanking the IRES sequence were regarded.

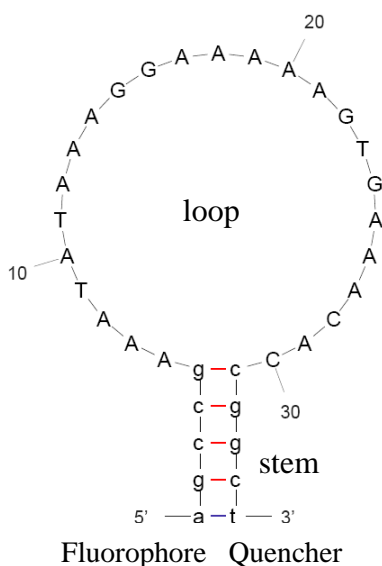


Fig. 46: Folded MB targeting the IRES sequence of HRV2. Folding was predicted [99 – 101] and the image obtained from [101].

## Results and Discussion

Our experiments intended to evolve a chip electrophoretic method to follow the viral RNA transfer of HRV2 through membranes. In order to do so, we first had to ensure correct folding of the MB in free solution to its closed state to arrange for intramolecular quenching. Quenching of MBs can be influenced via ionic strength and Mg<sup>2+</sup> content of respective buffer solutions as shown in the prediction above. Figure 47 demonstrates the resulting FL signals obtained via in-batch measurements of FAM labeled MB upon mixing with 50 mM sodium borate, pH 8.3 at different ionic strength values adjusted via NaCl (A)

or upon addition of  $\text{MgCl}_2$  (B). Quenching of the FL signal was found for NaCl concentrations of 100 mM or more or  $\text{MgCl}_2$  concentrations of 0.5 mM or higher. For further experiments, we opted for  $\text{MgCl}_2$  addition to buffers in anticipation of CE measurements; Application of buffers with high salt concentration creates high currents in CE and was therefore avoided.

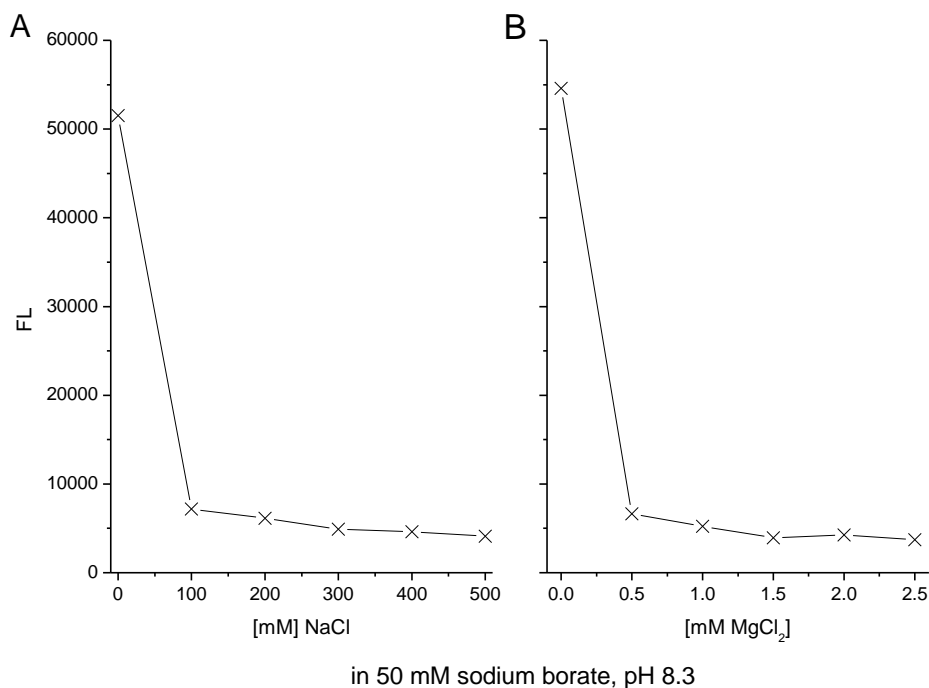


Fig. 47: In batch measurements of an HRV2 IRES targeting molecular beacon; beacon sequence: agccgAAATATAAAGGAAAAAGTGAAACACcgct. The beacon was modified via FAM (5') and via a BHQ (3'). Measurements were carried out with 100 nM MB concentration in 50 mM sodium borate, pH 8.3 and variable NaCl (A) or  $\text{MgCl}_2$  (B) concentration as indicated. Instrumentation: 1420 Multilabel Counter Victor<sup>2</sup> from Perkin Ellmer.

After preliminary experiments on intramolecular quenching of MBs, we checked the applicability of MB samples with  $\text{MgCl}_2$  containing buffers in CE. In order to minimize sample stacking effects, we introduced the same concentration of  $\text{MgCl}_2$  to both electrophoresis buffers, the BGE and the sample buffer, respectively. In good accordance with results from in-batch measurements, we found the  $\text{Mg}^{2+}$  concentration of buffers crucial for complete intramolecular FL quenching of the beacon. Up to  $\text{MgCl}_2$  concentrations of 0.25 mM we still obtained signals for completely or partially unquenched



MBs. Upon application of higher  $\text{MgCl}_2$  concentrations we did not obtain any FL peaks resulting from the beacon. Figure 48 depicts resulting electropherograms.

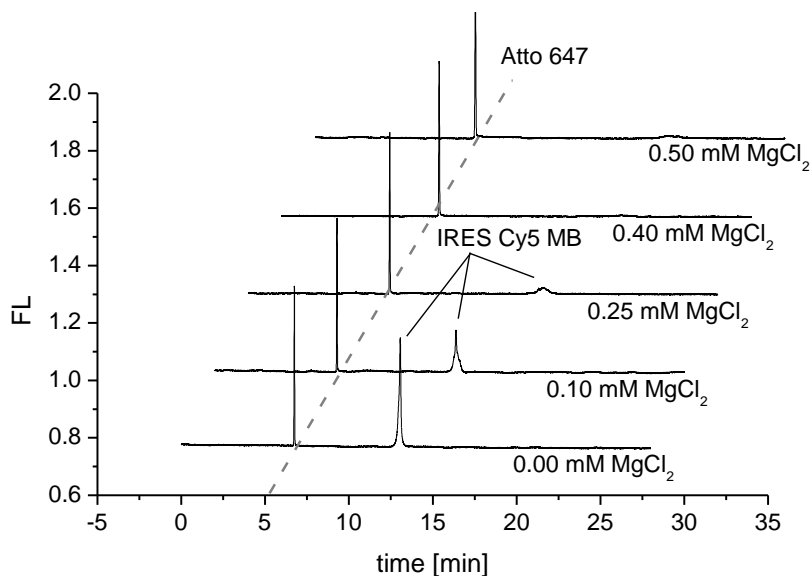


Fig. 48: CE of MBs depicting the influence of the  $\text{MgCl}_2$  content of electrophoresis buffers on MB conformation. A closed hairpin structure of the MB can be achieved by addition of 0.4 mM  $\text{MgCl}_2$  to electrophoresis buffers. CE at + 20 kV, 30.0°C and detection via Picometrics ZETALIF HeNe laser ( $\lambda_{\text{ex}} = 633 \text{ nm}$ ); Capillary: fused silica, 50  $\mu\text{m}$  inner diameter, 375  $\mu\text{m}$  outer diameter,  $L_{\text{tot}} = 72.2 \text{ cm}$ ,  $L_{\text{eff}} (\text{UV}) = 23.5 \text{ cm}$ ,  $L_{\text{eff}} (\text{FL}) = 57.2 \text{ cm}$ ; BGE: 100 mM sodium borate, pH 8.3 including variable  $\text{MgCl}_2$  concentrations; Sample: 100 nM MB targeting the HRV2 IRES sequence and labeled via Cy5, 25nM Atto 647 (internal standard) and DMSO 1 : 4 x 10<sup>3</sup> in 50 mM sodium borate, pH 8.3. The  $\text{MgCl}_2$  concentration of samples corresponded to respective BGE values.

However, upon application of  $\text{MgCl}_2$  in the BGE we experienced a drop in EOF from  $66.7 \pm 1.9 \times 10^{-9} \text{ m}^2/\text{Vs}$  (no  $\text{MgCl}_2$ ; n = 4 measurements) to  $50.5 \pm 0.6 \times 10^{-9} \text{ m}^2/\text{Vs}$  (0.5 mM  $\text{MgCl}_2$ ; n = 10 measurements). Because of this decline in EOF we did not investigate application of higher  $\text{MgCl}_2$  concentrations in electrophoresis buffers.

As shown in figure 48, the signal obtained for the MB declined upon addition of  $\text{MgCl}_2$  to electrophoresis buffers. Digestion of the MB via DNase I lead to regained FL. Such, we demonstrated the loss of FL upon application of  $\text{MgCl}_2$  to electrophoresis buffers to be related to intramolecular quenching of the beacon. Figure 49 depicts a respective

electropherogram for a digested MB sample. Upon application of electrophoresis conditions which previously yielded no FL signal for the beacon, we now obtained three FL peaks with mobility values of  $18.5 \pm 0.1$ ,  $23.4 \pm 0.2$  and  $26.3 \pm 0.2$  [ $10^{-9}$  m<sup>2</sup>/Vs]. The FL intensity of different MB fragment peaks varied according to incubation conditions. However, from these results we concluded that via addition of MgCl<sub>2</sub> to electrophoresis buffers we were able to shift the MB conformation to its closed state. For further measurements we finally opted for 0.5 mM MgCl<sub>2</sub> addition to electrophoresis buffers in order to obtain complete intramolecular quenching.

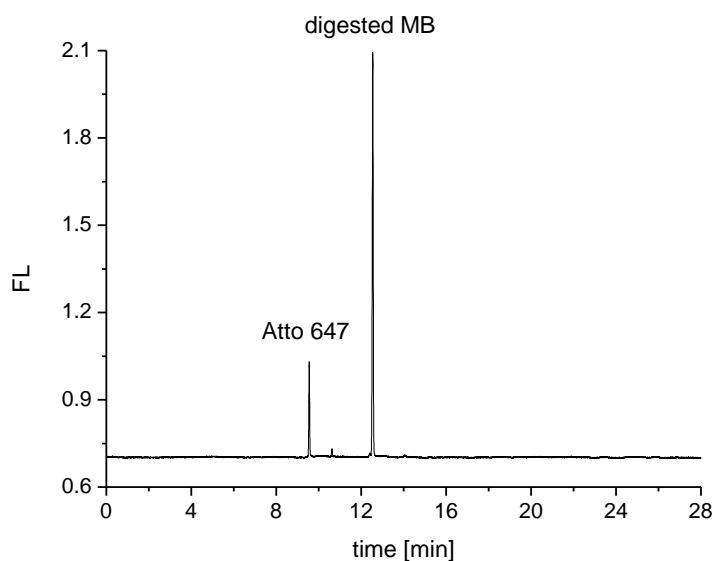


Fig. 49: Digest of HRV2 IRES targeting MB, Cy5 labeled. FL was recorded under CE conditions, which had previously not yielded a peak for the undigested beacon (compare to figure 48). CE and capillary as with figure 48. BGE: 100 mM sodium borate, pH 8.3 including 0.5 mM MgCl<sub>2</sub>. Sample: 100 nM IRES targeting MB, Cy5 labeled, 50 nM Atto 647 (internal standard) and DMSO 1 :  $4 \times 10^3$  in 50 mM sodium borate, pH 8.3 including 0.5 mM MgCl<sub>2</sub>. The sample was digested via DNase I.

As expected and demonstrated from figure 50, intramolecular quenching of the MB achieved via addition of MgCl<sub>2</sub> to electrophoresis buffers nevertheless did not influence the reactivity of the beacon towards its nucleotide target sequence. Upon incubation of MB samples with corresponding positive and negative control oligonucleotides under intramolecular quenching conditions, we only recorded a FL peak for samples including positive control oligomers. Interestingly, first results hinted a rather slow kinetic of duplex strand formation of the MB with the positive control oligonucleotide. In fact, even after

150 min incubation at ambient temperature we still recorded an increase in the product peak area related to the peak area of the internal standard (data not shown).

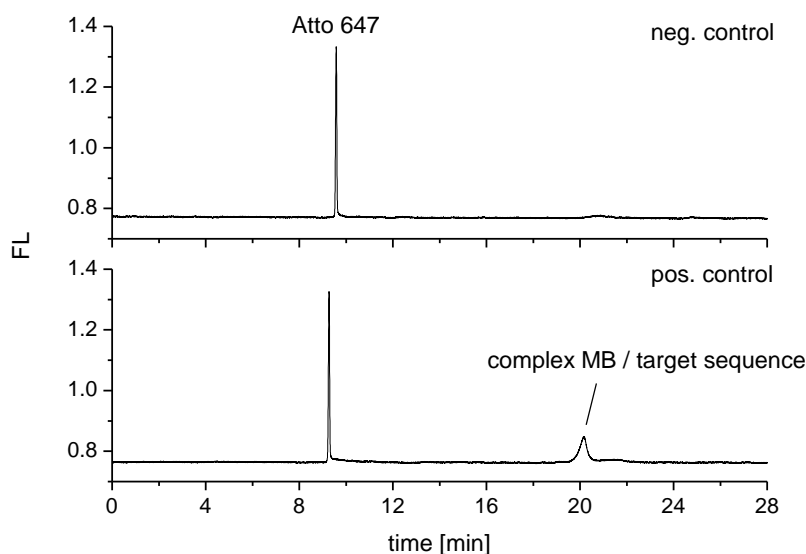


Fig. 50: Incubation of HRV2 IRES targeting MB, Cy5 labeled with negative and control oligonucleotide sequences. Only incubation with the positive control yielded an additional FL peak. CE and capillary as with figure 48, BGE and sample composition as with figure 49. Samples additionally contained 50 nM of control oligonucleotide sequences, respectively. Incubation was for approximately 40 min at 30.0°C in the sample tray of the instrument.

Upon incubation of MB with RNA released from HRV2 capsids through heat denaturation we obtained several sharp peaks as presented with figure 51. Obtained peaks were clearly no spikes and exhibited declining intensities. Recorded peak mobilities ranged from  $19.3 \pm 0.2$  to  $20.2 \pm 0.1$  [ $10^{-9}$  m<sup>2</sup>/Vs] for 67.5 nM HRV2 and from  $20.7 \pm 0.02$  to  $21.4 \pm 0.1$  [ $10^{-9}$  m<sup>2</sup>/Vs] for 33.8 nM HRV2 containing samples. Calculation of peak mobilities was carried out from duplicate measurements. From recorded mobilities we excluded the possibility that obtained peaks resulted from digested MBs (compare with mobility values presented above for DNase digested beacon). Peak sharpness may be related to large analyte size and charge; the molecular weight of viral RNA values around 2.2 MDa which leads to decreased longitudinal diffusion inside the capillary. Also interaction of nucleotides with Mg<sup>2+</sup> might cause a local gradient in the MgCl<sub>2</sub> concentration leading as well to peak sharpening. The unexpected high number of obtained FL peaks might be related to MB attachment to differently folded viral RNA molecules. Also several thermodynamically stable MB hybridization products with the roughly 7 100 nucleotides of the viral RNA are

reasonable (compare to [95]), however, because of high target length we skipped hybridization prediction with the full length target sequence.

Apart from heat denaturation of viral samples in the presence of MBs also acidification of HRV2 samples was tested (data not shown). In contrast to heated samples concentration conditions during acidification were such that mainly 135S particles were created (refer to 3.1). Thus, no signals for RNA attached MBs could be obtained after sample acidification.

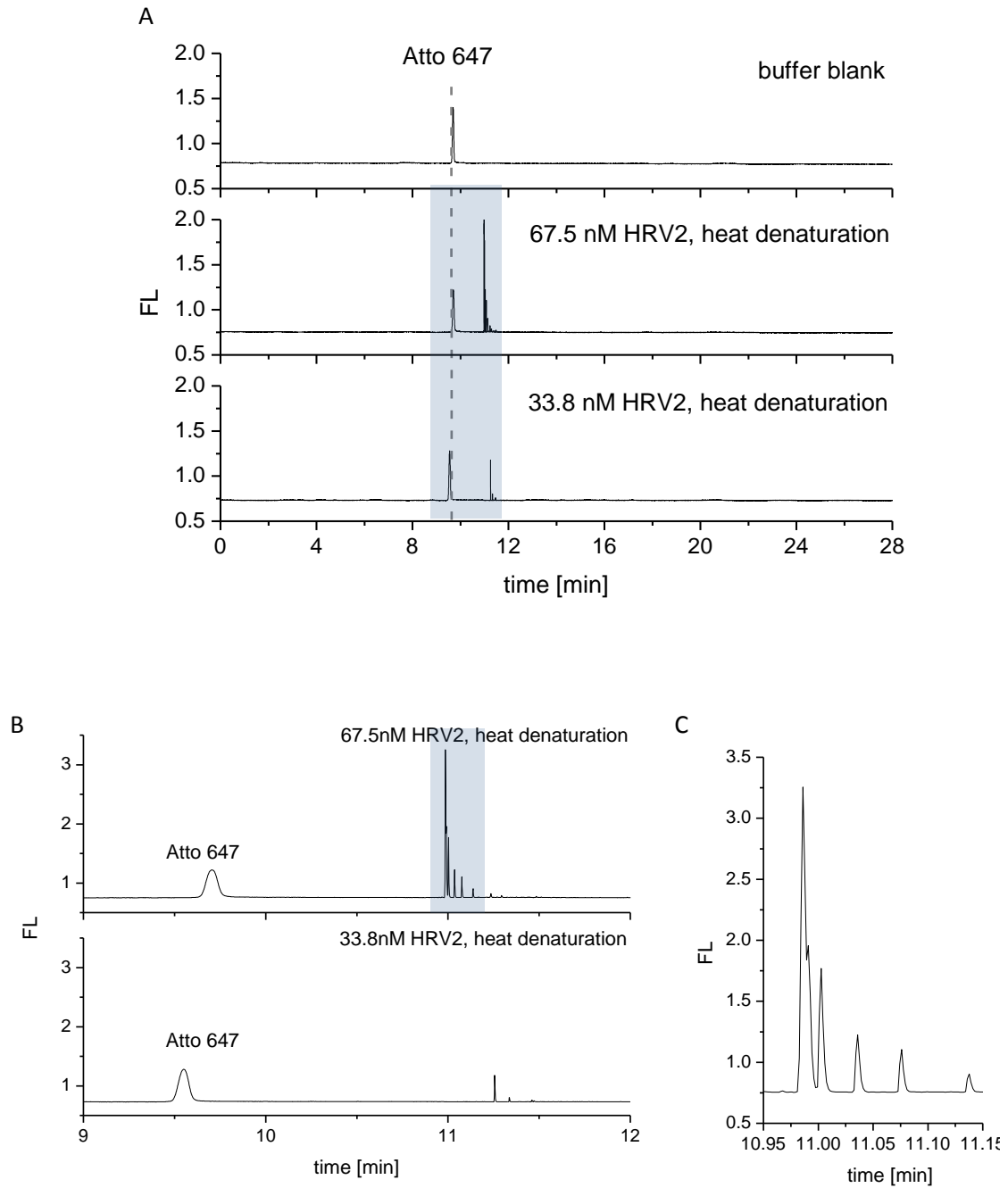


Fig. 51: FL signals obtained after hybridization of HRV2 IRES targeting MB, Cy5 labeled with full length viral RNA (A). Magnification of middle and lower trace from (A) depicted in (B);

magnification of upper trace from (B) depicted in (C). Magnified areas are highlighted, respectively. Viral RNA release was triggered via sample heating to 56.0°C for 10 min in the presence of MBs. CE and capillary as with figure 48, BGE and sample composition as with figure 49. Samples also included indicated concentrations of HRV2.

In a next step in developing a liposome based assay for elucidating viral RNA transfer through membranes we ported the CE analysis of MBs to the microchip scale, since we suggested higher sensitivity of the Agilent 2100 Bioanalyzer system. Indeed, upon comparison of limit-of-detection (LOD) values we found the LOD of the unquenched MB on the conventional CE instrument at 0.81 nM, whereas the LOD on the 2100 Bioanalyzer lay 2.25 fold lower at 0.36 nM. In good accordance with our findings upon application of conventional CE, we succeeded to close the MB hairpin structure in the chip format as well upon application of  $MgCl_2$  in electrophoresis buffers (figure 52).

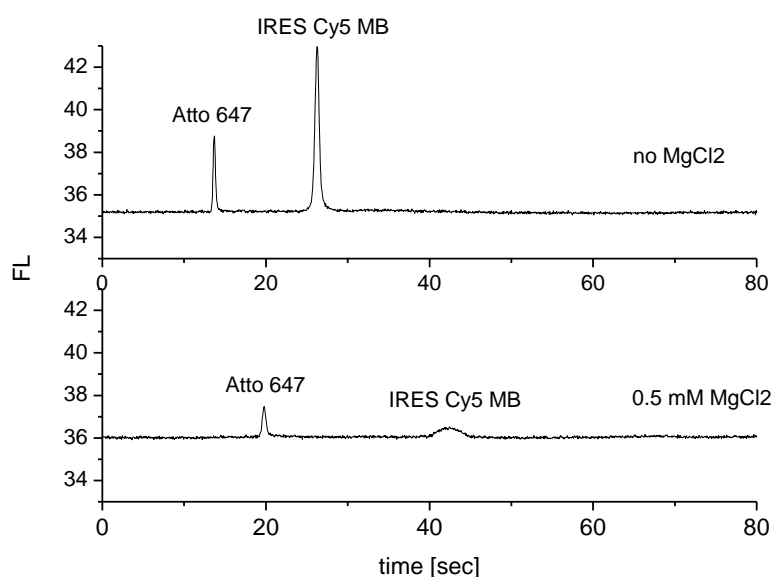


Fig. 52: Chip electrophoresis of HRV2 IRES targeting MB, Cy5 labeled. Analysis was carried out on the Agilent 2100 Bioanalyzer system upon application of DNA chips. Script changes were as described (refer to 3.2 – 3.4). BGE was 100 mM sodium borate, pH 8.3 either including 0.5 mM  $MgCl_2$  or not (as indicated). Samples consisted of 20 nM MB, 3.0  $\mu M$  Atto 495 (EOF marker for detection at  $\lambda_{ex}$  470 nm) and 2.5 nM Atto 647 (internal standard for detection at  $\lambda_{ex}$  630 nm) in BGE. Depicted are traces detected with the red laser ( $\lambda_{ex}$  630 nm) of the instrument.

Interestingly, although only 20 nM MB were applied to chip electrophoresis compared to the fivefold higher concentration with conventional CE, we still recorded a broad peak at

approximately 40s migration time originating from the closed MB upon application of MgCl<sub>2</sub> in electrophoresis buffers. However, FL of the closed MB was still significantly lower than for the beacon in the open conformation. Like on conventional CE we also experienced a decline in the EOF on chips of about 25%. We recorded EOF values of about  $53.9 \pm 0.5$  [ $10^{-9}$  m<sup>2</sup>/Vs] in the absence and  $40.7 \pm 1.2$  [ $10^{-9}$  m<sup>2</sup>/Vs] in the presence of 0.5 mM MgCl<sub>2</sub>. Measurements for elucidating EOF values were carried out in duplicates.

As a next step in developing a liposome based chip electrophoretic assay for viral RNA transfer through membranes, we encapsulated molecular beacons in liposomes. We chose the lipid composition of *n-phl* liposomes (refer to 3.2), that was also employed for chip electrophoretic leakage experiments. Again the MB targeting the IRES sequence of HRV2 was Cy5 labeled. It was encapsulated at 50 nM in 50 mM sodium borate buffer, pH 8.3 including 0.5 mM MgCl<sub>2</sub>. Initial experiments worked with conditions under MBP-V33333 receptor mediation, which previously did not yield any liposome leakage (up to approximately 20 nM HRV2 in incubation solution, refer to figure 42). Liposomes were decorated with recombinant receptor fragments before virus attachment. Receptor mediated adducts were then acidified to pH 5.1 and incubated for 15 min to allow for RNA transfer. After reneutralization and additional incubation at ambient temperature, samples were analyzed via chip electrophoresis. Although experimental conditions were employed that previously yielded good results in adduct formation and liposome leakage, experiments failed to detect the viral RNA transfer itself through membranes. However, influence of either the lipid membrane or of the Ni<sup>2+</sup> chelating DOGS-NTA lipid on the MB could be excluded. The obtained unquenched MB signal in the presence of DOGS-NTA lipid containing liposomes did not change (data not shown). Instead, gel electrophoresis experiments revealed partial digest of recombinant receptor fragments that such no longer exhibited virus binding characteristics. Therefore, we are of high spirits to get our experiments operating upon application of freshly prepared recombinant receptor solution. Further future modifications of our experimental setup for enhancing the sensitivity of this model system may include:

- (i) Longer incubation times for attachment of MB to target RNA since preliminary experiments showed slow kinetics of duplex strand formation.

- (ii) Adjustment of encapsulated MB concentration to obtain higher signals.
- (iii) Adjustment of MB nucleotide sequence to allow for faster RNA detection. Partial binding of the stem sequence to the target oligonucleotide [95] might increase the kinetics of duplex strand formation.
- (iv) Change in fluorophore from Cy5 to Atto 647 to further lower the LOD of MBs.
- (v) Targeting the poly A 3' end of the viral RNA. Although the exact length of the poly A tail is variable, more than one short MB might then be able to target the viral RNA leading to an approx. 2 - 3 fold increase in the obtained signal for a single target molecule.
- (vi) Application of Trolox<sup>TM</sup> as an additional component of electrophoresis buffers. Literature [103] reports an increase in dye photostability and decreased blinking of fluorophores thus yielding higher average photon counts per molecule. For Cy5 an approximately 200 fold increase in average photon counts to approx. 200 000 counts per molecule were reported, for Atto 647 an approximately 45 fold increase in average photon counts leads to even approx. 850 000 counts per molecule.
- (vii) Binding of His6-tagged recombinant receptor fragments to Ni<sup>2+</sup> chelating lipids was shown not to be complete although Ni<sup>2+</sup> was employed in molar excess over receptor fragments (refer to 3.4). Therefore, receptor fragments were able to stabilize virions in free solution or even virus particles already attached to liposomes against pH induced viral uncoating [7]. We therefore suggest to circumvent this additional virus stabilization via exchange of recombinant receptor fragments anchored via Ni<sup>2+</sup> and His- tags to lipid membranes to either recombinant receptor molecules including a transmembrane domain or to native receptor molecules obtained from cell culture. We propose that thereby a higher number of HRV2 particles is able to transfer its RNA genome through the liposomal membrane increasing the number of target molecules for MB detection.

- (viii) Application of a two step acidification process; *In vivo* bound virus particles dissociate from membrane receptors at mildly acidic pH values. However, under these conditions still no virus uncoating takes place. The pH threshold for virus uncoating was reported at lower pH values of 5.6 (refer to 2.1.1.), where already no virus / receptor complex was formed. Application of such acidification steps *in vitro* might increase virus infectivity, i.e. the number of viral RNA molecules that are shuttled through the liposomal membrane.

## Experimental Section

**Chemicals:** Boric acid (99.99%) and MgCl<sub>2</sub> hexahydrate (cell culture tested) were purchased from Sigma Aldrich (Steinheim, Germany). The FL dyes Atto 495 and Atto 647 (both in free acid form) were from Atto Tec (Siegen, Germany) and obtained as well from Sigma Aldrich. Cy5 was from Amersham Bioscience (Little Chalfont, England) and employed from a 25 mM stock solution in DMSO. DMSO (*p.a.*) was from Fluka (Buchs, Switzerland). A 1:200 dilution of DMSO in water was employed as intermediate DMSO stock for CE measurements. Sodium hydroxide (pellets pure) was from E. Merck (Darmstadt, Germany). DNase I (RNase free from bovine pancreas) was from Fermentas Life Science (St. Leon-Rot, Germany). Molecular Beacons and other oligonucleotides were composed of single stranded, unmodified DNA and obtained from VBC genomics (Vienna, Austria). The MB sequence was agccgAAATATAAAGGAAAAAGTGAAACACcggct for targeting the HRV2 IRES sequence. MBs were FL labeled at the 5' end via carboxyfluorescein (FAM) for in-batch and via Cy5 for CE and chip measurements. The 3' ends were modified via a black hole quenchers (BHQ), respectively. The oligonucleotide sequence for the positive control was tgggaccaactacttgggtgtccGTGTTTCACTTTTTCTTTATATTTgcttatggtgacaat and for the negative control tactctgttattacgtaacttgtacgccagtttatctccctccccatgtaacttagaag. MBs and oligonucleotides were solved in nuclease free water (Quiagen, Hilden, Germany) to obtain 100 μM stock solutions. All other water was of Millipore grade. Lipids were as described (refer to 3.2) and obtained from Avanti Lipids (Alabaster, AL, USA) *via* InstruChemie (Delfzyl, The Netherlands). Liposomes in non-physiologic composition (*n-phl*) were prepared in 50 mM sodium borate, pH 8.3 including 0.5 mM MgCl<sub>2</sub> and 50 nM of HRV2 IRES targeting MB, Cy5 labeled as previously described (refer to 3.2).

**Biological Material:** An HRV2 aliquot, produced as described [8, 46], in 50 mM sodium borate, pH 7.4 at a concentration of 5.4 mg/mL was employed for experiments. A recombinant receptor fragment of the VLDLR at 5.5 mg/mL in 20 mM Tris-HCl, pH 7.5, 150 mM NaCl and 20 mM CaCl<sub>2</sub> was used for formation of receptor mediated adducts between liposomes and virus particles. It consisted of five repeats of the VLDLR binding domain number 3 arranged in tandem, fused to a His6 tag at its C- and to MBP at its N-terminus [75].



**Instrumentation:** FL in-batch measurements were carried out on 96-well plates on a 1420 Multilabel Counter Victor<sup>2</sup> from Perkin Ellmer (Fremont, CA, USA). CE was carried out on an Agilent 3D CE coupled to a Picometrics (Ramonville, France) ZETALIF FL detection system equipped with a HeNe laser with  $\lambda_{\text{ex}} = 633$  nm (10mW from Melles Griot obtained via Merz Brothers, Haid, Austria). Electrophoresis was at + 20 kV and 30.0°C for 28 min runtime. The capillary was preconditioned for 2 min with BGE prior each run, postconditioning included flushing for 2 min with 1 M sodium hydroxide and 2 min with water. Samples were injected via application of 50 mbar pressure for 9 sec. Analytes were detected at 200, 205, 260 and 490 nm; the band width valued 10 nm for each UV detection wavelength, respectively. FL was recorded with the HeNe 594 nm setup of the Picometrics system. A fused silica capillary (50  $\mu\text{m}$  inner diameter, 375  $\mu\text{m}$  outer diameter) with  $L_{\text{tot}} = 72.2$  cm and  $L_{\text{eff}}$  (UV) = 23.5 cm and  $L_{\text{eff}}$  (FL) = 57.2 cm from Polymicro (Phoenix, USA) obtained via Optronis (Kehl, Germany) was employed for electrophoresis. Sodium borate (100 mM, pH 8.3) including variable  $\text{MgCl}_2$  concentrations was employed as BGE and sample buffer, respectively. Electrophoresis buffers were filtered through 0.45  $\mu\text{m}$  CA membrane syringe filters prior to application. Chip electrophoresis was carried out on the Agilent 2100 Bioanalyzer system (Agilent Technologies, Waldbronn, Germany) employing DNA chips. Modifications in chip handling and analysis were as described (refer to 3.2). BGE and sample buffer were as with conventional CE.

**Sample preparation:** For elucidating the impact of the  $\text{MgCl}_2$  concentration of electrophoresis buffers on the MB conformation samples consisting of 100 nM MB targeting the HRV2 IRES sequence and labeled via Cy5 and including 25 nM Atto 647 as internal standard and DMSO 1 : 4 x 10<sup>3</sup> as EOF marker in 50 mM sodium borate, pH 8.3 with variable  $\text{MgCl}_2$  concentrations corresponding to the respective BGE were prepared. Samples for digest included 100 nM Cy5 labeled MB, 50 nM Atto 647 and DMSO 1 : 4 x 10<sup>3</sup> in 50 mM sodium borate, pH 8.3 with 0.5 mM  $\text{MgCl}_2$ . Digestion was via DNase I at 0.05 units for an intermediate MB concentration of 400 nM for 10 min at 30.0°C before sample dilution to final concentrations. Diluted sample was additionally incubated for 35 min at 4.0°C (ice bath) and 35 min at 30.0°C (tray of CE instrument), respectively. For other conventional CE samples, an intermediate analyte solution of 111 nM MB including 55.5 nM Atto 647 and 1 : 3.6 x 10<sup>3</sup> DMSO in 55.5 mM sodium borate, pH 8.3 with 0.55 mM  $\text{MgCl}_2$  was prepared. 9  $\mu\text{L}$  of this intermediate solution were mixed with 1  $\mu\text{L}$  of oligonucleotide solutions (500 nM in water, respectively) or 1  $\mu\text{L}$  of virus stock solution. Alternatively, virus stock solution was diluted 1 : 2 in the corresponding preparation buffer before mixing with the beacon solution. Corresponding buffer without any virions was used for preparation of a blank sample. Incubation was for 40 min at 30.0°C in the tray of the CE instrument for control oligonucleotides and for 10 min at 56.0°C for hybridization of MBs to viral RNA. Chip electrophoretic samples consisted of 20 nM Cy5 labeled MB, 3.0  $\mu\text{M}$  Atto 495 (EOF marker for detection at  $\lambda_{\text{ex}}$  470 nm) and 2.5 nM Atto 647 (internal standard for detection at  $\lambda_{\text{ex}}$  630 nm) in BGE. BGE was 100 mM sodium borate, pH 8.3; for indicated experiments it included additionally 0.5 mM  $\text{MgCl}_2$ .

# 4 Method Development on the Agilent 2100 Bioanalyzer System

## 4.1 Application of a Fluorescent EOF Marker

In order to assess the EOF upon chip electrophoresis with FL detection, it was aimed to include a fluorophore with a known electrophoretic mobility in all respective samples (comparable to DMSO as EOF marker for UV detection). The Agilent 2100 Bioanalyzer offers the possibility of simultaneous detection at two wavelengths –  $\lambda_{\text{ex}}$  at 470 and 630 nm. Detection at  $\lambda_{\text{ex}} = 630$  nm showed higher sensitivity and was therefore employed for tracing FL labeled analytes. To circumvent possible separation problems between analyte peaks and a peak of a standard fluorophore, I opted for the second detection window offered by the instrument, with  $\lambda_{\text{ex}}$  at 470 nm (blue LED) for detection of a FL EOF marker. Several fluorophores were investigated for their applicability as FL standard.

### 4.1.1 Calcein

Calcein (HPCE grade) was obtained from Sigma Aldrich (Steinheim, Germany); figure 53 shows a respective molecule. Its absorption / emission characteristics ( $\lambda_{\text{ex}} / \text{em} = 470 / 509$  nm) correspond well to the blue detection window of the Agilent 2100 Bioanalyzer system ( $\lambda_{\text{ex}} / \text{em} = 470 / 525$  nm).

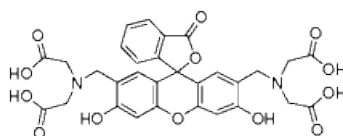


Fig. 53: Calcein (HPCE grade) from Sigma Aldrich, image taken from <http://www.sigmaaldrich.com>

Initial experiments showed detectability of Calcein with the Agilent 2100 Bioanalyzer system (figure 54). However, problems with the peak shape of the Calcein peak were experienced; heterogeneous and tailing peaks were obtained.

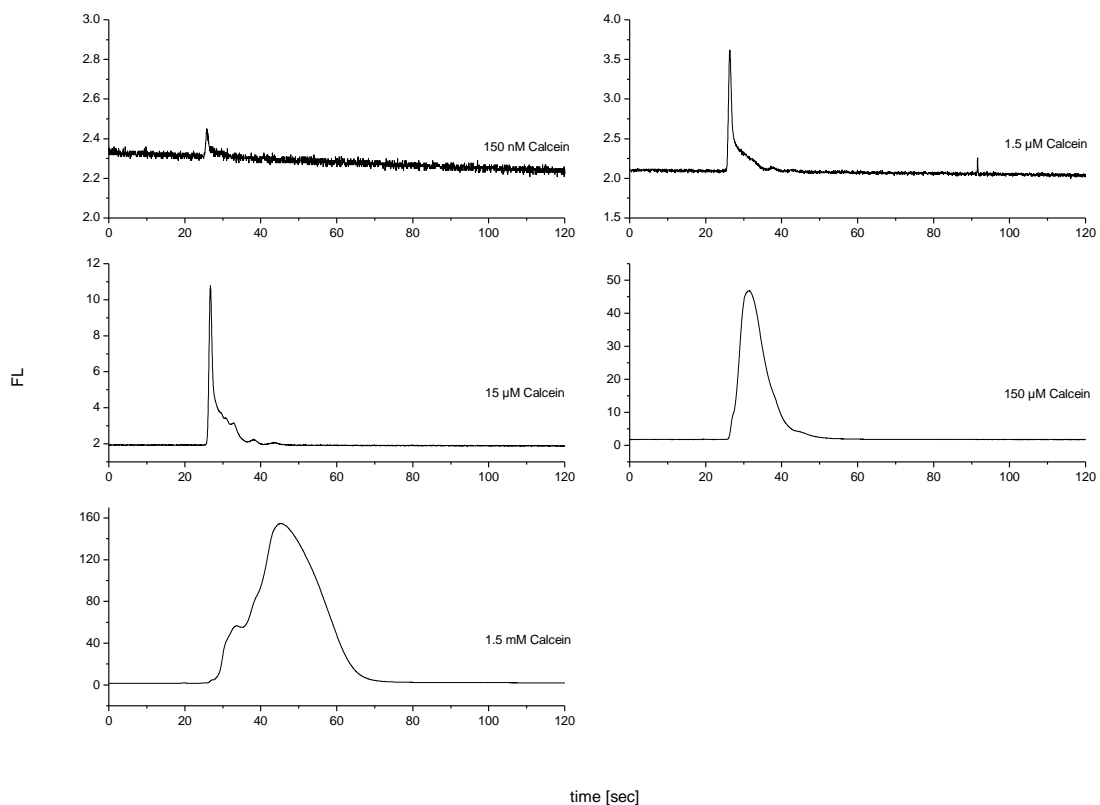


Fig. 54: Detection of Calcein employing the blue LED ( $\lambda_{\text{ex}} / \text{em} = 470 / 525 \text{ nm}$ ) of the Agilent 2100 Bioanalyzer System. Script modifications as detailed (refer to 3.2 - 3.5); measurements were carried out on DNA chips, BGE: 100 mM sodium borate, pH 8.3; Samples included Calcein at indicated concentrations.

Detection of heterogeneous Calcein peaks could be related to several possible reasons:

- (i) Contamination of obtained Calcein – An improbable assumption, since the supplying company guaranteed HPCE grade of the analyte substance.
- (ii) Wall adsorption to the chip separation channel – In order to exclude wall adsorption phenomena as reasons for obtained heterogeneous peaks, addition of

SDS at different concentrations to the BGE was tested (figure 55). At all investigated SDS concentrations the peak appearance did not change significantly. For higher SDS concentrations the observed effects seemed to be even more pronounced. Wall adsorption of Calcein as cause for tailing and heterogeneous peaks therefore could be excluded.

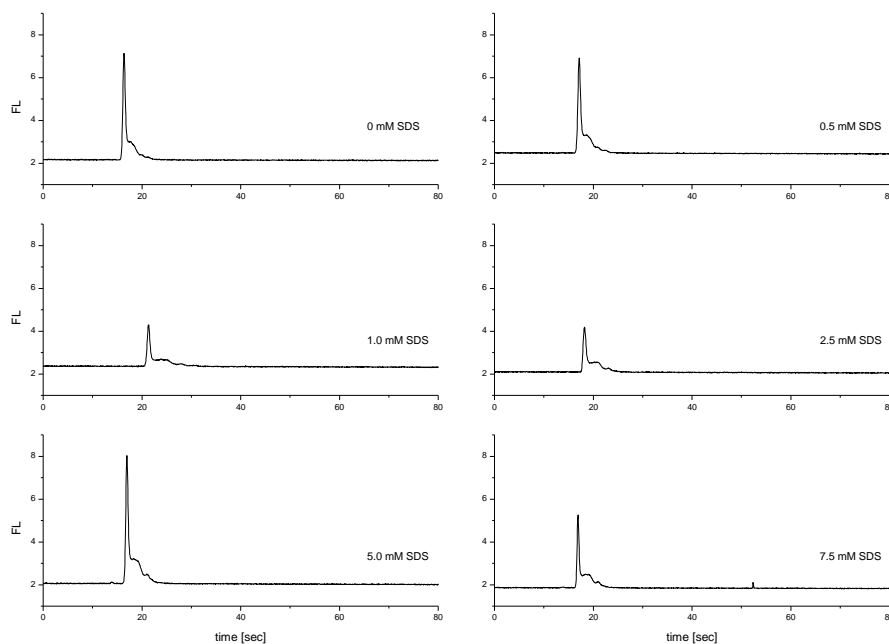


Fig. 55: Calcein peak shape depending on the SDS content of the BGE. Script modifications as detailed (refer to 3.2 - 3.5); measurements were carried out on DNA chips employing the blue LED of the instrument ( $\lambda_{\text{ex}} / \lambda_{\text{em}} = 470 / 525 \text{ nm}$ ) for detection; Sample: Calcein  $1.0 \mu\text{M}$  in BGE; BGE: 100 mM sodium borate, pH 8.3 at indicated SDS concentrations.

- (iii) Additional sample uptake at the injection cross during respective chip electrophoretic runs – Cleaning currents between sample injection to the separation channel and the analytical run itself were introduced to minimize additional analyte uptake at the injection cross. However, this did not lead to a significant improvement of peak shapes as presented in figure 56. In fact, increasing cleaning currents even lead to partial separation between three constituents of Calcein.

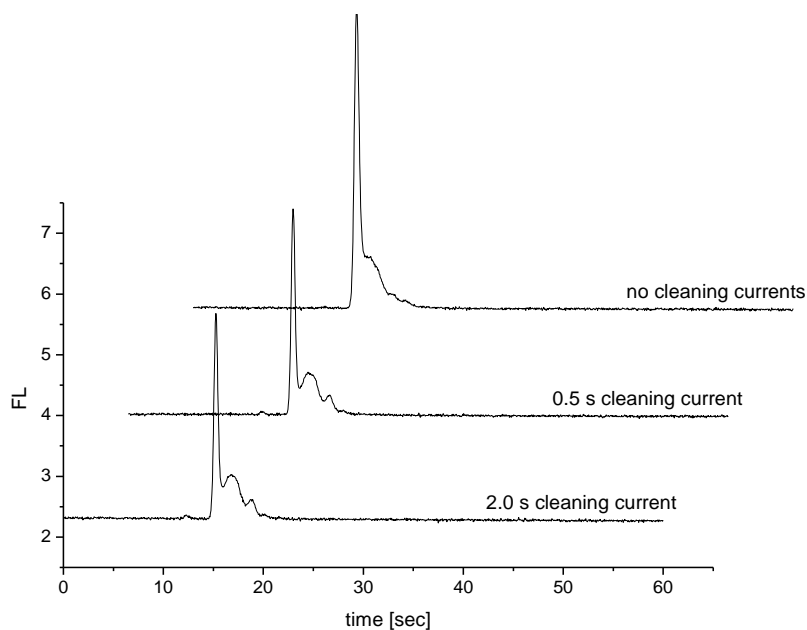


Fig. 56: Calcein peak shape depending on the introduction of cleaning currents after electrophoretic sample injection to the separation channel and before chip electrophoretic analysis to minimize additional sample uptake at the injection cross. Script modifications as detailed (refer to 3.2 - 3.5). Additional cleaning currents of indicated length were introduced to the chip electrophoretic setup. Measurements were carried out on DNA chips employing the blue LED of the instrument ( $\lambda_{\text{ex}} / \lambda_{\text{em}} = 470 / 525 \text{ nm}$ ) for detection; Sample: Calcein  $1.0 \mu\text{M}$  in BGE; BGE: 100 mM sodium borate, pH 8.3.

In overall, although the exact reason of heterogeneous and tailing peaks could not be resolved, Calcein did not seem suitable as FL EOF marker for chip electrophoretic analysis on the Agilent 2100 Bioanalyzer system upon employment of the blue detection window of the instrument. Also, its reactivity to divalent cations precluded the application of  $\text{Ni}^{2+}$  loaded liposome surfaces for receptor attachment. Therefore, in a next step, Atto 495 was tested as FL marker substance.

## 4.1.2 Atto 495

Atto 495 (HPCE grade) was obtained from Sigma Aldrich (Steinheim, Germany) in its free acid form. Figure 57 depicts a respective molecule. Its absorption / emission characteristics ( $\lambda_{\text{ex}} / \text{em} = 495 / 527 \text{ nm}$ ) corresponds well with the blue detection window of the Agilent 2100 Bioanalyzer system ( $\lambda_{\text{ex}} / \text{em} = 470 / 525 \text{ nm}$ ).

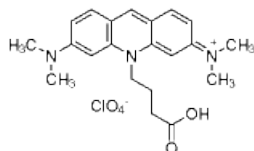


Fig. 57: Atto 495 (HPCE grade) from Sigma Aldrich, image taken from <http://www.sigmaldrich.com>

The pH value of the BGE for CE analysis of virions had to be chosen in the basic range (refer to 2.3.1); therefore, experiments had been carried out upon application of sodium borate buffer at pH 8.3. Chip electrophoretic analysis of liposomes and receptor mediated adducts between virions and liposomes also precludes the application of detergents in the BGE. From these considerations Atto 495 was electrophoresed in sodium borate buffer, pH 8.3 in the absence of any surfactants. Figure 58 depicts the UV adsorption spectra of all neutral compounds recorded under these conditions, i.e. DMSO and the Atto dye. As could be learned from these spectra, Atto 495 migrated with the EOF under such electrophoresis conditions – the fluorophore was recorded in its zwitterionic form.

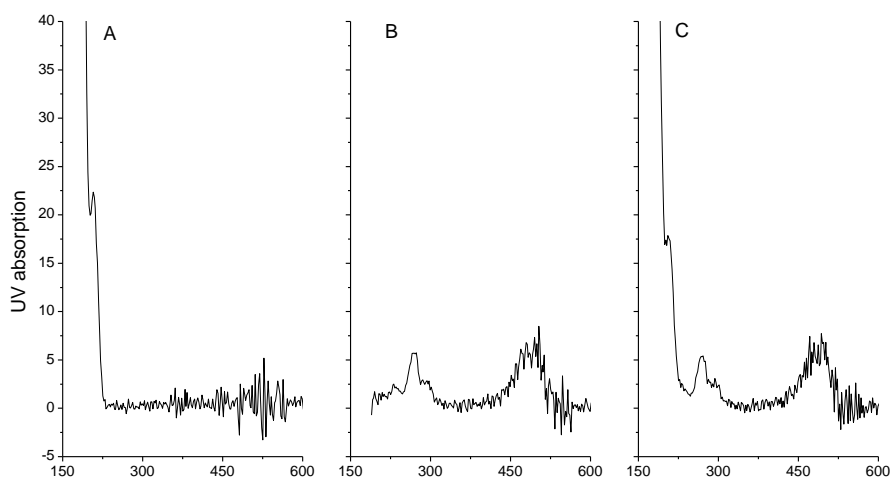


Fig. 58: UV absorption spectra for DMSO and Atto 495 containing samples – UV spectra of plain DMSO (A), of Atto 495 (B) and of a mix of these two components (C). From the UV absorption

spectra, comigration of Atto 495 with DMSO was concluded. Atto 495 was therefore recorded in its zwitterionic form. CE: fused silica capillary, 50  $\mu\text{m}$  inner diameter,  $L_{\text{tot}} = 60.0$  cm,  $L_{\text{eff}} = 51.6$  cm; CE was at + 20 kV, 20.0°C and sample injection at 400 mbar x sec; Analytes were detected at 200 nm and 470 nm via their UV absorption characteristics and UV spectra of corresponding peaks were obtained via the Agilent HPCHEM software; BGE: 100 mM sodium borate, pH 8.3; Samples: 31.5  $\mu\text{M}$  Atto 495 and / or DMSO 1 : 6.1 x 10<sup>3</sup> in BGE.

However, since CE of rhinoviruses had been carried out so far upon addition of surfactants to the BGE, I also tested the applicability of this marker in such an electrophoresis system. Upon SDS addition to the BGE, Atto 495 was found to interact with the detergent already below its respective CMC. Therefore, Atto 495 no longer migrated with the EOF but passed the detector at later time points (figure 59). It is of note that the EOF mobility of all three electropherograms presented below was comparable at approximately  $62.6 \pm 0.6 \times 10^{-9}$  m<sup>2</sup>/Vs. Electropherograms were recorded with FL detection (ZETALIF detector, Picometrics, Ramonville, France equipped with an Argon laser, model 163-M12 - 25 mW from Spectra-Physics, Mountain View, CA).

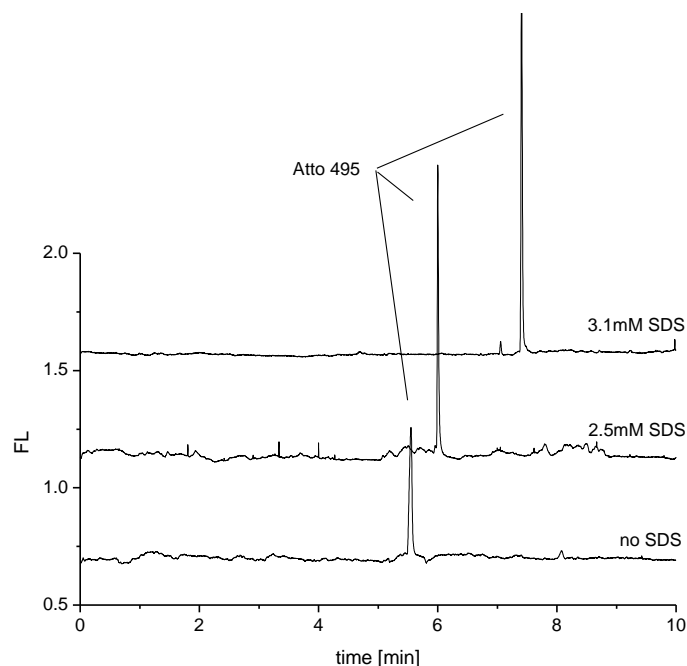


Fig. 59: Atto 495 signal in dependence of the SDS concentration of the BGE (100 mM sodium borate, pH 8.3) as indicated. Electrophoresis conditions: fused silica capillary, 75  $\mu\text{m}$  inner diameter,  $L_{\text{total}} = 73.0$  cm,  $L_{\text{UV}} = 23.5$  cm,  $L_{\text{FL}} = 58.0$  cm; sample injection at 200 mbar x sec; temperature of capillary at 20.0°C; electrophoresis at + 20 kV; detection at 200 nm (UV) and via ZETALIF system at  $\lambda_{\text{ex}} = 488$  nm (FL); The sample consisted of 30 nM Atto 495 and DMSO 1:6.1 x 10<sup>3</sup> in non SDS containing BGE.

Upon application of a theoretical approach we were able to predict shapes of the mobility dependence curves of Atto 495 on the SDS content of the BGE (above the CMC of SDS). For several assumed partition coefficients of Atto 495 between the bulk phase and SDS micelles we obtained (figure 60):

$$\mu_i^{\text{app}} = \mu_{\text{EOF}} - \left( \mu_{\text{EOF}} \cdot \frac{1}{1 + k_i} \right) + \left( \mu_{\text{SDS}} \cdot \frac{k_i}{1 + k_i} \right)$$

$$k_i = K_i \cdot \frac{V_{\text{SDS}}}{V_{\text{mob}}}$$

$$V_{\text{SDS}} = \frac{m_{\text{SDS}}}{\rho_{\text{SDS}}}$$

$$\rho_{\text{SDS}} = 1100 \frac{\text{kg}}{\text{m}^3}$$

$$M_{\text{SDS}} = 288.4 \frac{\text{g}}{\text{mol}}$$

$$\mu_{\text{EOF}} \cong 60 \cdot 10^{-9} \text{m}^2/\text{Vs}$$

$$\mu_{\text{SDS}} \cong 30 \cdot 10^{-9} \text{m}^2/\text{Vs}$$

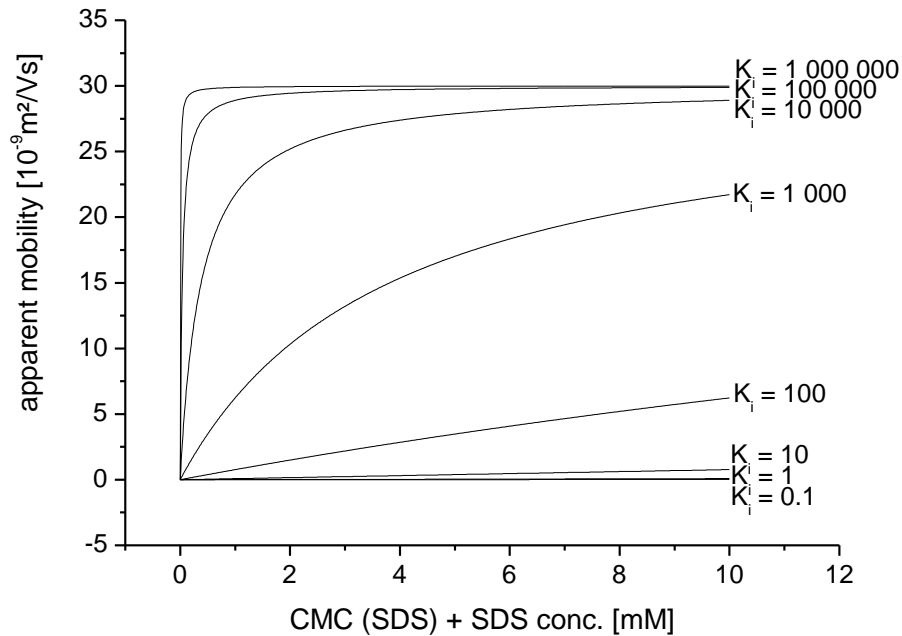


Fig. 60: Prediction of the electrophoretic mobility of Atto 495 in the presence of SDS in the BGE (100 mM sodium borate, pH 8.3) above the CMC. Depending on the partition coefficient of the FL dye between the bulk phase and SDS micelles different curves are fitted.



In following experiments we could demonstrate the mobility dependence of Atto 495 on the SDS content of the BGE according to our predictions for high partition coefficients. Measurements were carried out at least in duplicate on an Agilent 3D CE employing a ZETALIF FL detection system equipped with an Argon laser ( $\lambda_{\text{ex}} = 488 \text{ nm}$ ). In good agreement with obtained data points a linear fit was chosen for the description of the Atto 495 mobility behaviour below the CMC at approximately 2.4 mM SDS (figure 61). The migration of Atto 495 above the CMC of SDS in the BGE was similar as predicted for high partition coefficients. Slight variances in the curve shape (when compared to figure 60) are probably due to aggregating SDS monomers interacting with the dye. Such an effect had also been recorded previously [104].

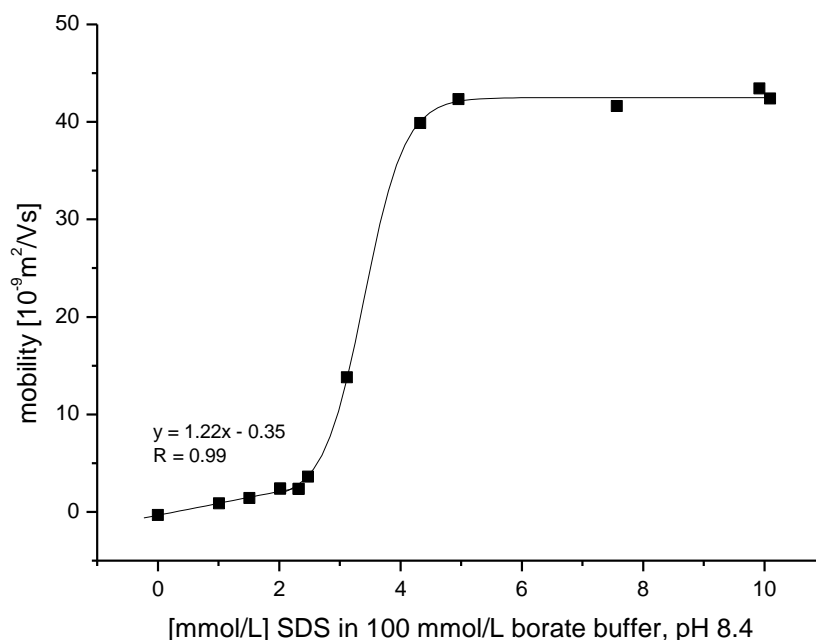


Fig. 61: Mobility of Atto 495 depending on the SDS content of the BGE (100 mM sodium borate, pH 8.3). For SDS concentrations below the CMC, a good correlation between obtained data points and an employed linear fit was found.

Electropherograms recorded on the Agilent 2100 Bioanalyzer system with the blue LED ( $\lambda_{\text{ex}} / \lambda_{\text{em}} = 470 / 525 \text{ nm}$ ) of the instrument and employing DNA chips demonstrated as well interaction of the fluorophore with SDS. At higher detergent concentrations of the BGE the migration time of the FL dye was shifted to higher values as experienced already in the capillary format (figure 62). Atto 495 is nevertheless suitable as FL marker for chip electrophoresis. However, for SDS containing BGEs the interaction between the dye and the surfactant has to be considered.

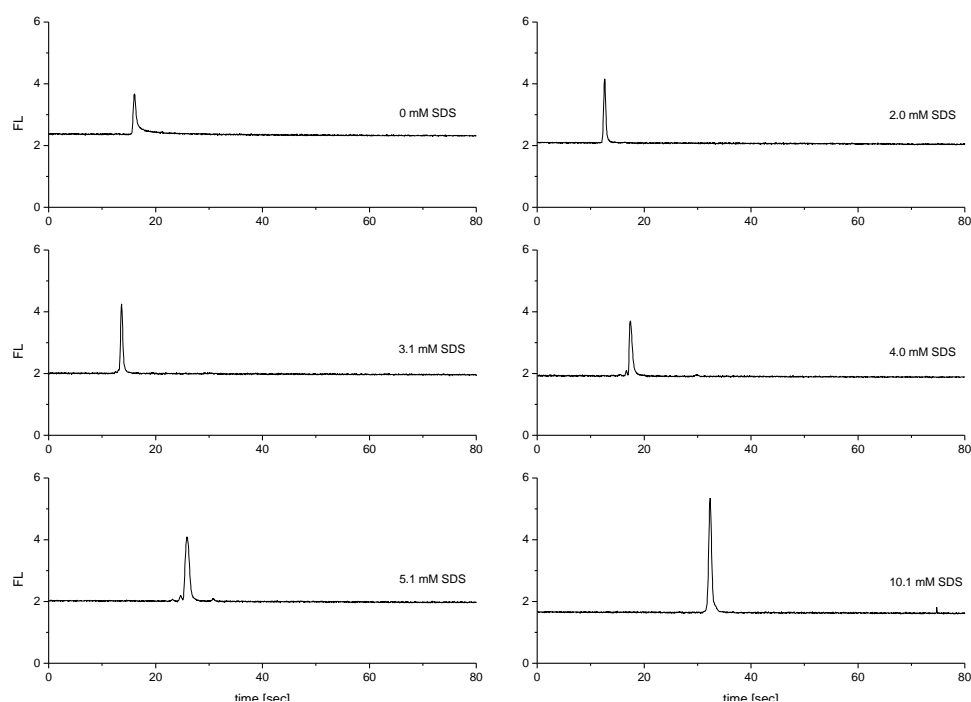


Fig. 62: Atto 495 signals recorded on the Agilent 2100 Bioanalyzer system employing a BGE (100 mM sodium borate, pH 8.3) with different SDS concentrations. Interactions between the FL dye and the surfactant can be deduced from prolonged migration times of Atto 495 in the presence of the detergent. Script modifications as presented under 3.2; measurements were carried out on DNA chips employing the blue LED of the instrument ( $\lambda_{\text{ex}} / \lambda_{\text{em}} = 470 / 525 \text{ nm}$ ) for detection; Sample: 3.0  $\mu\text{M}$  Atto 495 in BGE; BGE: 100 mM sodium borate, pH 8.3 including SDS at indicated levels.

In overall, Atto 495 performed well on the Agilent 2100 Bioanalyzer chip electrophoresis system. In the absence of SDS (as intended for analysis of liposomes) the dye even is suitable as FL EOF marker employing the blue detection window of the instrument. Atto 495 therefore was included in all subsequent samples at approximately 3.0  $\mu\text{M}$  concentration for EOF assessment.

## 4.2 Determination of Stable Electrophoresis Conditions for Chip Analysis

Upon application of 100 mM sodium borate, pH 8.3 without addition of surfactants as BGE during chip electrophoresis two sets of possible EOF values on Agilent 2100 Bioanalyzer DNA chips were experienced. The average EOF of one set was  $38.21 \pm 2.79$  [ $10^{-9}$  m<sup>2</sup>/Vs] (value obtained from 43 measurements), the other set yielded  $55.05 \pm 2.21$  [ $10^{-9}$  m<sup>2</sup>/Vs] (value obtained from 23 measurements) in average. EOF values were determined upon application of Atto 495 as FL EOF marker (refer to 4.1.2). Chip electrophoresis at high EOF values yields several advantages:

- (i) Short analysis times
- (ii) Sharper peaks for analytes with low electrophoretic mobility
- (iii) High reproducibility of peak migration times between electropherograms, especially upon sample analysis from different wells of the same chip
- (iv) Easier detection of peak mobility shifts in the course of bioaffinity reactions

These advantages were the reason why it was tried to obtain high EOF values for all chip electrophoretic measurements. Upon investigation of reasons for low EOF values several possible causes were considered:

- (i) BGE pH value – Upon application of a BGE with pH 8.3, silanol groups on the surface of the chip channels are deprotonated. Nevertheless, we investigated the EOF dependence on BGE pH values between 8.20 and 8.45. As expected, no connection between EOF and pH in the investigated pH range was found. Small variations in pH resulting from different BGE batches could therefore be excluded as reason for low EOF values.

- (ii) BGE ionic strength – Small differences in the pH value of various BGE batches led as well to variances in the respective buffer ionic strength values. However, like with pH variances, no connection between slightly varying ionic strength levels of the BGE and obtained EOF values could be drawn.
- (iii) Temperature of analysis – Agilent 2100 Bioanalyzer DNA chips are heated to 30.0°C during analysis. However, especially since our instrument was not equipped with a thermostatisation possibility, slight variances in temperature were expected to occur during analyses. Indeed, chip temperatures between 30.0°C and 33.3°C (regarding a representative set of 15 analyzed DNA chips) were recorded. However, as with investigated pH and ionic strength dependencies, it was not possible to deduce a correlation between elevated chip temperature during analysis and the two sets of obtained EOF values.
- (iv) Carry-over of detergents between different DNA chips – Control of HRV2 labeling via Cy5 was achieved in SDS containing BGE [1, 2]. However, since the analysis of liposome including samples precluded the application of surfactants in the BGE, SDS was omitted for other chip electrophoretic setups. The electrode cartridge of the instrument was, although thoroughly cleaned via the electrode cleaning chip between different analytical setups, the same for both applications. Therefore, SDS carry-over between DNA chips could not be completely excluded. Although upon addition of SDS to the BGE a stabilizing effect on the migration behavior of marker substances could be achieved, EOF values could not be stabilized on a high level via SDS addition to the BGE. Furthermore, surfactant addition to the BGE lead to tailing of liposome peaks upon electrophoresis and was thus omitted for further analyses.
- (v) Time depending alteration of the BGE – Buffer uptake of carbon dioxide as well as formation of polyborates with time was investigated as possible reason of shifting EOF values. However, low EOF values could not be related to either of these mechanisms, exclusively.
- (vi) Hydrodynamics – Another explanatory attempt considered hydrodynamics on chips as possible reason for different EOF values. In a series of experiments the

BGE content of the buffer outlet was varied by as much as 10 % in relation to the buffer inlet. Furthermore runtimes were reduced to minimize volume throughput to the outlet well. Again no correlation to different EOF sets was obtained.

- (vii) Finally, it was observed that preparation of BGE as well as of the Cy5 dilution in BGE for setup of the instrument optics had a significant impact on the EOF. Interestingly, only upon application of BGE and a Cy5 dilution in BGE prepared freshly on the day of analysis (i.e. not older than 7 hours at maximum), high EOF values were reproducibly obtained. The exact mechanism of this effect was not investigated in detail but the chip electrophoresis protocol was adapted according to these findings.

In accordance to these findings concerning high EOF values during chip electrophoresis the BGE was prepared freshly on the day of analysis from boric acid and 3M sodium hydroxide, equally prepared on the day of analysis. Cy5 stock (25 mM in DMSO) was diluted in DMSO to yield a less concentrated stock solution (62.5  $\mu$ M in DMSO). This less concentrated dye stock in DMSO was diluted 1 : 1 x 10<sup>3</sup> in BGE as well freshly on the respective day of analysis. Such, reproducible EOF values of  $54.17 \pm 0.88$  [ $10^{-9}$  m<sup>2</sup>/Vs] (n = 8 measurements from 8 chips measured on four consecutive days upon application of 4 independently prepared BGE aliquots) for chip electrophoresis on the Agilent 2100 Bioanalyzer system in the absence of any detergents were obtained.

## 4.3 Fluorescence Labeling of HRV2

Labeling of primary amino-groups of the HRV2 viral capsid was carried out via Cy5 to allow for detection via the red laser ( $\lambda_{\text{ex}} = 633 \text{ nm}$ ) of the Agilent 2100 Bioanalyzer system. According to literature [60 – 62], 50 mM sodium borate, pH 8.3 was employed as labeling buffer. The DMSO content of the labeling solution was limited to 5 % of the total volume, because of supposed virus instability in organic solvents. Such, 5  $\mu\text{L}$  of virus solution in 50 mM sodium borate, pH 7.4 were incubated with 4.5  $\mu\text{L}$  of 50 mM sodium borate, pH 8.3 and 0.5  $\mu\text{L}$  of Cy5 in DMSO. Cy5 was obtained in solid form from Amersham Bioscience (Little Chalfont, England) and dissolved in DMSO (*p.a.* from Sigma Aldrich, Steinheim, Germany) to yield a 25 mM stock solution. To adjust the molar excess value of dye over virus, Cy5 stock was diluted in DMSO to yield stocks of less concentration prior to labeling. Staining was carried out under light protection for approx. 12 - 20 hours at ambient temperature (approx. 20 - 25°C).

Primary amines on the virus surface originate from surface exposed lysines located on VP1 loops positioned on the starshaped dome of the capsid [61, 62]. This part of the virus capsid is also taking part in receptor recognition. Therefore, it was surprising that FL modification of virions still allowed for receptor binding. Cell infection, however, was significantly reduced upon labeling [61, 62].

A fairly large molar excess of dye molecules over virions was necessary for FL modification of viral capsids [61, 62]. Upon application of high molar excess levels of dye over virus, high FL signals for modified virions were obtained. However, we were interested in obtaining FL detectable particels with high resemblance to unmodified virions for application in bioaffinity reactions. Therefore, we opted for a compromise in labeling conditions – application of an approximately  $2.5 \times 10^3$  fold molar excess of dye over virus for capsid labeling modified approximately half of all lysines that were normally labeled upon application of higher molar excess levels of dye over virus (figure 63).

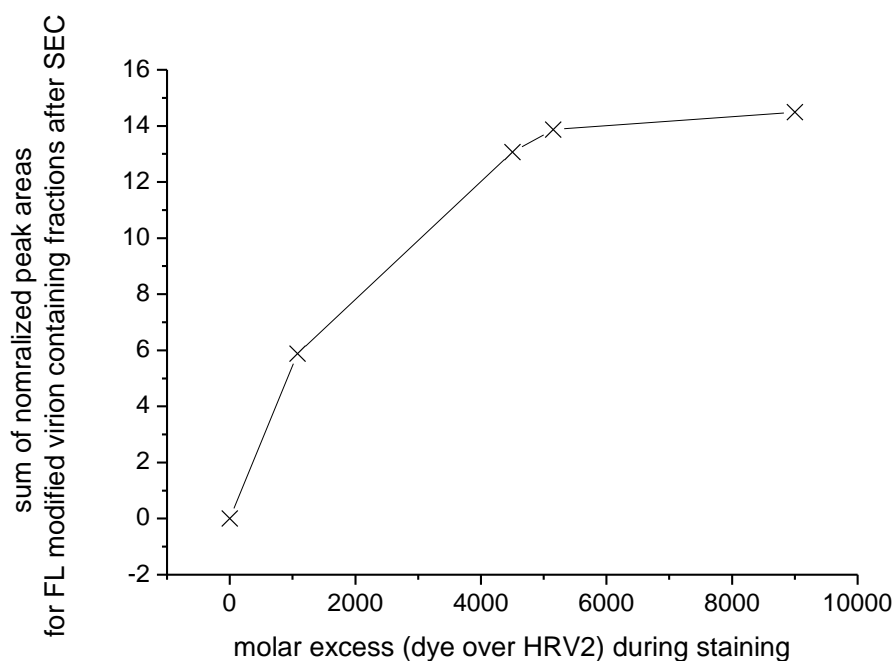


Fig. 63: The degree of virus surface modification during labeling (as expressed via the sum of normalized peak areas for SEC fractions containing labeled virions) is depending on the molar excess level of dye over virus molecules in the course of the labeling process. HRV2 was modified via the amine-reactive probe Cy5 at indicated molar excess levels. Low-molecular-mass material was removed from samples [1, 2] and SEC fractions were subjected to electrophoresis on the Agilent 2100 Bioanalyzer instrument. Obtained peak areas were normalized regarding the concentration of the virus starting material and the dilution in the course of sample preparation. Normalized peak areas from all SEC fractions of a respective HRV2 labeling experiment were summed up and plotted against the employed molar excess level of dye over virus particles.

The protocol for removal of low-molecular-mass material from virus labeling solutions was modified compared to the one found in literature [1, 2, 61, 62]. Instead of SEC on columns we opted for spin SEC. Corning X spin filter inlets (0.45 $\mu$ m CA membrane, figure 64, A) were filled with Sephadex G50 swelled in 50 mM sodium borate, pH 8.3. To obtain a maximum amount of SEC material inside these filter inlets, excess buffer was removed via spinning (30 sec at 100 rcf) on an Eppendorf table centrifuge (model 5415D) between SEC material additions. Such, 900  $\mu$ L of swelled material were applied to filter inlets in total. Consecutively, SEC material was dried via spinning (1 min at 400 rcf followed by 1 min at 800 rcf). This column was found to detach from the filter inlet wall and to sway upon touch of the filter inlet (figure 64, B). In such a way, sample dilution upon depletion of low molecular mass material was minimized. Application of other SEC

material was found not to be suitable for application in the spin SEC setup – Sephadex G15 did not detach from the tube wall and Sephadex G100 could not be dried via spinning.

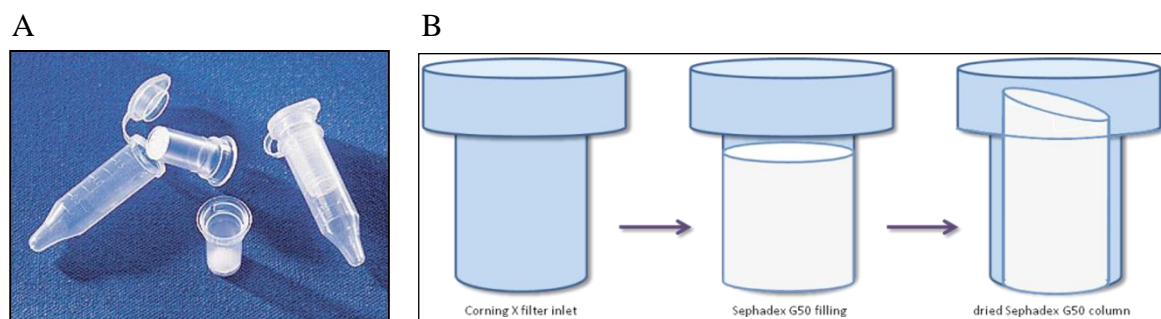


Fig. 64: Spin SEC upon application of Corning X spin filters (A). Filter inlets were filled with Sephadex G50 (B) consecutively spun dry on an Eppendorf table centrifuge to minimize sample dilution in the course of free dye depletion. Image A taken from <http://www.sigmaldrich.com>

The virus labeling solution (10  $\mu\text{L}$  in total) was applied to the SEC column and eluted via spinning (1 min at 800 rcf). Because of the high molecular weight of virus particles, elution of analytes was proposed already with this first elution step. Nevertheless, the column was rinsed thereafter with 20  $\mu\text{L}$  of 50 mM sodium borate, pH 8.3. The obtained combined volume of 30  $\mu\text{L}$  (termed fraction 1a) was subjected to spin SEC on a second column. This time the column was rinsed with 15  $\mu\text{L}$  of 50 mM sodium borate, pH 8.3. The obtained combined volume of 45  $\mu\text{L}$  (termed fraction 2a) contained the bulk of FL modified virions. Column rinsing with 20  $\mu\text{L}$  of 50 mM sodium borate, pH 8.3 for both SEC columns after collection of the main fraction, respectively, yielded fractions 1b and 2b. Collection of second fractions for both spin SEC passes was necessary to determine the content of FL labeled virions in the main SEC fraction.

SEC fractions were subjected to chip electrophoresis after dilution. Typically (depending on the amount of virus starting material), a 1 : 10 dilution of the SEC main fraction still yielded a sufficiently high peak for chip electrophoresis. As demonstrated (figure 65), fraction 2a indeed contained the highest number of FL modified particles. Free dye was depleted with a minimum of analyte dilution in the course of the purification process. Upon consideration of FL virus peak areas of fractions 1b, 2a and 2b approximately 94% of all modified virus particles were found in the main SEC fraction 2a.



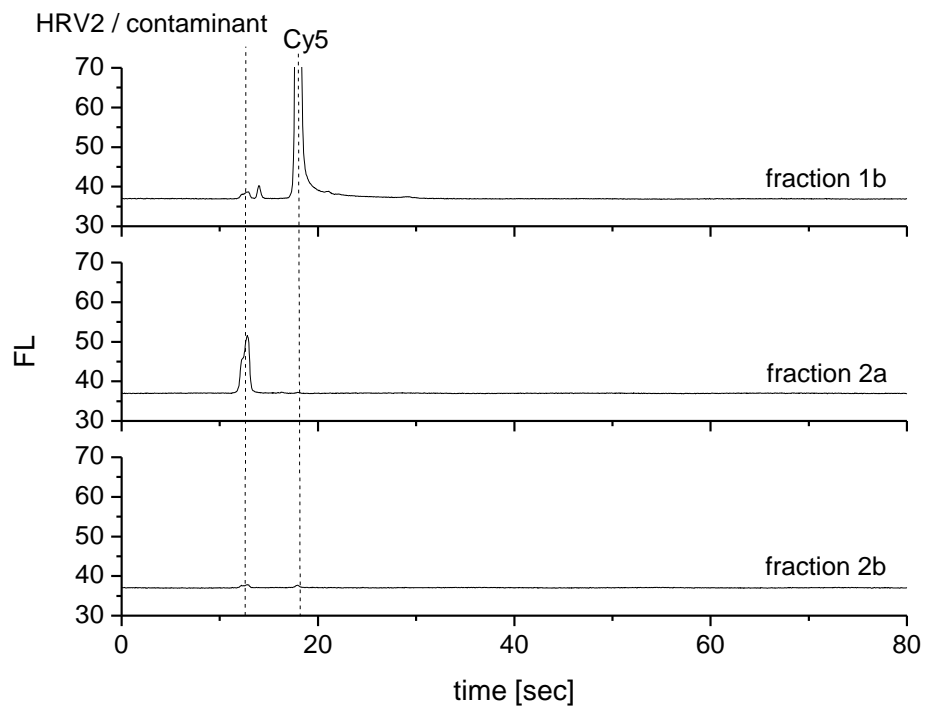


Fig. 65: Comparison of spin SEC fractions after 1 : 10 sample dilution. HRV2 was labeled via the amine-reactive probe Cy5 at an approx.  $2.5 \times 10^3$  fold molar excess level of dye over virus particles. The labeling solution was subjected to spin SEC purification as detailed in the text to deplete an analyte containing solution from free dye molecules with a minimum of further analyte dilution. Spin SEC fractions were analyzed via chip electrophoresis. As expected, fraction 2a was found to include the majority of FL modified viral particles. Free dye molecules however were mostly detected in fraction 1b.

## 6 Conclusion

Human Rhinoviruses belong to the picornavirus family and cause relative harmless infections of the upper respiratory tract. However, *picornaviridae* also include more hazardous viral species like polio-, hepatitis-A- and foot-and-mouth-disease virus. This fact accounts for the importance of carrying out experimental work with a relatively harmless member of this virus family for elucidating steps in the early infection pathway. Work in the course of my thesis concentrated on HRV2, the best studied serotype of HRVs binding to members of the LDLR family for cell entry.

In my research I was able to expand the applicability of capillary electrophoresis from the analysis of native virions to species of the HRV2 uncoating process. Refinement of sample preparation conditions allowed for specific targeting of particles trapped at a stage of viral uncoating, where virions still include the RNA genome but had already emitted part of their proteinaceous capsid to the surrounding solution (subviral 135S particles). Such, the stage was set for further structural elucidation of intermediates of the viral uncoating process.

Porting of CE conditions to a commercially available chip electrophoresis instrument – the Agilent 2100 Bioanalyzer system – allowed for virus analysis in the absence of detergents, which had not been possible with a conventional CE setup. Thus, electrophoresis of virions alongside lipid vesicles mimicking the cell surface environment under well defined conditions was achieved. Such, independent steps of early viral infection, ranging from virus attachment to receptor decorated particles to processes related to the viral genome transfer through membranes, could be discretely targeted. However, although it was possible to lay the basis for further elucidation of the viral genome transfer across membranes upon application of molecular beacons, this final step of viral infection could not be reached with the developed, liposome-based, chip electrophoretic setup. Therefore, future work will be directed to follow this last step of early viral infection. Nevertheless, in the course of the present work innovative applications of chip electrophoresis for targeting of questions related to infectious processes were worked out, even on a commercially available instrument.

# Literature

1. Weiss, V. U.; Kolivoska, V.; Kremser, L.; Gas, B.; Blaas, D.; Kenndler, E., Virus analysis by electrophoresis on a microfluidic chip. *J Chromatogr B* **2007**, 860, 173-179
2. Kolivoska, V.; Weiss, V. U.; Kremser, L.; Gas, B.; Blaas, D.; Kenndler, E., Electrophoresis on a microfluidic chip for analysis of fluorescence-labeled human rhinovirus. *Electrophoresis* **2007**, 28, 4734-4740
3. Fuchs, R.; Blaas, D., Human Rhinovirus Cell Entry and Uncoating. *from: Structure Based Study of Viral Replication* **2008**, Cheng, R. Holland, Miyamura, Tatsuo (Ed.), 1-42.
4. Abraham, G.; Colonno, R. J., Many rhinovirus serotypes share the same cellular receptor. *J Virol* **1984**, 51, (2), 340-5.
5. Tomassini, J. E.; Colonno, R. J., Isolation of a receptor protein involved in attachment of human rhinoviruses. *J Virol* **1986**, 58, (2), 290-5.
6. Hofer, F.; Gruenberger, M.; Kowalski, H.; Machat, H.; Huettinger, M.; Kuechler, E.; Blaas, D., Members of the low density lipoprotein receptor family mediate cell entry of a minor-group common cold virus. *Proc Natl Acad Sci U S A* **1994**, 91, (5), 1839-42.
7. Marlovits, T. C.; Zechmeister, T.; Gruenberger, M.; Ronacher, B.; Schwihla, H.; Blaas, D., Recombinant soluble low density lipoprotein receptor fragment inhibits minor group rhinovirus infection in vitro. *Faseb J* **1998**, 12, (9), 695-703.
8. Hewat, E. A.; Neumann, E.; Conway, J. F.; Moser, R.; Ronacher, B.; Marlovits, T. C.; Blaas, D., The cellular receptor to human rhinovirus 2 binds around the 5-fold axis and not in the canyon: a structural view. *Embo J* **2000**, 19, (23), 6317-25.
9. Neumann, E.; Moser, R.; Snyers, L.; Blaas, D.; Hewat, E. A., A cellular receptor of human rhinovirus type 2, the very-low-density lipoprotein receptor, binds to two neighboring proteins of the viral capsid. *J Virol* **2003**, 77, (15), 8504-11.
10. Wruss, J.; Ruenzler, D.; Steiger, C.; Chiba, P.; Koehler, G.; Blaas, D., Attachment of VLDL Receptors to an Icosahedral Virus along the 5-fold Symmetry Axis: Multiple Binding Modes Evidenced by Fluorescence Correlation Spectroscopy. *Biochemistry* **2007**, 46, (21), 6331-6339.
11. Querol-Audi, J.; Konecni, T.; Pous, J.; Carugo, O.; Fita, I.; Verdaguer, N.; Blaas, D., Minor group human rhinovirus-receptor interactions: Geometry of multimodular attachment and basis of recognition. *FEBS Letters* **2009**, 583, (1), 235-240.
12. Andries, K.; Dewindt, B.; Snoeks, J.; Wouters, L.; Moereels, H.; Lewi, P. J.; Janssen, P. A., Two groups of rhinoviruses revealed by a panel of antiviral compounds present sequence divergence and differential pathogenicity. *J Virol* **1990**, 64, (3), 1117-23.

13. Snyers, L.; Zwickl, H.; Blaas, D., Human rhinovirus type 2 is internalized by clathrin-mediated endocytosis. *J Virol* **2003**, *77*, (9), 5360-9.
14. Kienberger, F.; Zhu, R.; Moser, R.; Blaas, D.; Hinterdorfer, P., Monitoring RNA release from human rhinovirus by dynamic force microscopy. *J Virol* **2004**, *78*, (7), 3203-9.
15. Alberts, B.; Johnson, A.; Lewis, J.; Raff, M.; Roberts, K.; Walter, P., Intracellular Vesicular Traffic. *from: Molecular Biology of the Cell, 4th edition* **2002**, 711-767.
16. Prchla, E.; Kuechler, E.; Blaas, D.; Fuchs, R., Uncoating of human rhinovirus serotype 2 from late endosomes. *J Virol* **1994**, *68*, (6), 3713-23.
17. Brabec, M.; Schober, D.; Wagner, E.; Bayer, N.; Murphy, R. F.; Blaas, D.; Fuchs, R., Opening of size-selective pores in endosomes during human rhinovirus serotype 2 in vivo uncoating monitored by single-organelle flow analysis. *J Virol* **2005**, *79*, (2), 1008-16.
18. Sompayrac, L., Rhinovirus - A Virus that Surrenders. *from: How Pathogenic Viruses Work* **2002**, (Jones&Bartlett Publishers Inc., US), 25-28.
19. Gern, J. E., Rhinovirus respiratory infections and asthma. *American Journal of Medicine* **2002**, *112*, (6A), 19S-27S.
20. Heikkinen, T.; Jarvinen, A., The common cold. *Lancet* **2003**, *361*, (9351), 51-9.
21. Savolainen, C.; Blomqvist, S.; Hovi, T., Human rhinoviruses. *Paediatr Respir Rev* **2003**, *4*, (2), 91-8.
22. Yamaya, M.; Sasaki, H., Rhinovirus and airway allergy. *Allergology International* **2004**, *53*, (2), 37-45.
23. Alberts, B.; Johnson, A.; Lewis, J.; Raff, M.; Roberts, K.; Walter, P., Membrane Structure. *from: Molecular Biology of the Cell, 4th edition* **2002**, 583-593.
24. Gomez-Hens, A.; Fernandez-Romero, J. M., Analytical methods for the control of liposomal delivery systems. *TrAC* **2006**, *25*, (2), 167-178.
25. Gomez-Hens, A.; Manuel Fernandez-Romero, J., The role of liposomes in analytical processes. *TrAC* **2005**, *24*, (1), 9-19.
26. Jouyban, A.; Kenndler, E., Theoretical and empirical approaches to express the mobility of small ions in capillary electrophoresis. *Electrophoresis* **2006**, *27*, (5-6), 992-1005.
27. Landers, J. P., Introduction to Capillary Electrophoresis. *from: Handbook of Capillary and Microchip Electrophoresis and Associated Microtechniques, 3rd edition* **2008**, Landers, James P. (Ed.), 4-22.
28. Marina, M. L.; Ríos, A.; M., V., Fundamentals of Capillary Electrophoresis. *from: Analysis and Detection by Capillary Electrophoresis* **2005**, Marina, M. L., Ríos, A., Valcárcel; M. (Ed.), 2-11.
29. Lottspeich, F.; Zorbas, H., Kapillarelektrophorese. *from: Bioanalytik, 2nd edition* **2006**, 253-285.
30. Lottspeich, F.; Zorbas, H., Elektrophoretische Verfahren. *from: Bioanalytik, 2nd edition* **2006**, 217-252.

31. Gas, B.; Stedry, M.; Kenndler, E., Peak broadening in capillary zone electrophoresis. *Electrophoresis* **1997**, 18, (12-13), 2123-33.
32. Gas, B.; Kenndler, E., Dispersive phenomena in electromigration separation methods. *Electrophoresis* **2000**, 21, (18), 3888-97.
33. Gas, B.; Kenndler, E., Peak broadening in microchip electrophoresis: a discussion of the theoretical background. *Electrophoresis* **2002**, 23, (22-23), 3817-26.
34. Bousse, L.; Mouradian, S.; Minalla, A.; Yee, H.; Williams, K.; Dubrow, R., Protein sizing on a microchip. *Anal Chem* **2001**, 73, (6), 1207-1212.
35. Barthmaier, P.; Kuschel, M.; Neumann, T.; Kratzmeier, M., Use of a lab-on-a-chip based system for protein analysis. *American Biotechnology Laboratory* **2002**, 20, (9), 44, 46.
36. Kuschel, M.; Neumann, T.; Barthmaier, P.; Kratzmeier, M., Use of Lab-on-a-Chip Technology for Protein Sizing and Quantitation. *Journal of Biomolecular Techniques* **2002**, 13, (3, September 2002), 172-178.
37. Agilent 230 Protein Kit Guide. Edition 08 / 2006 from Agilent Technologies (Waldbronn, Germany); Manual Part Number G2938 - 90054
38. Mueller, O.; Hahnenberger, K.; Dittmann, M.; Yee, H.; Dubrow, R.; Nagle, R.; Ilsley, D., A microfluidic system for high-speed reproducible DNA sizing and quantitation. *Electrophoresis* **2000**, 21, (1), 128-134.
39. Hjerten, S., Free zone electrophoresis. *Chromatogr Rev* **1967**, 9, (2), 122-219.
40. Vegvari, A.; Hjerten, S., Hybrid microdevice electrophoresis of peptides, proteins, DNA, viruses, and bacteria in various separation media, using UV-detection. *Electrophoresis* **2003**, 24, (21), 3815-3820.
41. Liang, S.; Schneider, R. J., Capillary zone electrophoresis of Cowpea mosaic virus and peak identification. *Electrophoresis* **2009**, 30, 1-7
42. Mann, B.; Traina, J. A.; Soderblom, C.; Murakami, P. K.; Lehmborg, E.; Lee, D.; Irving, J.; Nestaas, E.; Pungor, E., Capillary zone electrophoresis of a recombinant adenovirus. *J Chromatogr A* **2000**, 895, (1-2), 329-37.
43. Kremser, L.; Bilek, G.; Blaas, D.; Kenndler, E., Capillary electrophoresis of viruses, subviral particles and virus complexes. *Journal of Separation Science* **2007**, 30, (11), 1704-1713.
44. Kremser, L.; Blaas, D.; Kenndler, E., Virus analysis using electromigration techniques. *Electrophoresis* **2009**, 30, (1), 133-40.
45. Oita, I.; Halewyck, H.; Pieters, S.; Dejaegher, B.; Thys, B.; Rombaut, B.; Heyden, Y. V., Improving the capillary electrophoretic analysis of poliovirus using a Plackett-Burman design. *J Pharm Biomed Anal* **2008**, 50, (4), 655-663
46. Okun, V. M.; Ronacher, B.; Blaas, D.; Kenndler, E., Analysis of Common Cold Virus (Human Rhinovirus Serotype 2) by Capillary Zone Electrophoresis: The Problem of Peak Identification. *Anal Chem* **1999**, 71, (10), 2028-2032.

47. Okun, V. M.; Blaas, D.; Kenndler, E., Separation and Biospecific Identification of Subviral Particles of Human Rhinovirus Serotype 2 by Capillary Zone Electrophoresis. *Anal Chem* **1999**, *71*, (20), 4480-4485.
48. Kremser, L.; Blaas, D.; Kenndler, E., Capillary electrophoresis of biological particles: Viruses, bacteria, and eukaryotic cells. *Electrophoresis* **2004**, *25*, (14), 2282-2291.
49. Kenndler, E.; Blaas, D., Capillary electrophoresis of macromolecular biological assemblies: bacteria and viruses. *TrAC* **2001**, *20*, (10), 543-551.
50. Schnabel, U.; Groiss, F.; Blaas, D.; Kenndler, E., Determination of the pI of human rhinovirus serotype 2 by capillary isoelectric focusing. *Anal Chem* **1996**, *68*, (23), 4300-3.
51. Kremser, L.; Petsch, M.; Blaas, D.; Kenndler, E., Influence of detergent additives on mobility of native and subviral rhinovirus particles in capillary electrophoresis. *Electrophoresis* **2006**, *27*, (5-6), 1112-1121.
52. Okun, V. M.; Nizet, S.; Blaas, D.; Kenndler, E., Kinetics of thermal denaturation of human rhinoviruses in the presence of anti-viral capsid binders analyzed by capillary electrophoresis. *Electrophoresis* **2002**, *23*, (6), 896-902.
53. Okun, V. M.; Ronacher, B.; Blaas, D.; Kenndler, E., Affinity capillary electrophoresis for the assessment of complex formation between viruses and monoclonal antibodies. *Anal Chem* **2000**, *72*, (19), 4634-9.
54. Okun, V. M.; Moser, R.; Ronacher, B.; Kenndler, E.; Blaas, D., VLDL receptor fragments of different lengths bind to human rhinovirus HRV2 with different stoichiometry: an analysis of virus-receptor complexes by capillary electrophoresis. *Journal of Biological Chemistry* **2001**, *276*, (2), 1057-1062.
55. Okun, V. M.; Moser, R.; Blaas, D.; Kenndler, E., Complexes between monoclonal antibodies and receptor fragments with a common cold virus: determination of stoichiometry by capillary electrophoresis. *Anal Chem* **2001**, *73*, (16), 3900-6.
56. Kremser, L.; Kenndler, E., Analysis of virus interactions by CE. *GIT Labor-Fachzeitschrift* **2004**, *48*, (2), 128-130.
57. Kremser, L.; Petsch, M.; Blaas, D.; Kenndler, E., Capillary electrophoresis of affinity complexes between subviral 80S particles of human rhinovirus and monoclonal antibody 2G2. *Electrophoresis* **2006**, *27*, (13), 2630-7.
58. Konecni, T.; Kremser, L.; Snyers, L.; Rankl, C.; Kilar, F.; Kenndler, E.; Blaas, D., Twelve receptor molecules attach per viral particle of human rhinovirus serotype 2 via multiple modules. *FEBS Letters* **2004**, *568*, (1-3), 99-104.
59. Okun, V.; Ronacher, B.; Blaas, D.; Kenndler, E., Capillary electrophoresis with postcolumn infectivity assay for the analysis of different serotypes of human rhinovirus (common cold virus). *Anal Chem* **2000**, *72*, (11), 2553-8.

60. Kremser, L.; Okun, V. M.; Nicodemou, A.; Blaas, D.; Kenndler, E., Binding of fluorescent dye to genomic RNA inside intact human rhinovirus after viral capsid penetration investigated by capillary electrophoresis. *Anal Chem* **2004**, 76, (4), 882-7.
61. Kremser, L.; Konecsni, T.; Blaas, D.; Kenndler, E., Fluorescence Labeling of Human Rhinovirus Capsid and Analysis by Capillary Electrophoresis. *Anal Chem* **2004**, 76, (14), 4175-4181.
62. Kremser, L.; Petsch, M.; Blaas, D.; Kenndler, E., Labeling of Capsid Proteins and Genomic RNA of Human Rhinovirus with Two Different Fluorescent Dyes for Selective Detection by Capillary Electrophoresis. *Anal Chem* **2004**, 76, (24), 7360-7365.
63. Bilek, G.; Kremser, L.; Blaas, D.; Kenndler, E., Analysis of liposomes by capillary electrophoresis and their use as carrier in electrokinetic chromatography. *J Chromatogr B* **2006**, 841, (1-2), 38-51.
64. Wiedmer, S. K.; Shimmo, R., Liposomes in capillary electromigration techniques. *Electrophoresis* **2009**, 30 Suppl 1, S240-57.
65. Terabe, S.; Otsuka, K.; Ando, T., Elektrokinetic chromatography with micellar solution and open-tubular capillary. *Anal Chem* **1985**, 57, (4), 834-841.
66. Terabe, S.; Otsuka, K.; Ichikawa, K.; Tsuchiya, A.; Ando, T., Elektrokinetic separations with micellar solutions and open-tubular capillaries. *Anal Chem* **1984**, 56, (1), 111-113.
67. Manetto, G.; Silvana Bellini, M.; Deyl, Z., Application of capillaries with minimized electroosmotic flow to the electrokinetic study of acidic drug-beta-oleoyl-gamma-palmitoyl-L-alpha-phosphatidyl choline liposome interactions. *J Chromatogr A* **2003**, 990, (1-2), 205-14.
68. Bilek, G.; Kremser, L.; Wruss, J.; Blaas, D.; Kenndler, E., Mimicking early events of virus infection: capillary electrophoretic analysis of virus attachment to receptor-decorated liposomes. *Anal Chem* **2007**, 79, (4), 1620-5.
69. Bilek, G.; Kremser, L.; Blaas, D.; Kenndler, E., Capillary electrophoresis of liposomes functionalized for protein binding. *Electrophoresis* **2006**, 27, (20), 3999-4007.
70. Chow, M., Newman, J. F., Filman, D., Hogle, J. M., Rowlands, D. J., Brown, F., Myristylation of picornavirus capsid protein VP4 and its structural significance. *Nature* **1987**, 327, (6122), 482-486.
71. Paul, A. V., Schultz, A., Pincus, S. E., Oroszlan, S., Wimmer, E., Capsid protein VP4 of poliovirus is N-myristoylated. *Proc Natl Acad Sci U S A* **1987**, 84, (22), 7827-7831.
72. Ward, T.; Powell, R. M.; Evans, D. J.; Almond, J. W., Serum albumin inhibits echovirus 7 uncoating. *J Gen Virol* **1999**, 80 ( Pt 2), 283-90.
73. Ward, T.; Powell, R. M.; Chaudhry, Y.; Meredith, J.; Almond, J. W.; Kraus, W.; Nelsen-Salz, B.; Eggers, H. J.; Evans, D. J., Fatty acid-depleted albumin induces the formation of echovirus A particles. *J Virol* **2000**, 74, (7), 3410-2.
74. Smyth, M., Pettitt, T., Symonds, A., Martin, J., Identification of the pocket factors in a picornavirus. *Arch Virol* **2003**, 148, (6), 1225-1233.

75. Moser, R.; Snyers, L.; Wruss, J.; Angulo, J.; Peters, H.; Peters, T.; Blaas, D., Neutralization of a common cold virus by concatemers of the third ligand binding module of the VLDL-receptor strongly depends on the number of modules. *Virology* **2005**, 338, (2), 259-69.
76. Zauner, W.; Blaas, D.; Kuechler, E.; Wagner, E., Rhinovirus-mediated endosomal release of transfection complexes. *J Virol* **1995**, 69, (2), 1085-92.
77. Smolarsky, M.; Teitelbaum, D.; Sela, M.; Gitler, C., A simple fluorescent method to determine complement-mediated liposome immune lysis. *Journal of Immunological Methods* **1977**, 15, (3), 255-65.
78. Ladokhin, A. S.; Wimley, W. C.; White, S. H., Leakage of membrane vesicle contents: determination of mechanism using fluorescence reequenching. *Biophys J* **1995**, 69, (5), 1964-71.
79. Rausch, J. M.; Wimley, W. C., A high-throughput screen for identifying transmembrane pore-forming peptides. *Analytical Biochemistry* **2001**, 293, (2), 258-263.
80. Sainz, B., Jr.; Rausch, J. M.; Gallaher, W. R.; Garry, R. F.; Wimley, W. C., The Aromatic Domain of the Coronavirus Class I Viral Fusion Protein Induces Membrane Permeabilization: Putative Role during Viral Entry. *Biochemistry* **2005**, 44, (3), 947-958.
81. Costin Joshua, M.; Rausch Joshua, M.; Garry Robert, F.; Wimley William, C., Viroporin potential of the lentivirus lytic peptide (LLP) domains of the HIV-1 gp41 protein. *Virol J* **2007**, 4, 123.
82. Li, W.; Nicol, F.; Szoka Francis, C., Jr., GALA: a designed synthetic pH-responsive amphipathic peptide with applications in drug and gene delivery. *Adv Drug Deliv Rev* **2004**, 56, (7), 967-85.
83. Nir, S.; Nieva, J. L., Interactions of peptides with liposomes: pore formation and fusion. *Prog Lipid Res* **2000**, 39, (2), 181-206.
84. Davis, M. P.; Bottley, G.; Beales, L. P.; Killington, R. A.; Rowlands, D. J.; Tuthill, T. J., Recombinant VP4 of human rhinovirus induces permeability in model membranes. *J Virol* **2008**, 82, (8), 4169-74.
85. Kramer, F. R., Introduction to Molecular Beacons. From <http://www.molecular-beacons.org/Introduction.html>.
86. Tyagi, S., Designing Molecular Beacons. From [http://www.molecular-beacons.org/PA\\_design.html](http://www.molecular-beacons.org/PA_design.html).
87. Tyagi, S.; Kramer, F. R., Molecular beacons: probes that fluoresce upon hybridization. *Nat Biotechnol* **1996**, 14, (3), 303-8.
88. Fang, X.; Li, J. J.; Perlette, J.; Tan, W.; Wang, K., Molecular beacons: novel fluorescent probes. *Anal Chem* **2000**, 72, (23), 747A-753A.
89. Antony, T.; Subramaniam, V., Molecular beacons: nucleic acid hybridization and emerging applications. *J Biomol Struct Dyn* **2001**, 19, (3), 497-504.
90. Silverman, A. P.; Kool, E. T., Quenched probes for highly specific detection of cellular RNAs. *Trends Biotechnol* **2005**, 23, (5), 225-30.



91. Li, Y.; Zhou, X.; Ye, D., Molecular beacons: an optimal multifunctional biological probe. *Biochem Biophys Res Commun* **2008**, 373, (4), 457-61.
92. Santangelo, P.; Nitin, N.; LaConte, L.; Woolums, A.; Bao, G., Live-cell characterization and analysis of a clinical isolate of bovine respiratory syncytial virus, using molecular beacons. *J Virol* **2006**, 80, (2), 682-8.
93. Wang, A.; Salazar, A. M.; Yates, M. V.; Mulchandani, A.; Chen, W., Visualization and detection of infectious coxsackievirus replication using a combined cell culture-molecular beacon assay. *Appl Environ Microbiol* **2005**, 71, (12), 8397-401.
94. Cui, Z. Q.; Zhang, Z. P.; Zhang, X. E.; Wen, J. K.; Zhou, Y. F.; Xie, W. H., Visualizing the dynamic behavior of poliovirus plus-strand RNA in living host cells. *Nucleic Acids Res* **2005**, 33, (10), 3245-52.
95. Ramachandran, A.; Zhang, M.; Goad, D.; Olah, G.; Malayer, J. R.; El Rassi, Z., Capillary electrophoresis and fluorescence studies on molecular beacon-based variable length oligonucleotide target discrimination. *Electrophoresis* **2003**, 24, (1-2), 70-77.
96. Koehler, R.T.; Peyret, N. Effects of DNA secondary structure on oligonucleotide probe binding efficiency. *Comput Biol Chem* **2005**, 29, (6), 393-7
97. Gamper, H. B.; Cimino, G. D.; Hearst, J. E., Solution hybridization of crosslinkable DNA oligonucleotides to bacteriophage M13 DNA. Effect of secondary structure on hybridization kinetics and equilibria. *J Mol Biol* **1987**, 197, (2), 349-62.
98. Technical information on oligonucleotides from: [www.biomers.net](http://www.biomers.net)
99. Mathews, D. H.; Sabina, J.; Zuker, M.; Turner, D. H., Expanded sequence dependence of thermodynamic parameters improves prediction of RNA secondary structure. *J Mol Biol* **1999**, 288, (5), 911-40.
100. Zuker, M., Mfold web server for nucleic acid folding and hybridization prediction. *Nucleic Acids Res* **2003**, 31, (13), 3406-15.
101. Rensselaer bioinformatics web page at: <http://mfold.bioinfo.rpi.edu/>
102. Behlke, M. A.; Huang, L.; Bogh, L.; Rose, S.; Devor, E. J., Fluorescence Quenching by Proximal G-bases. *Integrated DNA Technologies* **2005**.
103. Vogelsang, J.; Kasper, R.; Steinhauer, C.; Person, B.; Heilemann, M.; Sauer, M.; Tinnefeld, P., A reducing and oxidizing system minimizes photobleaching and blinking of fluorescent dyes. *Angewandte Chemie, International Edition* **2008**, 47, (29), 5465-5469.
104. Tellez, A.; Weiss, V. U.; Kenndler, E., An extended description of the effect of detergent monomers on migration in micellar electrokinetic chromatography. *Electrophoresis* **2008**, 29, (18), 3916-3923.

Mag. rer. nat. Victor U. Weiss

[victor.weiss@gmx.at](mailto:victor.weiss@gmx.at)

---



## Curriculum Vitae

### General Information:

Date of birth: 03.02.1981

Parents : Univ. Prof. DI Dr. Werner W. Weiss; Prof. Dr. Waltraud H. Weiss – Pyerin

### Education:

1987 – 1991 Elementary school: VS Cottagegasse 17, 1180 Vienna

1991 – 1999 Grammar school: BG XIX, Gymnasiumstrasse 83, 1190 Vienna

June 1999 School leaving examination qualifying for university admission: Chemistry, History, English, Maths and German with excellent A-level results

1999 – 2007 Academic studies: Chemistry at the University of Vienna, Waehringer Strasse 38 – 42, 1090 Vienna with special emphases on analytical and inorganic chemistry as well as on biochemistry

2006 – 2007 Diploma thesis: ‘Virus Analyses on Electrophoretic Microdevices’ at the Faculty of Chemistry, Department of Analytical and Food Chemistry, University of Vienna, Waehringer Strasse 38, 1090 Vienna, group ‘Microcolumn Separation Methods’ (Univ. Prof. Dr. Ernst Kenndler)

May 2007 Diploma examination: Univ. Prof. Dr. Wolfgang Lindner (chair), Univ. Prof. Dr. Ernst Kenndler (supervision of thesis), Univ. Prof. Rainer Prohaska

2007 – 2009 Ph.D. thesis: ‘Chip Electrophoresis of Human Rhinovirus and Receptor Decorated Liposomes as Model Membranes for the Analysis of Key Steps in the Viral Infection Pathway’ at the Faculty of Chemistry, Department of Analytical and Food Chemistry, University of Vienna, Waehringer Strasse 38, 1090 Vienna, group ‘Microcolumn Separation Methods’ (Univ. Prof. Dr. Ernst Kenndler) and at the Max F. Perutz Laboratories, Department of Biochemistry and Cell Biology, University of Vienna, Dr. Bohr Gasse 9, 1030 Vienna, group ‘Infection Biology’ (Univ. Prof. DI Dr. Dieter Blaas)

### **Internships:**

- 02.08. – 12.09.2004: Sandoz GmbH Vienna, Antibiotica Research Institute (ABRI), Analytical Laboratory I
- 18.07. – 11.09.2005: Senna Nahrungsmittel GmbH, Quality Control Department
- 26.06. – 21.07.2006: Senna Nahrungsmittel GmbH, Quality Control Department
- 16.08. – 08.09.2006: Senna Nahrungsmittel GmbH, Quality Control Department

### **Further Training:**

- 17.08. – 28.08.1998: English course, Cromer, GB
- 03.01. – 02.09.2000: Military service: Pioniertruppenschule (PITS) Klosterneuburg serving on board the navy ship MS Niederoesterreich
- December 2000: Driving licence A and B

### **List of Publications:**

1. Weiss, V. U.; Kolivoska, V.; Kremser, L.; Gas, B.; Blaas, D.; Kenndler, E., Virus analysis by electrophoresis on a microfluidic chip. *J Chromatogr B* **2007**, 860, 173-179
2. Kolivoska, V.; Weiss, V. U.; Kremser, L.; Gas, B.; Blaas, D.; Kenndler, E., Electrophoresis on a microfluidic chip for analysis of fluorescence-labeled human rhinovirus. *Electrophoresis* **2007**, 28, 4734-4740
3. Tellez, A.; Weiss, V. U.; Kenndler, E., An extended description of the effect of detergent monomers on migration in micellar electrokinetic chromatography. *Electrophoresis* **2008**, 29, (18), 3916-3923.
4. Weiss, V. U.; Bilek, G.; Pickl-Herk, A.; Blaas, D.; Kenndler, E., Mimicking virus attachment to host cells employing liposomes: analysis by chip electrophoresis. *Electrophoresis* **2009**, 30, (12), 2123-8.
5. Bilek, G.; Weiss, V. U.; Pickl-Herk, A.; Blaas, D.; Kenndler, E., Chip electrophoretic characterization of liposomes with biological lipid composition: Coming closer to a model for viral infection. *Electrophoresis* **2009**, in press, elps.200900382.R1.

**Participation on International Symposia:**

- 31.08. – 04.09.2008: ITP 2008, 16<sup>th</sup> International Symposium on Capillary Electroseparation Techniques, Catania, Italy: poster ‘Chip Electrophoretic Analysis of Viral Proteins Regarding their Membrane Disrupting Abilities’
- 15.11. – 16.11.2007: CECE 2007, 4<sup>th</sup> International Interdisciplinary Meeting on Bioanalysis, Brno, Czech Republic
- 27.06. – 29.06.2007: 13<sup>th</sup> International Symposium on Separation Sciences, High Tatras, Štrbské Pleso, Slovak Republic: presentation ‘Virus Analysis by Electrophoresis on a Microfluidic Chip’
- 13.11. – 14.11.2006: CECE 2006, 3<sup>rd</sup> International Workshop, Brno, Czech Republic

**Additional Skills and Specialization:**

Analytical chemistry and biochemistry

Capillary electrophoresis (CE) of viruses and subviral particles

Affinity CE of viruses to receptors and antibodies

Chip electrophoresis

Presentation techniques

Skilled in writing, speaking and reading English

Knowledge of MS Windows XP, Office, Origin, SciFinder Scholar, Endnote, Agilent Technologies ChemStation, Agilent Technologies 2100 Expert Software, Peakmaster



Victor U. Weiss

Vienna, October 2009

# Zusammenfassung der Dissertation (dt.)

Bis heute konnten in etwa 100 Serotypen von Humanen Rhinoviren (HRVs), welche eine der häufigsten Erkältungsursachen darstellen, unterschieden werden. Diese Serotypen werden nach dem jeweiligen Rezeptor, an den sie im Laufe der Zellinfektion binden, in zwei Gruppen unterteilt. Viren der Hauptgruppe binden an *intercellular adhesion molecule 1* (ICAM – 1), Viren der Nebengruppe an Vertreter der *low-density-lipoprotein* Rezeptor (LDLR) Familie. Chip Elektrophorese ermöglichte in der Vergangenheit bereits erfolgreich die Analyse von fluoreszenzmarkierten Viren sowie die Verfolgung entsprechender Bioaffinitätsreaktionen. Zum Beispiel konnte die Bindung von HRV2, einem Rhinovirus der Nebengruppe, an Rezeptorfragmente verfolgt werden [Weiss *et al.* (2007): Virus analysis by electrophoresis on a microfluidic chip, *J. Chromatogr. B* 860, 173 – 179 sowie Kolivoška *et al.* (2007): Electrophoresis on a microfluidic chip for analysis of fluorescence-labeled human rhinovirus, *Electrophoresis* 28, 4734 – 4740].

In Weiterführung dieser grundlegenden Experimente, versuchte ich, im Laufe dieser Dissertation, die spezifische, rezeptorvermittelte Bindung von fluoreszenzmarkiertem HRV2 an Zellen mit Hilfe von Chip Elektrophorese zu zeigen. Anstelle von Zellen arbeitete ich jedoch mit unilamellaren, rezeptordekorierten Vesikeln (Liposomen). Dieses Modellsystem ermöglichte Experimente unter gut definierten Bedingungen, anders als es bei Verwendung von tatsächlichem zellulären Material möglich gewesen wäre.

Zusätzlich zu reinen Bindungsexperimenten zwischen Viren und Membranen wurde auch der Transfer der viralen RNA in das Liposomeninnere untersucht. *In vivo* gelangen HRVs über rezeptorvermittelte Endocytose in das Zellinnere. Im Zuge dieser Transportroute werden Endosome angesäuert, was zur Konformationsänderung von aufgenommenen Viren führt. Bedingt durch diese Konformationsänderung gelingt es Viren, ihre RNA durch die Endosomenmembran in das Cytosol der infizierten Zelle zu transferieren. Daraus ergab sich mein Interesse an membrandestabilisierenden Fähigkeiten von viralen Proteinen sowie von ganzen Viren. Zusätzlich wurden auch grundlegende Experimente zum Transfer der viralen RNA selbst durch Membranen unter Zuhilfenahme von *molecular beacons* durchgeführt. *Molecular beacons* sind fluoreszenzmarkierten Sonden, die nach erfolgter Bindung an eine korrespondierende Nukleotidsequenz ein Fluoreszenzsignal ergeben.



## Lebenslauf (dt.)

### Allgemeine Informationen:

Geburtsdatum: 03.02.1981

Eltern: Univ. Prof. DI Dr. Werner W. Weiss; Prof. Dr. Waltraud H. Weiss – Pyerin

### Ausbildung:

1987 – 1991 Volksschule VS Cottagegasse 17, 1180 Wien

1991 – 1999 Gymnasium BG XIX, Gymnasiumstrasse 83, 1190 Wien

Juni 1999 Matura mit ausgezeichnetem Erfolg in den Fächern Chemie (mündlich), Geschichte (mündlich und Fachbereichsarbeit), Englisch (schriftlich und mündlich), Mathematik (schriftlich) und Deutsch (schriftlich)

1999 – 2007 Chemiestudium an der Universität Wien, Währinger Strasse 38 – 42, 1090 Wien mit Spezialisierung auf Analytische und Anorganische Chemie, sowie Biochemie

2006 – 2007 Diplomarbeit: ‘Virus Analyses on Electrophoretic Microdevices’ am Institut für Analytische Chemie und Lebensmittelchemie der Universität Wien, Währinger Strasse 38, 1090 Wien in der Arbeitsgruppe ‘Microcolumn Separation Methods’ (Univ. Prof. Dr. Ernst Kenndler)

Mai 2007 Diplomprüfung durch Univ. Prof. Dr. Wolfgang Lindner (Vorsitz), Univ. Prof. Dr. Ernst Kenndler (Betreuer), Univ. Prof. Rainer Prohaska

2007 – 2009 Dissertation: ‘Chip Electrophoresis of Human Rhinovirus and Receptor Decorated Liposomes as Model Membranes for the Analysis of Key Steps in the Viral Infection Pathway’ am Institut für Analytische Chemie und Lebensmittelchemie der Universität Wien, Währinger Strasse 38, 1090 Wien in der Arbeitsgruppe ‘Microcolumn Separation Methods’ (Univ. Prof. Dr. Ernst Kenndler) sowie an den Max F. Perutz Laboratories, Department für Biochemie und Zellbiologie der Universität Wien, Dr. Bohr Gasse 9, 1030 Wien, Arbeitsgruppe ‘Infection Biology’ (Univ. Prof. DI Dr. Dieter Blaas)

### **Ferialpraxis:**

- 02.08. – 12.09.2004: Sandoz GmbH Vienna, Antibiotica Research Insitute (ABRI),  
Analytik Labor I
- 18.07. – 11.09.2005: Senna Nahrungsmittel GmbH, Qualitätssicherungslabor
- 26.06. – 21.07.2006: Senna Nahrungsmittel GmbH, Qualitätssicherungslabor
- 16.08. – 08.09.2006: Senna Nahrungsmittel GmbH, Qualitätssicherungslabor

### **Weitere Ausbildung:**

- 17.08. – 28.08.1998: Besuch eines 30 stündigen Englischsprachkurses in Cromer, GB,  
mit Abschlusszertifikat
- 03.01. – 02.09.2000: Präsenzdienst an der Pioniertruppenschule (PITS) Klosterneuburg  
als Erster Matrose der MS Niederösterreich mit Beförderung zum  
Gefreiten
- Dezember 2000: Führerscheinprüfung A und B

### **Publikationsliste:**

1. Weiss, V. U.; Kolivoska, V.; Kremser, L.; Gas, B.; Blaas, D.; Kenndler, E., Virus  
analysis by electrophoresis on a microfluidic chip. *J Chromatogr B* **2007**, 860, 173-  
179
2. Kolivoska, V.; Weiss, V. U.; Kremser, L.; Gas, B.; Blaas, D.; Kenndler, E.,  
Electrophoresis on a microfluidic chip for analysis of fluorescence-labeled human  
rhinovirus. *Electrophoresis* **2007**, 28, 4734-4740
3. Tellez, A.; Weiss, V. U.; Kenndler, E., An extended description of the effect of  
detergent monomers on migration in micellar electrokinetic chromatography.  
*Electrophoresis* **2008**, 29, (18), 3916-3923.
4. Weiss, V. U.; Bilek, G.; Pickl-Herk, A.; Blaas, D.; Kenndler, E., Mimicking virus  
attachment to host cells employing liposomes: analysis by chip electrophoresis.  
*Electrophoresis* **2009**, 30, (12), 2123-8.
5. Bilek, G.; Weiss, V. U.; Pickl-Herk, A.; Blaas, D.; Kenndler, E., Chip  
electrophoretic characterization of liposomes with biological lipid composition:  
Coming closer to a model for viral infection. *Electrophoresis* **2009**, in press,  
elps.200900382.R1.

**Teilnahme an internationalen Symposien:**

- 31.08. – 04.09.2008: ITP 2008, 16<sup>th</sup> International Symposium on Capillary Electroseparation Techniques, Catania, Italien: Posterbeitrag zu ‘Chip Electrophoretic Analysis of Viral Proteins Regarding their Membrane Disrupting Abilities’
- 15.11. – 16.11.2007: CECE 2007, 4<sup>th</sup> International Interdisciplinary Meeting on Bioanalysis, Brno, Tschechische Republik
- 27.06. – 29.06.2007: 13<sup>th</sup> International Symposium on Separation Sciences, High Tatras, Štrbské Pleso, Slowakische Republik: Präsentation ‘Virus Analysis by Electrophoresis on a Microfluidic Chip’
- 13.11. – 14.11.2006: CECE 2006, 3<sup>rd</sup> International Workshop, Brno, Tschechische Republik

**Zusätzliche Fähigkeiten und Spezialisierung:**

Analytische Chemie und Biochemie

Kapillarelektrophorese (CE) von Viren und Subviralen Partikeln

Affinitäts – CE von Viren mit Rezeptoren und Antikörpern

Chip Elektrophorese

Präsentationstechnik

Ausgezeichnete Englischkenntnisse in Wort und Schrift

Kenntnisse in MS Windows XP, Office, Origin, SciFinder Scholar, Endnote, Agilent Technologies ChemStation, Agilent Technologies 2100 Expert Software, Peakmaster



Victor U. Weiss

Wien, Oktober 2009